Removal of Arsenic from Water and Immobilization in Soil Using Iron/Copper Nanoparticles

Fatemeh Yassaman Babaee

A thesis submitted to Concordia University in partial fulfillment of the requirements for the degree of:

Doctor of Philosophy

Department of Building, Civil and Environmental Engineering

Faculty of Engineering and Computer Science

Concordia University

Montreal, Quebec, Canada

July 2016

CONCORDIA UNIVERSITY

School of Graduate Studies

This is to certify that the thesis prepared

By: Fatemeh Yassaman Babaee

Entitled: Removal of Arsenic from Water and Immobilization in Soil

Using Iron/Copper Nanoparticles

and submitted in partial fulfillment of the requirements for the degree of

Doctor of Philosophy

complies with the regulations of the University and meets the accepted standards with respect to originality and quality. Signed by the final Examining Committee:

Pouya Valizadeh	Chair
John Capobianco	Examiner's name
Rajesh Seth	Examiner's name
Zhi Chen	Examiner's name
Fariborz Haghighat	Examiner's name
Catherine Mulligan	Supervisor's name
Saifur Rahaman	Supervisor's name

Approved by: Fariborz Haghighat Graduate Program Director

ABSTRACT

Removal of Arsenic from Water and Immobilization in Soil Using Iron/Copper Nanoparticles

Fatemeh Yassaman Babaee, PhD.

Concordia University, 2016

In this research, iron/copper bimetallic nanoparticles were used to remove arsenic from aqueous solutions as well as its immobilization in soil matrix. Nanoparticles were synthesized using two different protocols, resulting in two different sizes of particles and the physicochemical characterization was determined using XRD, TEM, BET and XPS techniques. To apply the nanoparticles in a soil environment, nanoparticles were stabilized with various starch concentrations. Characterization of nanoparticles resulting from the two methods of synthesis indicated that the mean diameter of nanoparticles were 13.17 nm and 27.15 nm. For both nanoparticles, adsorption isotherms fit well with the Langmuir equation and the maximum sorption capacities for As(III) and As(V) were 19.68 mg/g, and 21.32 mg/g respectively at pH 7.0 for the first nanoparticle size and 5.55 mg/g and 10.41 mg/g for As(III) and As(V) respectively for the second nanoparticle size. The kinetic test revealed that sorption follows pseudo-second-order and coexisting HCO_3^-, SO_4^{2-} , and PO_4^{3-} had an insignificant influence on arsenic adsorption at equal initial concentrations to As. Based on transport studies, for immobilization of arsenic in contaminated soil, 0.04 wt.% starch stabilized Fe/Cu nanoparticles were used. For this nanoparticle, the Langmuir adsorption isotherm was fitted and showed the maximum sorption capacity of 90.1 mg/g, and 126.58 mg/g for As(III) and As(V) respectively. Soil column breakthrough tests and elution profiles proved the mobility of the starch stabilized nanoparticles when 15% of the nanoparticles were retained in the soil bed. Starch stabilized Fe/Cu nanoparticles were highly effective for arsenic immobilizing in the contaminated soil. When the soil was treated in batch experiments with nanoparticles (0.4 g/L) at a soil to liquid

ratio of 0.1, the water leachable arsenic was reduced from 55 µg/L to 4.23 µg/L. Column elution tests indicated that application of a starch stabilized Fe/Cu suspension transferred nearly all water-soluble arsenic to nanoparticle phase. Then arsenic can become immobilized in the soil bed as the nanoparticles are immobilized in the soil matrix. The results of this research can lead to introducing an effective and efficient alternative adsorbent for removal of arsenic from water and its stabilization in contaminated soils.

Acknowledgement

Firstly, I would like to express my sincere gratitude to my advisors Professor Catherine Mulligan and Doctor Saifur Rahaman for the continuous support of my Ph.D study and related research, for their patience, motivation, and immense knowledge. Their guidance helped me in all the time of research and writing of this thesis.

Besides my advisors, I would like to thank Mr. Mazen Samara in Concordia university laboratory of thermodynamics of materials for his insightful comments, assistance and encouragement.

My sincere thanks also goes to Ms. Hong Guan in Concordia university lab of environmental engineering who provided me with anything which was needed to conduct the experiments in terms of research facilities or materials.

Finally, I would give my special thanks to my family: my mother and, brother who deserve much more appreciation than I can give. My father always encouraged me to pursue my dream and even after he passed away, his spirit still bestirred me to surmount the difficulties in my study.

TABLE OF CONTENTS

List of Tables

List of Figures

List of abbreviations

AA	Activated Alumina
AC	Activated Carbon
BET	Brunauer–Emmett–Teller
BNPs	Bimetallic Nanoscale Particles
CCA	Chromated Copper Arsenate
CEC	Cation Exchange Capacity
CMC	Carboxymethyl Cellulose
DI	Deionized
DLVO	Derjaguin, Landau, Verwey, and Overbeek
DO	Dissolved Oxygen
EBCT	Empty Bed Contact Time
EDL	Electrical Double-Layer
EDS	Energy-Dispersive X-ray Spectroscopy
EPA	Environmental Protection Agency
ESCA	Electron Spectroscopy for Chemical Analysis
FTIR	Fourier Transform Infrared Spectroscopy
FWHM	Full width at half maximum
HTMR	High Temperature Metals Recovery
ICP-MS	Inductively Coupled Plasma Mass Spectrometry
LC	Liquid Chromatography
MF	Microfiltration
NF	Nanofiltration
NRC	National Research Council

nZVI	Nanoscale Zero-Valent Iron
PAP	Polyaspartate
PRB	Permeable Reactive Barrier
PV	Pore Volume
PZC	Point of Zero Charge
RO	Reverse Osmosis
SGW	Simulated Groundwater
SLR	Soil to Liquid Ratio
SSE	Selective Sequential Extraction
TCLP	Toxicity Characteristic Leaching Procedure
TEM	Transmission Electron Microscopy
UF	Ultrafiltration
VDW	Van Der Waals
WHO	World Health Organization
XPS	Photoelectron Spectroscopy
XRD	X-ray Diffraction

Chapter 1

Introduction

1.1 Problem Statement

Arsenic has been recognized as a poison to human since ancient times and intake of it over long periods of time can lead to chronic arsenic poisoning. Health effects, which can develop over the years depending on the level of exposure, include skin lesions, peripheral neuropathy, gastrointestinal symptoms, diabetes, renal system effects, cardiovascular disease and cancer (IPCS 2001). Arsenic is widely dispersed in the nature and its increasing concern is due to its high toxicity and non-biodegradability. It has many different forms and can exist in both inorganic and organic forms.

Arsenic is released into the environment from a variety of natural and anthropogenic sources. Naturally it enters into the groundwater and the food chain due to its association with rocks, sediments and soils which contains arsenic. On average, in the earth's crust arsenic

concentrations are reported to range from 1.5 to 5 mg/kg (Cullen and Reimer, 1989) although, in some igneous and sedimentary rocks, higher concentrations of arsenic can be found, particularly in iron and manganese ores (Welch et al., 1988). Anthropogenic sources of arsenic include its use in the lumber (wood preservatives), agriculture (pesticides, insecticides, etc.), livestock (food additives, disease preventatives, etc.), and general industries (glassware, catalysts, alloys, ceramics, etc.) (Azcue & Nriagu, 1994).

The presence of naturally occurring arsenic in groundwater is a tremendous public health threat to millions of people all around the world. Bangladesh, India, China, Taiwan, Thailand, Chile and Romania are the countries most affected by high concentrations of inorganic arsenic present in ground water (Maharjan et al., 2005). To reduce the health risks of arsenic, the World Health Organization (WHO) has set a provisional guideline value of 10 µg/L for arsenic in drinking water as the practical quantification limit, a level five times stricter than the previous standard (50 µg/L). Even this limit may not be entirely free of health risks. However there are practical problems in many areas of the world in reducing levels in drinking water below this limit.

Several remediation methods have been employed to mitigate arsenic contamination in groundwater. These include coagulation and flocculation (by applying ferric chloride, ferric sulfate, ferric hydroxide and alum as coagulant), adsorption (on Activated alumina, activated carbon, copper-zinc granules, granular ferric hydroxide, iron oxide coated sand and surfactant-modified zeolite), ion exchange (using strong base resins usually loaded with chloride ions) and membrane filtration (only NF and RO membrane) (EPA, 2002; Shih, 2005; Choong et al., 2007). On the other hand, methods such as solidification and stabilization, vitrification, soil washing/acid extraction, pyrometallurgical recovery and in situ soil flushing are being used to stabilize or remediate the arsenic contaminated soils through prevention of arsenic leaching into ground water.

Although the aforementioned methods are effective in the remediation of arsenic, there are some concerns and limitations related to their use. Firstly, the cost of applying these technologies is relatively high, making them economically unfeasible for use in rural or less developed communities. Secondly, these technologies involve the production of significant amounts of

sludge by-products that create further costs in handling and management. In order to overcome these problems, it is indispensable to find new materials and/or techniques for arsenic remediation which are effective, affordable and applicable in diverse situations.

1.2 Nanoparticles as a new tool for remediation of contaminants

Adsorption is a commonly used process for the treatment of arsenic containing groundwater and drinking water. Traditionally, some adsorbents, like activated alumina (AA), and activated carbon (AC) have been used to remove arsenic from contaminated water. However, in recent years, due to some unique features, nanoparticles have emerged as a new class of adsorbents suited for contaminant removal. The extremely small size of nanomaterials, provides a large specific surface area, allowing a higher number of adsorption sites compared with micro-sized materials of the same volume (Khin et al., 2012). Moreover, due to their smaller sizes, nanoparticles can easily be transported to the target zone of a contaminated aquifer for in-situ remediation where they can remain in suspension for extended periods of time, establishing an in situ treatment zone (Zhang, 2003).

Different types of nanoparticles have been tested for the removal of pollutants from the environment; among them nanoscale zero-valent iron (nZVI) is the most widely used nanoparticle that has been investigated as a tool for the remediation of contaminated water and soil (Liang et al., 2014). Metallic or zero-valent iron (Fe^0) is a moderate reducing reagent, which can react with dissolved oxygen (DO), and to some extent water. Contaminants readily accept the electrons from the oxidation of iron and become reduced. The application of metallic iron in an environmental context has been known since the 1990s, largely due to the low cost and an absence of any known toxicity induced through the use of iron. Use of metallic iron in packed bed reactors and permeable reactive barriers has been reported widely. By using ZVI, the contaminants are being removed through redox reactions, precipitation, adsorption or transformation processes in contact with the ZVI surface (Gu et al., 1999, Scherer et al., 2000).

The successful use of ZVI in permeable reactive barriers led to the synthesis and development of iron nanoparticles for contaminant remediation. Studies have demonstrated the effectiveness of nZVI particles in the remediation of a wide range of contaminants including chlorinated organics (Cheng et al., 2007), chlorinated solvents (Choe et al., 2001), chlorinated pesticides (Elliott et al., 2009), inorganic anions (Mondal et al., 2004), and metals and metalloids (O'Carroll et al., 2013).

However, limitations and concerns have been expressed regarding the use of zero-valent iron nanoparticles. For one, it is known that in water iron reacts with oxygen and forms a layer of oxyhydroxide. This layer may inhibit further electron transfer from the Fe^0 core to the contaminants at later reaction times. This indicates that efforts need to be made to extend the functionality of ZVI nanoparticles.

Recently, there has been increasing interest in the synthesis of iron bimetallic nanoparticles. It has been hypothesized that the combination of iron and a more noble metal (e.g. Pd, Pt, Ag, Ni, Cu) will enhance reactivity. Bimetallic nanoscale particles (BNPs) increase the kinetics of the redox reactions involved in contaminant remediation, and as a result, act as a catalyst in the reaction. Equally important, bimetallic iron nanoparticles play an important role in overcoming the self-inhibition of metal removal reactions by preventing oxide formation on the nZVI surface (O'Carroll et al., 2013) as the second metal deposits on the surface of iron during the synthesis.

1.3 Scope of the project

Although varieties of iron bimetallic nanoparticles are being used for the purpose of environmental remediation, this project is limited to the use of iron/copper bimetallic nanoparticles (with or without stabilizer) for removal of arsenic from aqueous solution and its stabilization in an anthropogenic contaminated soil. The outcome of this study can lead to the introduction of a new adsorbent for removal of arsenic and possibly other heavy metals from water and soil.

1.4 Objectives

The overall goal of this study is to investigate the effectiveness of iron/copper nanoparticles in the removal of arsenic from water and stabilization of arsenic in contaminated soil. The efficiency of these nanoparticles in arsenic remediation will be investigated, as well as developing optimal conditions for application of this adsorbent on polluted media. Therefore, the main objectives of this research are as follows:

- To evaluate the efficiency of iron/copper nanoparticles as a new adsorbent for arsenic removal from water and soil.

- To determine the effect of different parameters (e.g., size and dosage of nanoparticles, and initial arsenic concentration) on removal efficiency.

- To evaluate the critical parameters (such as the presence of co-existing anions and pH) in order to enhance removal efficiency.

- To improve the overall understanding of metal removal mechanisms by Fe/Cu bimetallic nanoparticles.

- To investigate the effect of stabilization of nanoparticles on their mobility and colloidal stability.

- To evaluate soil mobility and breakthrough behaviors of Fe/Cu nanoparticles and the potential for in situ immobilization of arsenic contaminated soils.

- To determine the effect of nanoparticles on leachability of arsenic from different fractions of soil by performing selective sequential extraction.

1.5 Organization of Thesis

This thesis consists of six chapters which include the introduction, general literature review, materials and methods, results and discussions, conclusions, and bibliography.

Chapter 1 gives an introduction of the context and description of the problem and the objectives as well as the organization of the thesis.

Chapter 2 briefly reviews the chemistry of arsenic, natural and anthropogenic sources of arsenic in the environment, and the health effects of arsenic. As well, it surveys environmental levels of arsenic in Canada and established guidelines, arsenic treatment techniques in water (coagulation and flocculation, adsorption, ion exchange, membrane filtration), arsenic treatment technologies for soil and sediment (solidification and stabilization treatment, vitrification, soil washing/ acid extraction, pyrometallurgical recovery, in situ soil flushing), and emerging technologies for arsenic removal from both soil and water (biological treatments, new generation of adsorbents).

Chapter 3 describes the materials and methods used to synthesize and characterize the nanoparticles used as well as the methods used for adsorption experiments. For removal of arsenic from water, iron/copper nanoparticles were synthesized using two different methods resulting in two differing sizes to see the effect of size on adsorption. Both nanoparticles were characterized through TEM, XRD, XPS and BET surface area analyser tests. The nanoparticle with the higher adsorption capacity was selected for the remainder of the experiments to determine the reaction kinetics, effect of pH, effect of competing ions, etc. For the soil experiments, a complete physiochemical characterization of the soil was conducted. Nanoparticles were stabilized with different concentrations of a stabilizing compound (starch). After performing soil transport tests to determine the optimum concentration of starch, adsorption isotherm and kinetic tests, batch and column arsenic immobilization, and arsenic-soil leachability tests were performed.

Chapter 4 presents the result and complete description of the characteristics of the nanoparticles, interpretation the results of the water batch experiments followed by a description of the adsorption mechanism.

Chapter 5 presents the complete physiochemical characteristics of the soil and the stabilized nanoparticles, as well as the result of the soil batch and column tests, transportability, and leachability studies. The results are discussed following each section.

Chapter 6 presents a project summary and the overall conclusions from the complete research project, including the contributions to knowledge and suggestions for further research. A complete list of references cited in the thesis is presented at the end.

Chapter 2

Literature Review

2.1 Arsenic Chemistry

Arsenic is a metalloid of Group 5A elements with the electronic configuration [Ar] $3d^{10}$ $4s^2$ $4p^3$ and has only one stable isotope (^{75}As) (Mance et al., 1984). Exhibiting both metallic and nonmetallic properties, arsenic can occur in four oxidation states as arsine (-3), arsenic metal (0), arsenite (+3), and arsenate (+5). Arsenic bonds covalently with most nonmetals and metals and forms stable organic compounds in both its trivalent and pentavalent states. Arsenic is rarely found in its elemental form in nature and occurs most commonly as sulphides and as complexes with iron, nickel, copper, and cobalt (Ignatow et al., 1991).

The chemistry of arsenic in soil and aquatic environments is complicated. However, two forms are common in natural waters. At the high Eh (redox potential) values encountered in oxygenated waters, arsenic acid species (H_3AsO_4, $H_2AsO_4^-$, $HAsO_4^{2-}$, AsO_4^{3-}), referred to arsenic

(V) or pentavalent arsenic, are stable. Under mild reducing conditions arsenous acid species (H_3AsO_3, $H_2AsO_3^-$, $HAsO_3^{2-}$, AsO_3^{3-}) become stable (Figure 2-1) (Ferguson& Gavis, 1972). The equilibrium equations for both As(V) and As(III) in aqueous solutions are provided (with their respective acid dissociation constants) in Eqs. 1-6 (O'Neill, 1990).

Arsenic acid

$H_3AsO_4 + H_2O \leftrightarrow H_2AsO_4^- + H_3O^+$ pKa 2.20 (1)

$H_2AsO_4^- + H_2O \leftrightarrow HAsO_4^{2-} + H_3O^+$ pKa 6.97 (2)

$HAsO_4^{2-} + H_2O \leftrightarrow AsO_4^{3-} + H_3O^+$ pKa 11.53 (3)

Arsenous acid

$H_3AsO_3 + H_2O \leftrightarrow H_2AsO_3^- + H_3O^+$ pKa 9.22 (4)

$H_2AsO_3^- + H_2O \leftrightarrow AsO_3^{2-} + H_3O^+$ pKa 12.13 (5)

$HAsO_3^{2-} + H_2O \leftrightarrow AsO_3^{3-} + H_3O^+$ pKa 13.4 (6)

The speciation of arsenic [both As(III) and As(V)] as a function of pH is presented in Figure 2-2. As seen in Figure 2-2, in the neutral pH range (pH 6.0-8.0), the most thermodynamically stable compounds of As(V) are $H_2AsO_4^-$, $HAsO_4^{2-}$, and As(III), found mostly

as the uncharged species H_3AsO_3. In the alkaline pH range, AsO_4^{3-} and $H_2AsO_3^-$ are the dominant ionic forms.

Arsenic can be found in different forms of inorganic and organic compounds in soils. Similar to aqueous solutions under oxic soil conditions (Eh > 200 mV; pH 5-8), arsenic is mainly present in the +5 oxidation state. However, As(III) is the principal form under reducing conditions. Both As(V) and As(III) species can undergo chemical and/or microbial oxidation-reduction and methylation reactions in soils and sediments (Smith et al., 1998). A wide variety of arsenic compounds have been recognized in soil environments, and as mentioned earlier they can be categorized into two main groups: a) inorganic arsenic compounds, b) organic arsenic compounds (Smith et al., 1998; Matschullat, 2000).

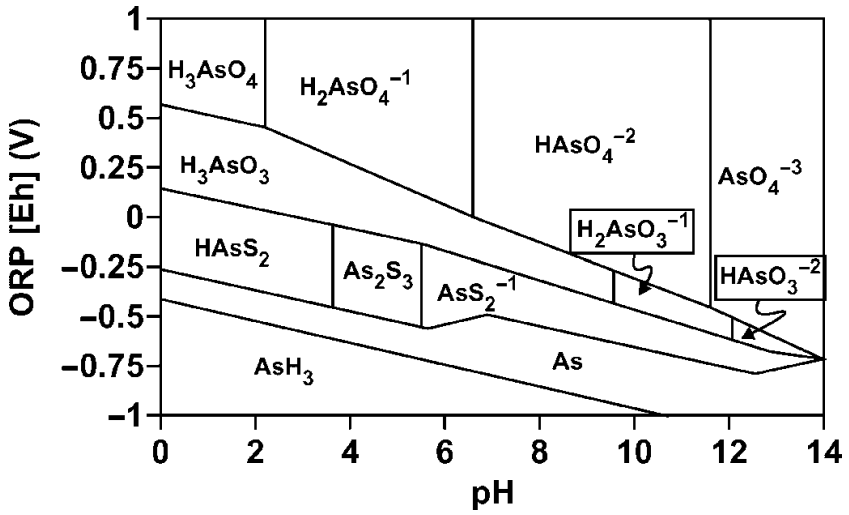

Figure 2-1: Eh-pH diagram for arsenic at 25ºC and 1 atmosphere with total arsenic 10^5 mol/L and total sulfur 10^{-3} mol/L (Ferguson & Gavis, 1972).

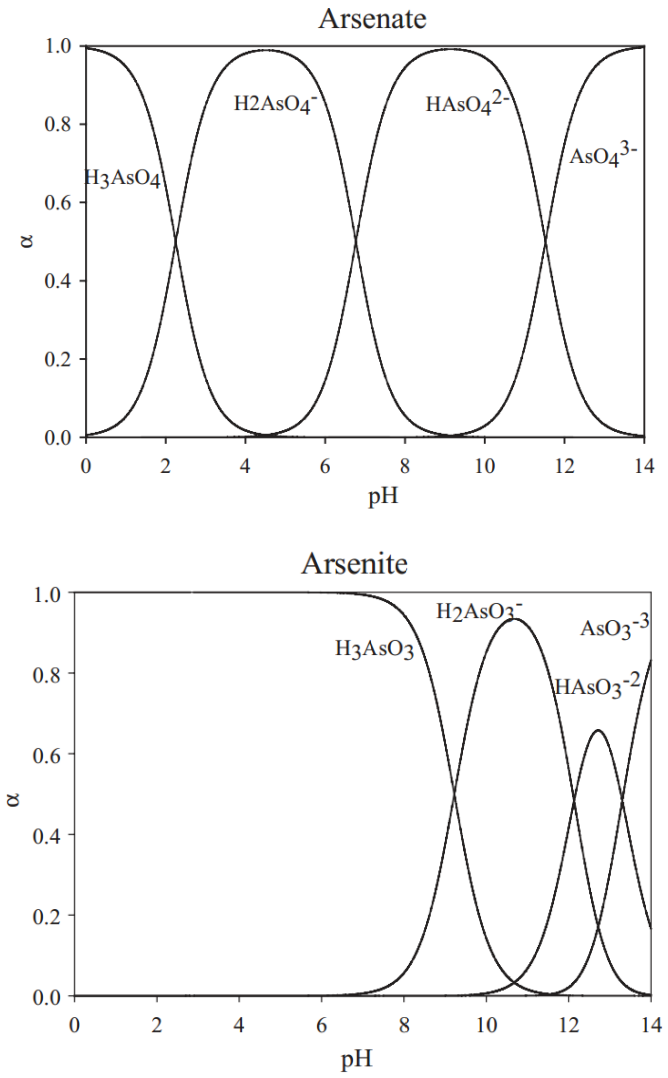

Figure 2-2: Distribution of arsenate and arsenite as a function of pH (Ghimirea et al., 2003)

2.1.1 Inorganic Arsenic Compounds

Arsenic occurs as different chemical species in different soil environments. These differences affect arsenic mobility and availability. Arsenate (As(V)) and arsenite (As(III)) compounds are the most significant inorganic arsenic species existing in soil environments and

the solubility of these compounds in water is high (Smith et al., 1998; Ravenscroft et al., 2009). Generally, geochemical systems are described in terms of their reaction due to redox potential (Eh) and pH. The most thermodynamically stable inorganic arsenic species in normal soil in the pH range of 4 to 8 are H_3AsO_3 (As(III)), $H_2AsO_4^-$, and $HAsO_4^{2-}$ (As(V)).

2.1.2 Organic Arsenic Compounds

Organic arsenic compounds are found in both trivalent and pentavalent states in soils. Microbial methylation of the arsenic oxyanions may occur in soil environments and will produce methylarsenic compounds such as monomethylarsonics, di- and trimethylarsines (O'Neill, 1990), and may produce arsine gas (Smith et al., 1998). Various microorganisms have the ability to methylate inorganic arsenic compounds present in the soil. The methylation pathway for bacteria and fungi is different. For example, biomethylation of arsenic by bacteria produces only di-methylarsine in the absence of oxygen (Smith et al., 1998). The methylarsonic acid and dimethylarsinic acid equilibria in aqueous solution are seen in Eqs.7-9 (O'Neill, 1990).

Monomethylarsenic acid

$$(CH_3)AsO(OH)_2 + H_2O \leftrightarrow (CH_3)AsO_2(OH)^- + H_3O^+ \qquad \text{pKa 4.19 (7)}$$

$$(CH_3)AsO_2(OH)^- + H_2O \leftrightarrow (CH_3)AsO_3^{2-} + H_3O^+ \qquad \text{pKa, 8.77 (8)}$$

Dimethylarsenic acid

$$(CH_3)_2AsO(OH) + H_2O \leftrightarrow (CH_3)_2AsO_2^- + H_3O^+ \qquad \text{pKa 6.27 (9)}$$

2.2 Arsenic Origin and Sources in the Environment

Arsenic is released to the environment from a variety of natural and anthropogenic sources.

2.2.1 Natural Sources of Arsenic

In the environment, arsenic occurs naturally in rocks, soil, water, air, and in biota. A variety of common minerals contain arsenic. In the earth's crust, average concentrations are reported to range from 1.5 to 5 mg/kg (Cullen and Reimer, 1989). In some igneous and sedimentary rocks, higher concentrations of arsenic can be found, particularly in iron and manganese ores (Welch et al., 1988).

Other important natural sources of arsenic include volcanoes and forest fires. Volcanic activity is the original source of much of the arsenic in sedimentary rocks. Recently this process has reached an equilibrium state, where the weathering of arsenic is approximately in balance with deposition of arsenic in sediments.

As reported by National Research Council (NRC) (1999), natural concentrations of arsenic in soil typically range from 0.1 to 40 mg/kg, with an average concentration of 5 to 6 mg/kg of soil.

Arsenic can be released from the soil to ground or surface water through erosion, weathering, and dissolution. Geothermal waters can also be sources of arsenic in ground water, particularly in the western United States (Nimick et al., 1998; Welch et al., 1988).

Arsenic occurs as a major constituent of more than 200 minerals. Among them, arsenopyrite (FeAsS) is the most abundant arsenic ore mineral. Table 2-1 provides a list of the most common arsenic minerals. Most of them are ore minerals or their alteration products. However, most of these minerals are relatively rare in the natural environment. The greatest concentrations of these minerals occur in mineralized areas and are found in close association

with the transition metals, as well as Cd, Pb, Ag, Au, Sb, P, W, and Mo. It is generally accepted that arsenopyrite, together with the other dominant As-sulphide minerals such as realgar and orpiment, are only formed under high temperature conditions in the earth's crust.

Table 2-1: Major arsenic minerals occurring in nature (Smedley & Kinniburgh, 2002)

Mineral	**Composition**	**Occurrence**
Native arsenic	As	Hydrothermal veins
Niccolite	NiAs	Vein deposits and norites
Realgar	AsS	Vein deposits, often associated with orpiment, clays and limestones, also deposits from hot springs
Orpiment	As_2S_3	Hydrothermal veins, hot springs, volcanic sublimation product
Cobaltite	CoAsS	High-temperature deposits, metamorphic rocks
Arsenopyrite	FeAsS	Most abundant As mineral, dominant in mineral veins
Tennantite	$(Cu,Fe)_{12}As_4S_{13}$	Hydrothermal veins
Enargite	Cu_3AsS_4	Hydrothermal veins
Arsenolite	As_2O_3	Secondary mineral formed by oxidation of arsenopyrite, native arsenic and other As minerals
Claudetite	As_2O_3	Secondary mineral formed by oxidation of realgar, arsenopyrite and other As minerals
Scorodite	$FeAsO_4.2H_2O$	Secondary mineral
Annabergite	$(Ni,Co)_3(AsO_4)_2.8H_2O$	Secondary mineral
Hoernesite	$Mg_3(AsO_4)_2.8H_2O$	Secondary mineral, smelter wastes
Haematolite	$(Mn,Mg)_4Al(AsO_4)(OH)_8$	
Conichalcite	$CaCu(AsO_4)(OH)$	Secondary mineral
Pharmacosiderite	$Fe_3(AsO_4)_2(OH)_3.5H_2O$	Oxidation product of arsenopyrite and other As minerals

2.2.2 Anthropogenic Sources of Arsenic

Anthropogenic sources of arsenic include its use in the lumber (wood preservatives), agriculture (pesticides, insecticides, etc.), livestock (food additives, disease preventatives, etc.), and general industries (glassware, catalysts, alloys, ceramics, etc.) (Azcue & Nriagu, 1994). Arsenic is also released from industrial processes, including the burning of fuels and wastes, mining and smelting, pulp and paper production, glass manufacturing, and cement manufacturing. Coal-fired power plants and incinerators are other sources that may release small amounts of arsenic into the atmosphere as coal and waste products often contain some level of arsenic (US EPA, 1998b).

Historically, use of arsenic-containing pesticides has left large tracts of agricultural land contaminated with arsenic. Most agricultural uses of arsenic have been banned in the United States (USEPA, 1999b). In the 1990s, around 90% of arsenic used in the United States was for the production of the wood preservative, chromated copper arsenate (CCA) (Reese, 1998 & Reese, 1999). CCA is used to pressure treat lumber and is classified as a restricted use pesticide by the USEPA (1999b). The use of arsenic in the preservation of timber has also led to contamination of the environment (EPA, 2000).

Another significant industrial use of arsenic is the production of lead-acid batteries, while small amounts of pure arsenic metal are used to produce the semi conductive crystalline gallium arsenide, which is used in computers and other electronic applications. In addition, abandoned waste disposal sites may be contaminated with arsenic. Mining, smelting of non-ferrous metals, and burning of fossil fuels are major industrial processes that contribute to anthropogenic arsenic contamination of air, water, and soil.

2.3 Health Effects of Arsenic

Arsenic and associated compounds are known to be toxic and carcinogenic. Many people all around the world are exposed to arsenic through different routes. The primary routes that arsenic enters into the body are through ingestion and inhalation, with dermal exposure serving as a secondary route (Maharjan et al., 2005).

Generally, contaminated ground water is the main source of exposure to inorganic arsenic to the human population. Bangladesh, India, China, Taiwan, Thailand, Chile and Romania are the most affected countries where inorganic arsenic is present in the ground water with high concentrations (Maharjan et al., 2005).

Chronic ingestion of arsenic can cause adverse health effects in multiple body systems. Regarding inorganic arsenic, the major metabolic pathway in humans body and in most animal species is biotransformation. Chemical speciation of inorganic arsenic has important effects on health (Sing et al., 2007). As (III) binds strongly to sulfhydryl groups of amino acids such as cysteine in proteins inactivating a wide range of enzymes in intermediate metabolism then it is more toxic than As (V) (Tamaki and Frankenberger,1992).

High doses of arsenic in drinking water causes characteristic symptoms including skin manifestation, vascular diseases, cardiovascular disease, cerebrovascular disease, renal disease, chronic lung disease, neurological effects, reproductive effects, and many types of cancer including skin, lungs, liver, kidney, and bladder cancer. Arsenic is also associated with growth retardation in children. Arsenic contaminated drinking water is also responsible for effects on pregnancy including spontaneous abortion, stillbirth, and infant mortality (Aschengrau et al., 1989; Hopenhayn-Rich et al., 2000).

2.4 Environmental Levels of Arsenic in Canada and Guidelines

Table 2-2 presents the concentration of arsenic and its corresponding guideline values in different media in Canada.

Table 2-2: Environmental Levels of Arsenic in Canada and Guideline levels

Media	Average concentrations of arsenic	Guideline levels of arsenic
Air	0.001µg/m^3 (Environment Canada, 1990)	0.03 µg/m^3 (Wang & Mulligan, 2006)
Soil	4.8 to 13.6 mg/kg (CED, 2003)	12 mg/kg (Environment Canada, 1996).
Sediment	6 and 100 mg/kg (Ollson, 1999)	12 mg/kg (Environment Canada, 1996)
Water	0.001 to 0.002 mg/L (BCMWLAP, 2002)	0.01 mg/L (Health Canada, 2012)

2.5 Arsenic Treatment and Remediation Methods

2.5.1 Arsenic Treatment Techniques in Water

There are several techniques for reducing arsenic concentration in water, but most of them are primarily effective in removing arsenic in its pentavalent form. Therefore, in most cases, removal of arsenic from water includes an oxidation step as a pretreatment process to convert arsenite to arsenate. The most common oxidizing agents for these purposes are: oxygen, ozone, free chlorine, hypochlorite, permanganate and hydrogen peroxide (EPA, 2002; Vaclavikova et al., 2008).

The conventional physical and chemical processes for arsenic removal from contaminated waters can be classified into four groups (EPA, 2002; Shih, 2005; Choong et al., 2007).

1- Coagulation and flocculation
2- Adsorption
3- Ion Exchange
4- Membrane Filtration

Here is a brief description of each process.

2.5.1.1 Coagulation and Flocculation

Coagulation and flocculation are the most traditional methods in arsenic removal processes. It is effective in removing arsenic from groundwater, surface water, leachate, mine drainage, drinking water, and wastewater (EPA, 2002). The first step in this process is the addition of a chemical precipitant or coagulant. The most common coagulants for arsenic removal are ferric salts, (e.g. ferric chloride, ferric sulfate, ferric hydroxide) and alum (aluminum hydroxide). After dissolving these chemicals in water while stirring, flocs will be formed rapidly and will agglomerate to larger settleable flocs. During this flocculation process, the negatively charged ions will be adsorbed to the flocs through electrostatic interactions. In this process arsenic is also adsorbed onto coagulated flocs. Oxidation of arsenite to its less soluble state (e.g. As(V)) can increase the effectiveness of the precipitation/coprecipitation processes, and can be done as a separate pretreatment step or as part of the precipitation process. After mixing treatment chemicals into the water and the formation of a solid matrix through precipitation and coprecipitation, separation of the solid matrix from the water should be performed. In this phase, clarification or filtration are commonly used to remove the solid precipitates (EPA, 2002; Choong et al., 2007).

2.5.1.2 Adsorption

Adsorption is a widely used process for treating ground and drinking water containing arsenic (EPA, 2002). In this process solids are used to remove contaminants from liquid

solutions. Removal of contaminants is accompanied by its accumulation or concentration at the surface of solids, and thereby their concentration will be reduced in the bulk liquid phase. Adsorption is mostly caused by van der Waals and electrostatic forces between adsorbate molecules and the atoms which compose the adsorbent surface (Choong et al., 2007). The adsorption media is usually placed into a column, then, as the contaminated water passes through the column, contaminants become adsorbed at the surface of media adsorbents. When adsorption sites become filled, the column must be regenerated or disposed of and then replaced with new media. The most commonly used adsorbents for arsenic removal are: activated alumina (AA), activated carbon (AC), copper-zinc granules, granular ferric hydroxide, ferric hydroxide coated newspaper pulp, iron oxide coated sand, iron filings mixed with sand, greensand ($KMnO_4$ coated glauconite), and surfactant-modified zeolite (EPA, 2002; Choong et al., 2007; Vaclavikova et al., 2008).

2.5.1.3 Ion Exchange

Ion exchange is a physical-chemical process that is usually used for removal of specific undesirable cations or anions from water. In this process, ions in a solution are exchanged for ions of similar charge that held electrostatically on the surface of a solid (EPA, 2002). It removes ions from the aqueous phase by the exchange of cations or anions between the contaminants and the exchange medium. Ion exchange is normally used to remove arsenic from groundwater, drinking water and surface water. Four types of ion exchange media have been used (EPA, 2000): strong acids, weak acids, strong bases, and weak bases.

Strong and weak acid resin exchange cations while strong and weak base resin exchange anions. Because dissolved arsenic is usually in an anionic form, and weak base resins tend to be effective only over a limited pH range, strong base resins are typically used for arsenic treatment (USEPA, 2000). For this purpose, an ion exchange resin, usually loaded with chloride ions at the exchange sites, is placed in the vessels. Arsenic containing water is passed through the vessels

and the arsenic is “exchanged” for chloride ions. As the resin becomes exhausted, it needs to be regenerated (Choong et al., 2007).

2.5.1.4 Membrane Filtration

Pressure-driven membrane filtration can remove a wide range of dissolved contaminants and suspended solids from water. For arsenic removal, membranes are commonly used to treat groundwater and drinking water (EPA, 2002). Membrane filtration separates contaminants from water by passing the contaminated water through a semipermeable barrier or membrane. The membrane allows some contaminants to pass through, while preventing the others. There are four types of membrane processes: microfiltration (MF), ultrafiltration (UF), nanofiltration (NF), and reverse osmosis (RO).All four of these processes are pressure-driven and classified into two categories: high pressure membrane (RO & NF) and low pressure membrane (MF&UF). They are also categorized by the size of the particles that can pass through the membranes or by the pore size of the membrane (EPA, 2002; Shih, 2005).

MF and UF membranes cannot remove dissolved arsenic from water due to the large pore size of the membranes. Due to the relatively low molecular weights of arsenic species dissolved in water, only NF and RO membrane processes are considered effective in the treatment of dissolved arsenic from the contaminated water (USEPA, 2000; Shih, 2005). In Table 2-3, a comparison of the advantages and disadvantages of different arsenic removal technologies is presented.

Table 2-3: Comparison of main arsenic removal technologies (Mohana et al., 2007)

Major process	Advantages	Disadvantages
Coagulation and flocculation	Chemicals are available commercially, relatively low capital cost and simplicity in operation	Produces toxic sludge; low removal of arsenic; pre-oxidation may be required
Adsorption	Adsorbents are relatively well known and commercially available, relatively inexpensive	Needs replacement, produces toxic solid waste
Ion Exchange	Well-defined medium and capacity; pH independent; exclusive ion specific resin to remove arsenic	High cost medium; high-tech operation and maintenance
Membrane Filtration	Well-defined and high-removal efficiency, No toxic solid waste is produced, Capable of removing of other contaminants	High-capital and running cost, pre-conditioning; high water rejection, toxic retentate is produced

2.5.2 Arsenic Treatment Technologies for Soil and Sediment

Arsenic treatment technologies that are applicable to soil and sediment are:

1) Solidification and stabilization, 2) Vitrification, 3) Soil washing/acid extraction,

4) Pyrometallurgical recovery and 5) In situ soil flushing (EPA, 2002).

2.5.2.1 Solidification and Stabilization Treatment

Solidification and stabilization is a kind of immobilization technology, which is the most common treatment option for metal-contaminated sites (Choi et al., 2009; Evanko and Dzombak, 1997). S/S is a widely used treatment technology to suppress migration of contaminants from a contaminated media. This media can be soil, sludge, sediment, or a waste site in general (EPA, 2009). For stabilization processes a soil or sediment is mixed with a binding agent such as portland cement, lime, fly ash, cement kiln dust, or polymers. This creates a slurry, paste, or other semi-liquid state and cure into a solid form over time (Mulligan et al., 2001; EPA, 2002). Pozzolanic binders such as cement and fly ash are used most frequently for the S/S of arsenic (EPA, 2002). In this process through physical and chemical means the mobility of hazardous substances and contaminants are reduced because they entrapped within a stabilized mass. Then contaminants are converted into less soluble, less mobile, or less toxic forms.

In the solidification and stabilization process for changing the stability state of arsenic and making it less soluble, some materials like pH adjustment agents, ferric sulfate, persulfates, and other proprietary reagents would be added. It is also possible to convert As(III) to As(V) with a pretreatment phase, making it less toxic and soluble. Pretreatment with incineration in order to convert arsenic into ferric arsenate has also been studied, but limited data is available on this process (EPA, 2002).

2.5.2.2 Vitrification

Vitrification (in-situ or ex-situ) is another S/S treatment process. In the vitrification process, high temperatures are used to reduce the mobility of metals by incorporating them into a chemically durable, leach resistant, and vitreous mass of glass (Choi et al., 2009, Evanko and Dzombak, 1997). In this process of melting the soil or other earthen materials present in the

environment, direct-fired kiln or other heat sources at extremely high temperatures (1,600 - 2,000°C or 2,900 - 3,650°F) are commonly used. In the vitrification process, inorganics will be immobilized and/or organic pollutants will be destroyed by pyrolysis. Inorganic pollutants such as arsenic will be incorporated within the vitrified glass (EPA, 2009). Through this process it is possible for some contaminants to volatilize or undergo thermal destruction, and as a result their concentration will be reduced in the contaminated media. During the treatment process, the metals become surrounded by a glass matrix and are chemically bonded inside the matrix. For example, arsenates can be converted into silicoarsenates during vitrification (EPA, 2002).

2.5.2.3 Soil Washing/ Acid Extraction

Soil washing can extract heavy metals or metalloids adsorbed onto soil particles through physico-chemical processes. By using this technique, the amount of contaminated soil that needs further treatment would be reduced (Jang et al., 2005). This process relies on the fact that most contaminants tend to bind to finer soil particles (clay, silt) rather than larger particles (sand, gravel). Therefore, physical methods must be employed to separate the relatively clean larger particles from the finer particles.

After this, soil is mixed with the wash solution. Wash solutions can be water or water enhanced with chemical additives such as leaching agents, surfactants, acids, or chelating agents to help remove organics and heavy metals.. Obviously the coarser-grained soil is relatively clean and there is no need for further treatment. Methods used for treating the wastewater, including ion exchange and solvent extraction, will then be employed for the treatment of wash water to use it again in the cycle (EPA, 2002).

2.5.2.4 Pyrometallurgical Recovery

A variety of pyrometallurgical technologies have been employed to recover arsenic from soils and waste containing arsenic. In high temperature metal recovery (HTMR), a heat source is used in an attempt to make a waste feed containing heavy metals, such as arsenic, to volatilize.

The airborne metals are then removed and recovered from the off-gas and the residual solid materials are disposed. Arsenic may need pretreatment with reducing or fluxing agents to assist melting and provide a uniform feed (Mulligan et al., 2001). Other pyrometallurgical technologies typically involve modifications at metal refining facilities to recover arsenic from process residuals. In fact in the pyrometallurgical recovery processes an arsenic contaminated waste feed will be transformed into a product with a high arsenic concentration through the use of heat. This product then can be reused or sold (EPA, 2002).

2.5.2.5 In Situ Soil flushing

In situ soil flushing process uses water or a mixture of water and some additives as flushing solution. Additives like acids (sulfuric, hydrochloric, nitric, phosphoric, or carbonic acid), bases (sodium hydroxide), chelating or complexing agents (such as EDTA), reducing agents, or surfactant aide in the desorption and dissolution of heavy metals like arsenic (EPA, 2002). Soil pH, soil type, cation exchange capacity (CEC), particle size, permeability, and type of contaminant will affect the whole process. In this technology it is possible to use subsurface containment barriers or other hydraulic controls to help control the flow of flushing solution fluids. Also, impermeable membranes have been used in some cases to prevent infiltration of groundwater, which may cause dilution of flushing solutions and loss of hydraulic control.

With in situ soil flushing techniques there is no need to excavate soil because the wash solution dissolves contaminants while passing through the contaminated zone. In this process, the solution is injected into or sprayed onto the contaminated area, allowing the contaminants to become mobilized through dissolution or emulsification. After passing through the contamination zone, by using down gradient wells or trenches, the contaminant-bearing flushing solution will be collected and pumped to the surface for further treatment or removal (EPA, 2002; Mulligan et al., 2001).

2.5.3 Emerging Technologies for Arsenic Removal from Soil and Water

Recently new processes have been tried for removal of arsenic from different media including water, soil and sediment. These emerging technologies are divided in two categories. Here is a brief description of each one.

2.5.3.1 Biological Treatments - Bioremediation and Phytoremediation

Biological treatment has gained increased attention due to the benefits offered in comparison with conventional physico-chemical treatment methods (Zouboulis & Katsoyiannis, 2005). For arsenic, bioremediation of contaminated soils and groundwater holds great advantages because of its general environmental compatibility and cost-effective nature (Wang & Zhao, 2009).

In the bioremediation process, microorganisms are used to reduce, eliminate, contain, or transform contaminants in soils, sediments, and water into harmless products. One major advantage is that metals are non-biodegradable, but by using this process they can be transformed to less toxic substances through sorption, methylation, and complexation (Adeniji, 2004).

Other than microorganisms, certain plant species that can accumulate high concentrations of heavy metals also have the potential to remove contaminants from the environment (Shah & Nongkynrih, 2007). In this process (known as phytoremediation), plants uptake heavy metals and other contaminants present in soil and in groundwater via their roots and translocate them to the above-ground shoots where they accumulate (Jadia & Fulekar, 2009). The rate of bioremediation by plants is directly proportional to plant growth rate and the total amount is dependent on total plant biomass (Shah & Nongkynrih, 2007).

For arsenic removal, bioremediation relies on microbial or plant activity to reduce, mobilize, or immobilize arsenic through sorption, biomethylation, complexation, and oxidation–

reduction processes (Wang & Zhao, 2009). Microbially mediated redox reactions involving organic carbon, Fe, Mn, and S are the basic underlying mechanisms affecting arsenic mobility. Microorganisms have evolved biochemical mechanisms to exploit arsenic oxyanions, either as an electron acceptor (e.g. As(V)) in anaerobic respiration, or as an electron donor (e.g. As(III)) supporting chemoautotrophic fixation of carbon dioxide (CO_2) into cell carbon (Silver & Phung, 2005; Rhine et al., 2006).

2.5.3.2 New Generation of Adsorbents–(Nanoparticles)

With increased concerns over human health issues associated with drinking of arsenic contaminated water, regulations regarding arsenic acceptable levels in water has been tightened during recent years. In 2006, the US EPA reduced the maximum contaminant level of arsenic in water from 50 µg/L to 10 µg/L which requires water suppliers to implement more efficient advanced technologies to meet the new standard.

As it was discussed earlier, there are several technologies for removal of arsenic from water, and adsorption is among the most cited ones (Chen et al., 1999). Traditionally, some adsorbents like activated alumina (AA), activated carbon (AC), copper-zinc granules, and granular ferric hydroxide have been used to remove arsenic from contaminated water (EPA, 2002; Choong et al., 2007; Vaclavikova et al., 2008). Although those adsorbents have been successful in arsenic removal, recently nanoparticles due to their unique features have emerged as an effective new class of adsorbents introduced for this purpose.

Different types of nanoparticles have been employed in polluted environments for removal of a variety of contaminants including arsenic. The extremely small size of nanomaterials, typically in the range of 1 to 100 nanometres, generates a large surface-to-volume ratio, providing them with enhanced surface reactivity (Khin et al., 2012). As particle size decreases, the proportion of surface and near surface atoms increases. Surface atoms tend to have more unsatisfied bonds with higher surface energy. Thus, the surface atoms have a stronger tendency to interact, adsorb, and react with other atoms or molecules in order to achieve surface stabilization (Li et al., 2006). Silver, iron, gold, and titanium oxides and iron oxides are the most

frequently cited nanoscale metals and metal oxides used in environmental remediation (Khin et al., 2012).

Among these nanoparticles, nanoscale zero-valent iron (nZVI) is the most widely used nanoparticle that has been investigated as a new class of material for the remediation of contaminated water and soil (Liang et al., 2014). Although it has been more than 10 years since nZVI began to be used in many countries worldwide, use of zero valent iron (ZVI) as a remediation tool dates back to early the 1990s (Li et al., 2006). In fact, first ZVI in granular form was employed in permeable reactive barrier (PRBs) systems (Gavaskar et al., 1998). In a PRB structure, a migrating plume of contaminated groundwater flows through an engineered wall (packed with iron powder) where the contaminants are removed through redox reactions, precipitation, adsorption, or transformation processes in contact with the ZVI surface (Gu et al., 1999, Scherer et al., 2000). Over the last 20 years, a significant number of polluted sites have been successfully treated with zero-valent iron PRBs. The efficiency of these systems has been proven in remediation of acid mine drainage, dissolved nutrients, numerous heavy metals, radio nuclides and other inorganics such as phosphorous, arsenic, and selenium at shallow depths. However, important challenges such as the large amounts (e.g. tonnes) of iron powder required and the costs associated with the construction and even relocating the barrier or modification after installation still exist (Blowes et al., 2000; Li et al., 2006).

The use of nZVI for environmental remediation can be considered as an extension of the ZVI PRB technology (Zhang, 2003; Li et al., 2006). Because of its higher specific surface area and greater surface energy, nZVI offers superior reactivity and is able to degrade contaminants more rapidly than the bulk granular iron used in PRBs. Also, because of a lower amount of material needed for remediation, in comparison with reactive barriers, the use of nZVI particles is more cost effective (Karn et al, 2009). Moreover, due to their smaller sizes, nZVI particles can be easily transported to the target contaminated site.

Over the past few years, many studies have demonstrated the effectiveness of nZVI particles for remediation of a wide range of contaminants including chlorinated organics (Cheng et al., 2007), chlorinated solvents (Choe et al., 2001), chlorinated pesticides (Elliott et al., 2009), inorganic anions (Mondal et al., 2004), metals, and metalloids such as lead (Li and Zhang 2007),

chromium (López-Téllez et al., 2011), copper (Üzüm et al., 2009), arsenic (Raj Kanel et al., 2005; Lien and Wilkin, 2005), cobalt (Uzum et al., 2008), nickel (Li and Zhang 2007), cadmium (Boparai et al., 2011), zinc (Li and Zhang 2007) and uranium (Klimkova et al., 2011).

Despite the benefits offered through the use of nZVI particles, there are still some challenges with the technology, such as rapid oxidation of iron nanoparticles, aggregation due to magnetic forces, and decreased efficiency because of the aging process.

To solve these problems, over the past 10 years, there has been an increasing interest in developing iron bimetallic nanoparticles. It has been hypothesized that through combination of iron with a more noble metal (e.g. Pd, Pt, Ag, Ni, Cu), reactivity will improve (Altavilla & Ciliberto, 2011).

Iron is oxidized more rapidly when it is attached to a less active (noble) metal. Therefore, the transformation and reduction of contaminants can be enhanced by combining iron to a noble metal. The iron-noble metal will create numerous galvanic cells, wherein the noble metal (cathode) is protected as the iron (anode) sacrificially corrodes. Studies also suggest that noble metals can promote transformation of contaminants through catalytic functions such as hydrogenation (Elliott & Zhang, 2001) as hydrogen gas, a reductant species may subsequently undergo desirable remedial interactions with contaminants (Altavilla & Ciliberto, 2011).

Another reason for developing iron bimetallic nanoparticles is overcoming the formation of mixed metal hydroxides layer on the oxidized nZVI surface, which may inhibit further electron transfer from the Fe^0 core at later reaction times. By preventing oxide formation on the nZVI surface (metal catalyst deposits on the surface of iron), bimetallic iron nanoparticles overcome the self-inhibition of metal removal reactions of nZVI (O'Carroll et al., 2013).

Among metal catalysts, copper is known as a mild hydrogenation catalyst (Satterfield, 1991). Due to its lower cost, as compared to other noble metals, copper is a good choice for incorporation with iron to make iron/copper bimetallic nanoparticles. Some studies have shown the efficiency of the iron/copper nanoparticle in the remediation of other contaminants. Liou et al. (2005) evaluated the effects of three metals including Pd, Pt, and Cu deposited onto nano-Fe^0

surface to test their reactivity to NO_3^--N reduction. The results indicate that the reactivity of three bimetallic nanoparticles can be ranked as Cu>Pd>Pt. Hosseini et al. (2011) showed a successful reduction of nitrate by nano-Fe/Cu particles in packed column. Cao et al. (2011) achieved near 90% reduction efficiency of 1, 2, 4-trichlorobenzene by Carboxymethyl cellulose CMC-stabilized Fe/Cu bimetal nanoparticles in a 24 h treatment. Although in these studies iron/copper nanoparticles have been synthesized by different methods resulting in different characteristics, they all show good efficiency for decontamination of the polluted media.

Therefore, in the first phase of this study, iron/copper nanoparticles were prepared using two different methods resulting in two different sizes which were then used to remove arsenic from water.

In the second phase of this research, Fe/Cu nanoparticles were stabilized to immobilize arsenic in a chromated copper arsenate soil. The use of nanoparticles in the subsurface environment is limited by rapid particle aggregation and media pore clogging which both are systemic problems for environmental application of nanoparticles. The very limited movement of iron based nanoparticles in the subsurface environment can be attributed to one or more of the following reasons (Altavilla & Ciliberto, 2011):

1) Particle aggregation and subsequent gelation caused by colloidal instability, followed by pore clogging.
2) Particle oxidation causing formation of voluminous surface precipitates and rust which can lead to further sedimentation and pore clogging.
3) Particle removal from suspension via interaction with soil or sediment components.

The most important of these three mechanisms is particle aggregation which attributes to the imbalance of attractive and repulsive forces. Traditionally, attractive and repulsive forces that govern the stability of colloidal material have been described through the DLVO theory. Following the DLVO theory, the sum of van der Waals (VDW) attractive forces (influenced by particle size, chemistry, and aqueous concentration) and electrical double-layer (EDL) forces (influenced by particle surface potential and ionic strength of the solution) will determine the final interaction of two approaching particles. However, non-DLVO forces, such as steric,

magnetic, and hydration forces can also play an important role in the aggregation and deposition of engineered nanomaterials (Petosa et al., 2010).

In order to lower the effect of interacting forces, nanoparticles are either supported onto larger particles (e.g. activated carbon supported or embedded in a silica matrix) (Hoch et al., 2008; Zhan et al., 2008) or the surface becomes modified directly (Kim et al., 2012). Surface modification, which has been more frequently used to suppress the attractive forces among nanoparticles, can be accomplished by using surfactants or polymeric surface coatings.

By using surfactants, nanoparticles become stabilized via steric hindrance as the surfactant molecules counteract the electrical and dipolar attractions between particles. Surfactants attach themselves to the particle surfaces while forming hemimicelles. When the concentration of surfactant is low, hydrophobic groups are in contact to the aqueous phase while under higher concentrations, the hydrophilic head is subjected to the aqueous media and prevents flocculation via steric repulsion. This provide much longer suspension stability via Brownian motion in aqueous media. As has been defined in previous studies a high ratio of surfactant to iron leads to colloidal stability through the formation of a hydrophilic hemi-micelle. Surfactant stabilization of nanoparticles for subsurface uses is not favorable because of some limitations: in particle suspensions of high concentartion, typical of injection slurries, surfactants may cause aggregation and in sub surface environments, surfactants can easily be washed in water and stop acting as a stabilizer (Altavilla & Ciliberto, 2011). Using high molecular weight polymers for stabilization of nanoparticles is more favorable, as their adsorption on nanoparticle surfaces is an irreversible process (Saleh et al., 2007).

Polyelectrolytes, including polyaspartate (PAP) and polystyrene sulfonate (PSS) (Phenart et al., 2008), polyacrylic acid (Schrick et al., 2004), polymethacrylic acid, butyl methacrylate (Sirk et al., 2009), carboxymethyl cellulose (CMC), and potato starch (Liang et al., 2012) have been shown as effective surface modifiers. They provide electrosteric stabilization against aggregation and reduce deposition of nanoparticles onto aquifer materials through electrosteric repulsion with negatively charged soil minerals (Sirk et al., 2009). In this study, starch as a green polysaccharide was used to stabilize the nanoparticles.

Chapter 3

Materials and Methods

This chapter includes the methods used for the preparation of iron/copper nanoparticles with two different protocols and investigation of their efficacy in removal of arsenic from solution. As well this chapter details the preparation of starch stabilized nanoparticles for immobilization of arsenic in a chromated copper arsenate (CCA) contaminated soil. To characterize the nanoparticles XRD, TEM, and BET surface area analyses were performed. For water experiments, batch arsenic adsorption and kinetic tests with both As(III) and As(V) were performed, as well as experiments to elucidate the effect of nanoparticle dose, effect of competing ions, the effect of pH, and the possibility of desorption of arsenic from nanoparticles. To have an understanding of the adsorption mechanism, XPS spectra were obtained before and after adsorption and examined carefully.

To determine the effect of starch-stabilized nanoparticles for immobilization of arsenic in soil, following the water experiments, the complete characterization of starch-stabilized nanoparticles and contaminated soil were performed in detail as well as soil batch and column tests, transport and TCLP studies.

3.1 Chemicals

Ferrous sulfate ($FeSO_4.7H_2O$) and ferric chloride ($FeCl_3.6H_2O$) were purchased from Sigma-Aldrich (St Louis, MO, USA). Cupric sulfate ($CuSO_4.5H_2O$) and copper(II) chloride ($CuCl_2.2H_2O$) were obtained from Fisher (Nazareth, PA, USA). Hydrochloric acid (HCl) and acetone (C_3H_6O) were purchased from Fisher Scientific (Lane Fair Lawn, New Jersey, USA). Sodium borohydride ($NaBH_4$, 98%) was obtained from Acros (Lane Fair Lawn, New Jersey, USA). Sodium hydroxide (NaOH) was obtained from Fisher Scientific (Pittsburgh, PA, USA). Water soluble potato starch (hydrolyzed for electrophoresis), was obtained from Acros Organics (Pittsburgh, PA, USA). Deionized (DI) water generated by a Milli-Q water purification system from Millipore, (Bedford, MA, USA) was used as the solvent for preparing all solutions.

3.2 Preparation of Fe/Cu nanoparticles (method 1)

Synthesis of Fe/Cu bimetallic nanoparticles was carried out by reduction of $FeSO_4 \cdot 7H_2O$ and $CuSO_4 \cdot 5H_2O$ aqueous mixture using sodium borohydride. The reaction for this synthesis can be described as follows (Morales-Luckie et al. 2008):

$$4Fe^{+2} + 4Cu^{+2} + 3BH^{-}_4 + 12H_2O \rightarrow 4Fe^0Cu^0 + 3B(OH)^{-}_4 + 24H^+$$

First, a 5 mM aqueous solution of $FeSO_4.7H_2O$ and a 5mM $CuSO_4.5H_2O$ aqueous solution were prepared using de-ionized water. Then 500 mL of each metal salt solution were mixed under nitrogen and vigorous stirring for 20 min. After that, pH was adjusted to 7.0 with 1 N and 0.1 N NaOH solutions; subsequently, 100 ml of a 10 mM aqueous solution of $NaBH_4$ were added drop wise to the metal salt solution over a 20 min period. A fine black precipitate of hybrid nanoparticles was obtained. The precipitates were then washed three times with de-ionized water, and finally the water was removed with acetone.

3.3 Preparation of Fe/Cu nanoparticles (method 2)

In this alternate method, iron nanoparticles were prepared first and then iron-copper nanoparticles were made by adding $CuCl_2$ solution. The reaction for the synthesis of nano zero valent iron (NZVI) can be described as follows (Zin et al., 2013):

$$4Fe^{3+} + 3BH_4^- + 9H_2O \rightarrow 4Fe^o + 3H_2BO_3^- + 12H^+ + 6H_2$$

In order to synthesize nanoscale zero valent iron (nZVI), 1 L of 0.018 M ferric chloride solution was prepared by dissolving $FeCl_3$ salt in 1 L of 9:1 (v/v) ethanol/water mixture (900 ml ethanol + 100 ml deionized water) and stirring with a mechanic stirrer. At the same time, 2.8 g $NaBH_4$ was dissolved in 100 mL of deionized water to produce a sodium borohydride solution which was added dropwise to the iron chloride solution at a rate of 7 to 7.5 mL per minute with vigorous stirring under nitrogen. After adding the whole borohydride solution leading to the formation of the black precipitate (by adding the first drop of $NaBH_4$, formation of NZVI begins), 100 ml of 0.0018 M $CuCl_2$ solution, prepared by mixing $CuCl_2.2H_2O$ salt with ethanol-water (9:1) solution, was poured into the reactor. The mixture was left for another 10 minutes of stirring. Finally, the solid particles were washed three times with ethanol.

3.4 Preparation of Starch Stabilized Fe/Cu Nanoparticles

The starch stabilized Fe/Cu nanoparticles were prepared by a modified version of the method proposed by Morales-Luckie et al. (2008). The key modification was the use of starch as a low-cost and environmentally benign polysaccharide stabilizer during particle formation.

The stabilized nanoparticles were prepared in 250 mL or 1000 ml flasks in the presence of the starch. First, a 1 wt % starch stock solution was prepared and heated under magnetic stirring (heating was required to dissolve starch in deionized (DI) water) then cooled to room

temperature. Meanwhile, aqueous solutions of iron and copper were prepared by dissolving $FeSO_4.7H_2O$ and $CuSO_4.5H_2O$ salts in DI water respectively. For preparation of 0.1 g/L Fe/Cu nanoparticles (0.5 mg/L iron and 0.5 mg/L copper), 0.9 mM aqueous solutions of $FeSO_4.7H_2O$ and $CuSO_4.5H_2O$ were prepared separately, in DI water, and mixed with a fraction of the stock stabilizer solution to yield mixtures of desirable concentrations of stabilizer ranging from 0 to 0.06 wt %. The mixtures were purged under nitrogen and vigorous stirring for 20 min. The pH of the resulting solutions were adjusted to 7.0 by using 1 M and 0.1 M NaOH solutions; subsequently, 10 mL of a 0.675 mM aqueous solution of $NaBH_4$ was injected to the solution under stirring. The suspensions were created freshly for each set of experiments.

3.5 Physico-chemical characterization of nanoparticles

In order to characterize the synthesized particles, X-ray Diffraction (XRD), X-ray photoelectron spectroscopy (XPS), transmission electron microscopy (TEM), and Brunauer–Emmett–Teller (BET) surface area analyses were performed.

XRD reveals information about the chemical composition and crystallographic structure of the bimetallic Fe/Cu nanoparticles. XRD patterns of the nanoparticles were obtained using a MiniFlex X-ray diffractometer (Philips X'Pert Pro Multipurpose, Netherlands) equipped with Cu K-alpha radiation. Air dried samples were ground and were diffracted over a 2θ range from 10° to 90°.

X-ray photoelectron spectroscopy (XPS), also known as ESCA (electron spectroscopy for chemical analysis) provides both elemental and chemical state information virtually without restriction on the type of material analyzed. In this experiment (XPS, SK-Alpha, USA) was used and measurements were done with monochromatized Al-KαX-ray source hv= 1350 eV on dried samples.

TEM is an imaging analysis technique which shows the morphology of synthesized nanoparticles. The size of the synthesized bimetallic Fe/Cu nanoparticles can be measured by

using high resolution TEM. The TEM images also reveal if the synthesized nanoparticles occur as single particles or tend to agglomerate in nanoclusters. The localized essential information of iron/copper nanoparticles was viewed with transmission electron microscopy (TEM) (Tecnai G2 F20 S/TEM, USA) photographs.

Specific surface area of nanoparticles can be determined with the BET method. Systematic sorption and desorption of nitrogen in the NOVA 1000e analyzer will produce a BET isotherm and consequently provide fundamental information on the surface characteristics and the total surface area. BET (Micromeritics Tri Star 3000, USA) was used to perform the analysis in this experiment.

The zeta (ζ) potential of the stabilized Fe/Cu nanoparticles (0.04% w/w starch) was measured using a Zeta Potential/Particle Size Analyzer (BrookHaven Instrument Corp., ZetaPlus / Bl-PALS, Holtsville, NY) at a 173° scattering angle with two replicates.

3.6 Efficiency of bare Fe/Cu nanoparticles for removal of arsenic from water

Batch experiments were conducted to determine arsenic sorption of the Fe/Cu nanoparticles. These experiments were carried out in 50 mL centrifuge tubes at ambient room temperature (20 ± 2◦C). 100 and 10 mg/L concentrations of trivalent and pentavalent arsenic solutions were prepared by dissolving an accurately weighed quantity of arsenic salts (As_2O & Na_2HAsO_4) in 1 L of DI water. Solutions of the desired concentrations were obtained by successive dilution of stock solutions.

First, in order to investigate the effect of contact time, a preliminary experiment was carried out over 48 hours with initial concentrations of 100, 500, 1000 µg/L of As (III) and As(V) and 50 mg/L of nanoparticles. For uniform dispersion of NPs, the suspensions were probe sonicated for 15 minutes with a probe sonicator (Branson model 102 C(CE), USA). Then the sorption tests were initiated by adding the appropriate amounts of As(III) and As(V) stock solutions to the nanoparticle suspensions in order to generate arsenic concentrations of 100, 500 and 1000 µg/L. After rigorous mixing, the tubes were continuously shaken by a platform shaker, operated at 200 rpm. The solution pH was adjusted at 7.0 ± 0.1 using 1M and 0.1 M NaOH or

HCl. At predetermined time intervals, samples were taken and centrifuged for 10 minutes (12000 rpm) to separate nanoparticles, leaving only dissolved arsenic in the solutions. To become sure that nanoparticles have been removed completely, the aliquots were filtered through a 25 nm membrane of mixed cellulose esters (MilliporeCorp., Billerica, MA, USA) and then analyzed for arsenic remaining in the aqueous phase using ICP-MS (Agilent Technologies, 7700 Series, USA). For the first 6 hours, samples were taken every hour, and after that, sampling was performed at 12-hour intervals. As the results revealed that reactions occur within the first hour, therefore, samples in consequent experiments were taken within one hour unless otherwise mentioned. Control experiments were conducted at the same time and same conditions without the presence of nanoparticles.

To elucidate the effect of adsorbent dose, different doses of nanoparticles were tested on arsenic adsorption. Fe/Cu nanoparticle suspensions were prepared by adding 10, 50 and 100 mg of Fe/Cu NPs in 1 L of DI water of three different initial concentrations of arsenic (100, 500 and 1000 µg/L). After one-hour, samples were taken and analyzed for remaining arsenic.

In order to study the adsorption isotherms, 100 mg/L of nanoparticles suspensions were prepared with different concentrations of arsenic (from 100 to 5000 µg/L) at pH 7 (adjusted by 1M and 0.1 M NaOH and HCl). The solutions were shaken on a platform shaker (200 rpm) at ambient room temperature of 20 ± 2◦C. The amount of arsenic adsorbed (mg/g) on the surface of the NPs was determined by calculating the difference in arsenic concentration before and after exposure. After one hour, samples were analyzed by ICP-MS. It should be noted that for the rest of experiments, only the nanoparticle with the higher rate of adsorption was used.

The adsorption kinetics of As(III) and As(V) at pH 7.0 were also studied. Fixed initial concentrations of arsenic at 0.5, 1, 2 and 4 mg/L were used. The dosage of adsorbent used was 100 mg/L, and the total reaction time was 1h. The solutions were sampled at 1, 4, 7, 10, 15, 20, 30, 45 and 60 minutes.

The effect of competing ions on As(III) and As(V) adsorption on nanoparticles were studied using batch adsorption experiments with three different competing ions. Batch tests were performed with competitive anions using solutions of 0.5 mg/L of As(III) and As(V) in 0.5 mg/L solutions of PO_4^{3-} (prepared by dissolving NaH_2PO_4 in DI water), SO_4^{2-} (prepared by dissolving Na_2SO_4 salt in DI water), and CO_3^{2-} (prepared by dissolving $NaHCO_3$ in water) separately. The

suspensions were centrifuged, filtered through a 25 nm membrane filter (Millipore), and analyzed for arsenic as described above. This experiment continued for 24 hours.

To study the desorption capability of As from Fe/Cu nanoparticles, As(III) and As(V) (0.5 mg/L) were reacted with Fe/Cu nanoparticles (0.1 g/L) in DI water. Then, the arsenic-treated nanoparticles were separated and gently washed with water to remove any extraneous aqueous As. The arsenic-treated Fe/Cu nanoparticles were agitated for 24 h with 0.10 and 0.01 M NaOH, similar to previous studies (Reddy et al., 2013; Pillewan et al., 2011), then the aliquots of supernatant solution were analyzed for the amount of arsenic released. This experiment was also continued for 24 hours.

Finally, in order to investigate the effect of pH on adsorption, a series of batch tests were conducted with 0.5 mg/L solutions of As(III) and As(V). The pH of solutions was initially adjusted (from 4 to 11) by using 0.1 M and 1 M NaOH or 0.1M and 1M HCl. After one hour of shaking at 200 rpm, samples were centrifuged and filtered for analysis. Duplicate experiments were carried out for all operating variables studied and the mean values are presented.

3.7 Adsorption mechanism

X-ray photoelectron spectroscopy (XPS), also known as ESCA (electron spectroscopy for chemical analysis), provides both elemental and chemical state information virtually, without restriction on the type of material analyzed. In this experiment in order to have an understanding about the adsorption mechanism of arsenic on nanoparticles, XPS (SK-Alpha, USA) was used and measurements were performed with monochromatized Al-KαX-ray source hv= 1350 eV.

3.8 Soil Characterization

A chromated copper arsenate (CCA) polluted soil was extracted from a contaminated site in Quebec and brought to the lab. In order to characterize the soil, some physical and chemical characteristics were determined.

Among physical characteristics of soils, information about their texture and size distribution is the most useful. Analysis of the particle size distribution of soil samples was conducted by use of the laser scattering particle size distribution analyzer (Horiba LA-950, Japan). The D10, D30, D50, D60 and D90 of each sample (which, respectively, represents the diameter of grain sizes at which 10, 30, 50, 60 and 90 percent of the soil sample is finer than) were determined. Moreover, the percentage of clay, silt, and sand was calculated as it is important to know the percentage composition of fine soil with a tendency to adsorb the pollutants.

Beside the physical characteristics, some chemical features of soil samples were measured as well. One important factor is pH, which was determined according to ASTM method D4972–01. For this purpose, 10 g of air dried soil was placed into a glass container and approximately 10 mL of the 0.01 M $CaCl_2$ solution or distilled water was added. Samples were mixed thoroughly and let stand for 1h, then the pH was read by a pH meter.

Estimation of organic content in the soil sample is vital for analyzing the role of organic material in adsorption process. Therefore, loss on ignition (LOI) was chosen to estimate organic content in the soil. According to the ASTM D2974 method, oven dried soil samples (105^{o} C) were placed in a furnace at 440^{o} C overnight. After this, the samples were cooled in a desiccator, and their weights (w) were measured, loss on ignition (%) in each sample was calculated. This measurement is an approximation of sample organic content.

Selective sequential extraction tests were performed to evaluate the fractionation of As among soil fractions and the impact of nanoparticle treatment on that. A SSE procedure, based on Wang & Mulligan (2009), was applied. For each procedure, 1.0 g samples of dried soil were used. Between each successive extraction, separation was conducted by centrifugation at 3000

rpm for 15 min. The supernatant was collected and the residue was washed with distilled water. Each of the fractions was collected and the concentrations of arsenic were determined. The amount of arsenic extracted from the soil by each of the extractants were then calculated. The sequential extraction procedure that was used is as follows:

F1. Water soluble: 8 ml of distilled water or washing solution were added, shaken at room temperature for 30 min.

F2. Exchangeable: 8 ml of 1 M $MgCl_2$ were added, pH 7, 1h of shaking at room temperature.

F3. Carbonate associated: 8 ml of 1 M NaOAc were added, pH was adjusted to 5 with acetic acid, 5h of shaking at room temperature.

F4. Oxide and hydroxide associated: 8 ml of 0.04 M $NH_2OH{\cdot}HCl$ in 25% (v/v) acetic acid were, pH 2.5, at 96 ◦C in a water bath for 6 h.

F5. Organic matter and sulphide associated: 3 ml of 0.02 M HNO_3 and 5 ml of 30% H_2O_2 (pH 2) were added at 85 ◦C for 2 h, followed by 3 ml of 30% H_2O_2 (pH 2) at 85 ◦C for 3 h, and then 5 ml of 3.2 M NH_4OAc in 20% (v/v) HNO_3 were added and diluted to 20 ml at room temperature for 30 min.

F6. Residual fraction: digestion at 90 ◦C with 25 ml of dilute aqua regia (50 ml HCl + 200 ml HNO_3 + 750 ml water) for 3 h.

3.9 Determination of total arsenic in contaminated soil

To determine the total concentration of arsenic in soil, samples were digested according to the EPA method 3050B. Using this method, arsenic was extracted sequentially by adding nitric acid, hydrogen peroxide and hydrochloric acid then the total concentration was measured using ICP-MS (Agilent Technologies, 7700 Series, USA).

3.10 Effects of Starch Concentration on Stability of Fe/Cu Nanoparticles

To test the effect of the stabilizers, Fe/Cu nanoparticles were prepared at a fixed concentration of 0.1 g/L, but with 0, 0.02, 0.04 and 0.06 % (wt/wt) starch. Particle stability was then determined by comparing the visual transparency and particle concentrations in the supernatants.

The particle concentration was determined through dissolution of the nanoparticles with concentrated nitric acid and measuring the total dissolved iron concentration by atomic absorption (Perkin Elmer pin AAcle 700F).

3.11 Efficiency of starch stabilized Fe/Cu nanoparticles for removal of arsenic from groundwater

The efficiency of stabilized (with 0.04 wt % starch) Fe/Cu nanoparticles for removal of arsenic (As (III) and As (V)) from ground water was determined in batch experiments. First, nanoparticle suspensions of 0.1 g/L of stabilized Fe/Cu were prepared. In 50 mL centrifuge tubes, As (III) and As (V) from stock solutions were added to the suspensions to create initial arsenic concentrations of 0.5, 1, 2, 3, 4, 5, 10, 15 and 20 mg/L. The pH of the suspensions was adjusted to 7± 0.1 using 1 M and 0.1 M hydrochloric acid or sodium hydroxide, then the centrifuge tubes were placed on a platform shaker at 200 rpm for 48 hours. After this time had passed, samples were centrifuged at 12000 rpm for 10 minutes and supernatant were then filtered through a 25 nm membrane of mixed cellulose esters (MilliporeCorp., Billerica, MA, USA) to separate the nanoparticles from the suspension and measure the concentration of remaining arsenic in water. The aliquots were then analyzed for arsenic remaining in the aqueous phase by use of ICP-MS (Agilent Technologies, 7700 Series, USA).

To examine the effect of time on adsorption (kinetic studies), the initial As (III) and As (V) concentrations were set at 4.0 and 10 mg/L as As and the concentration of Fe/Cu nanoparticles was fixed at 0.1 g/L. The pH of the suspensions was initially adjusted to 7± 0.1 using 1 M and 0.1 M hydrochloric acid or sodium hydroxide. The suspensions were placed in 50

ml centrifuge tubes and were continuously shaken with a platform shaker operated at 200 rpm and samples were taken and tested for remaining arsenic at hours 1, 2, 4, 8, 24 and 48. It should be noted that control experiments were conducted at the same time and same conditions without the presence of nanoparticles.

3.12 Arsenic immobilization in soil: batch tests

To study the effect of nanoparticles on arsenic immobilization in the soil matrix, batch tests of arsenic leaching from soil were carried out in the presence and absence of starch-stabilized nanoparticles.

The tests were conducted in a batch of Corning plastic centrifuge tubes (50 mL). Typically, 1.5 or 6 g of air dried arsenic polluted soil (sieved through a standard sieve of 2mm opening) was added to the centrifuge tubes, each containing 15 ml of the nanoparticle suspension (with 0.04 wt % starch) at a concentration of 0.1 g/L or 0.4 g/L. This resulted in soil to liquid ratios (SLR) of 0.1 and 0.4. The tubes were then capped and equilibrated on a platform shaker at 100 rpm at room temperature (20 ± 2◦C) for 24 h (preliminary experiments showed this time is enough to reach the equilibrium). The solution pH was initially adjusted to 7 ± 0.1. Samples were prepared for total arsenic analysis by centrifuging the mixtures at 12000 rpm for 20 minutes and passing the supernatant through a 25 nm Millipore membrane filter. This analysis provided the total leachable As in the system after nanoparticle tretment. To compare the effect of the stabilized Fe/Cu nanoparticles on the leachability of soil sorbed arsenic, arsenic desorption tests were also carried out in the absence of the nanoparticles by mixing the contaminated soil with DI water and a simulated groundwater (SGW) with a chemical composition of 7 mM NaCl + 0.86 mM $CaSO_4$ prepared following the method by Liang and Zhao (2014). All tests were conducted in duplicate.

3.13 Soil sorption and transport of starch-stabilized Fe/Cu nanoparticles

To test the transportability of starch stabilized nanoparticles, column breakthrough tests were carried out. The experimental setup included a Cole Palmer peristaltic pump (Masterflex L/S, PA, USA), a Plexiglas column (ID = 10 mm, length = 100 mm), and a fraction collector (Spectrum Labs, CA, USA). Approximately 12 g of air-dried contaminated soil samples were packed in the column (a metal mesh was placed at the bottom of the column to retain the soil, but allowed water to pass) resulting in a soil porosity of 0.38 (measured by dividing the pore volume by the total volume (Wu, 1976)), a bulk bed volume of 7.85 ml, and hydraulic conductivity of 9.5×10^{-3}cm/s. Hydraulic conductivity was determined by measuring flow rate, surface area, hydraulic gradient, and the time which was needed for water to reach from one section to another according to constant head method ASTM D7100-06.

Then, the Fe/Cu nanoparticle suspensions at a concentration of 0.1 g/L, stabilized with various concentrations of starch (adjusted pH of 7 ± 0.1) were pumped through the column in the down-flow mode at an EBCT (Empty Bed Contact Time) of 17.5 min and at a pore water velocity of 4.17×10^{-3} cm/s. The effluent was collected by the fraction collector, and the samples were then acidified by concentrated (5 M) nitric acid to dissolve the nanoparticles. The concentration of the nanoparticles was then determined by measuring the total iron and copper content. For comparison, the breakthrough behavior of a control tracer solution (50 mg/L Br^-) was tested in parallel (Liang and Zhao, 2014; An and Zhao, 2012).

3.14 Immobilization of arsenic in soil: column tests

To evaluate the effectiveness of the nanoparticles for potential in situ immobilization of arsenic, the same column setup was used under the same hydrodynamic conditions. Then, the effluent arsenic concentration was determined in two ways. First, the samples, which included both dissolved and nanoparticle-associated arsenic, were digested with 5M HNO_3 and analyzed for total arsenic; second, the effluent samples were first centrifuged for 10 minutes at 12000 rpm

and filtered through the 25 nm membrane to remove the nanoparticles and arsenic- sorbed on them, and then filtrates were analyzed for arsenic, which provided the soluble arsenic. For comparison, arsenic elution history was also determined by introducing the contaminated soil bed to DI water as well as a simulated groundwater (SGW) with a chemical composition of 7 mM NaCl+0.86 mM $CaSO_4$ which was prepared following the method of Liang & Zhao (2014) under the same hydrodynamic conditions.

3.15 Leachability of arsenic in soil

The toxicity characteristic leaching procedure (TCLP) specified in EPA Method 1311 was employed to determine the leachability of arsenic from untreated and treated nanoparticle amended soil. Soil samples after the batch or column tests were first air-dried at room temperature and then mixed with the #1 TCLP fluid (pH 4.93) at a solid-to-solution ratio of 1:20 (i.e. 2 g dried soil and 40 mL of #1 TCLP fluid). The mixtures were rotated for 18 h at 30 rpm and then centrifuged at 6500 rpm for 20 min. The supernatants were then analyzed for leached arsenic.

Chapter 4

Experimental results of arsenic adsorption from water by Fe/Cu nanoparticles and discussion

4.1 Characterization of Fe/Cu nanoparticles by XRD, TEM and BET (method 1)

4.1.1 X-ray Diffraction

Figure 4-1 shows the XRD peaks of synthesized bimetallic Fe/Cu nanoparticles. According to XRD analyses of the synthesized bimetallic Fe/Cu nanoparticles, the peaks are composed of phases of ferric oxide (Fe_3O_4) and copper oxide (CuO) with a higher percentage of copper oxide. Peaks at 30.2 [220], 35.6 [311], 43.3 [400], 57.3 [511], and 62.9 [440] º 2θ correspond to iron oxide (Fe_3O_4), which conforms to that reported by Peng & Sun (2007). This layer of ferric oxide around the metallic core is due to oxidation of iron and will be discussed later. In addition, the peaks at 36.4 [111], 39.1 [111], 49 [220] º 2θ can be associated with copper oxide (CuO). This is in agreement with the work of Zhu et al. (2007) and Xu et al. (1999). It should be noted that these CuO peaks corresponds to the thin layer of CuO which

forms on the metallic surface of copper in presence of air (Keil et al., 2006). This thin layer will not interfere with copper electrochemical conductivity.

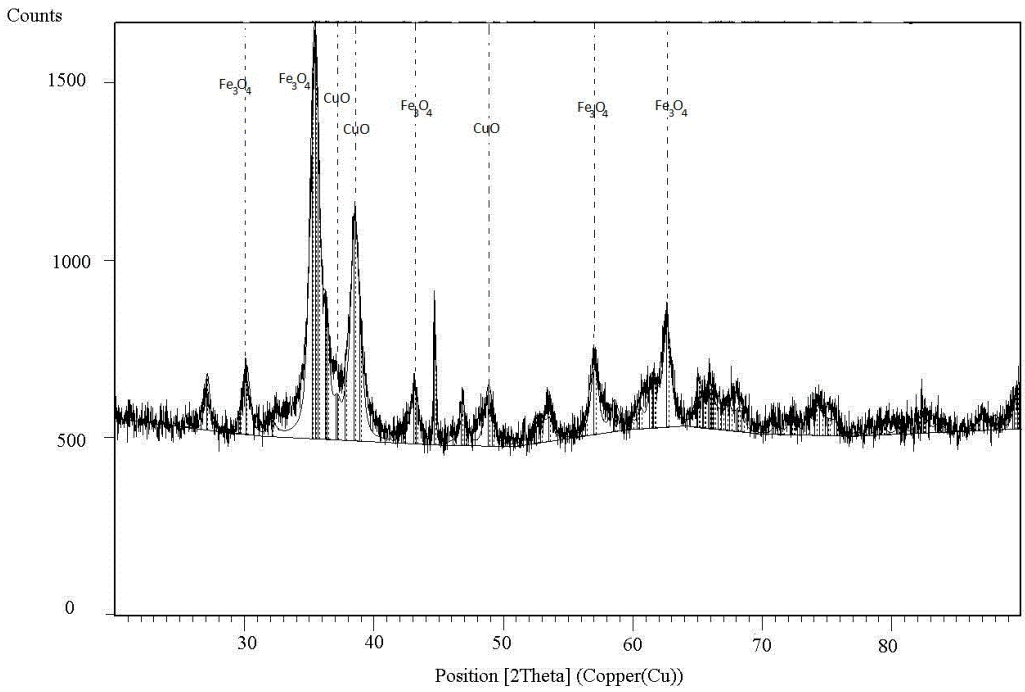

Figure 4-1: XRD pattern of Fe/Cu nanoparticles (method 1)

4.1.2 Transmission Electron Microscopy

The representative TEM images of the synthesized sample shown in Figure 4-2 indicate that Fe/Cu nanoparticles were obtained. An overview image (Fig 4-2 (a)), at low magnification, illustrates that the sample consists of nano-sized individual particles with a relatively narrow size distribution. The particles are mostly spherical and almost uniform in size and shape. Measuring the size of approximately 100 particles in different high resolution TEM images revealed that the particle diameter ranges from 4 to 22 nm with a mean size of 13.17 nm. However using the Scherrer's equation the mean size of the nanoparticles was calculated as 10.38 nm.

$$\tau = \frac{K\gamma}{\beta \cos\theta} \quad (4\text{-}1)$$

(τ: mean size of the ordered (crystalline) domains.

K: dimensionless shape factor, with a value close to unity.

γ: X-ray wavelength.

β: line broadening at half the maximum intensity (FWHM).

θ: Bragg angle.

The image of an isolated nanocrystal at higher magnification (Fig 4-2 (b)) shows a distinct core–shell structure, which indicates the presence of zero valent iron at the core. Other authors mentioned similar results indicating the importance of this core–shell structure as the zero valent iron at the core provides the electron for reductive transformation of contaminants while the oxide layer at the shell (containing copper in this case) acts as an appropriate surface for sorption of contaminants via surface complexation or electrostatic interactions (Yan et al., 2010; O'Carroll et al., 2013). Figure 4-3 shows the size distribution information of the Fe/Cu nanoparticles, obtained by measuring each nanoparticle on the same TEM photograph. It can be seen in Figure 4-3 that the 15 nm grouping is the largest group, and the 10 nm group is the second highest. The percentage of the nanoparticles with diameters of 15 and 10 nm are 50.1% and 20%, respectively. This means about 70.1% nanoparticles have a diameter between 7.5 and 17.5 nm. The elemental distribution of the sample for Fe/Cu nanoparticles is illustrated in Fig. 4-4.

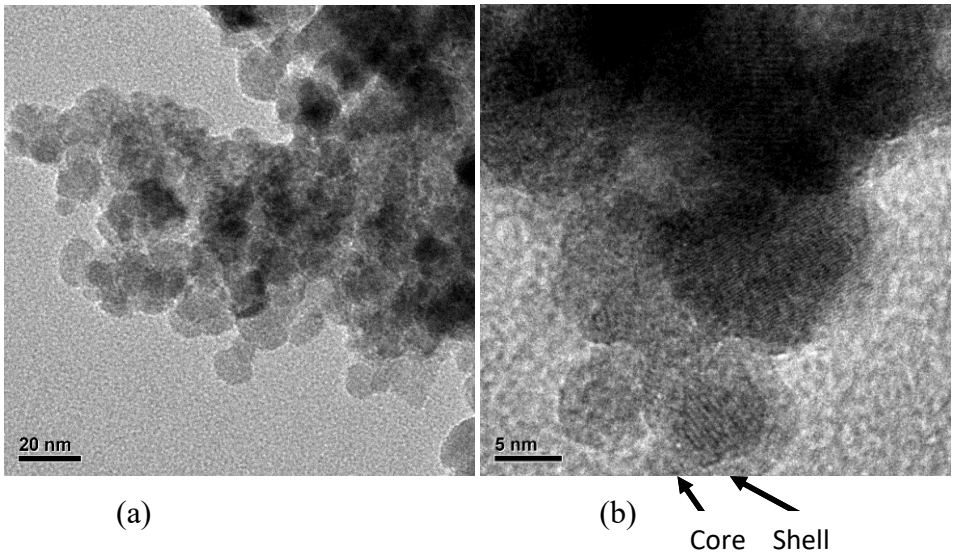

Figure 4-2: TEM images of Fe/Cu nanoparticles (method 1)

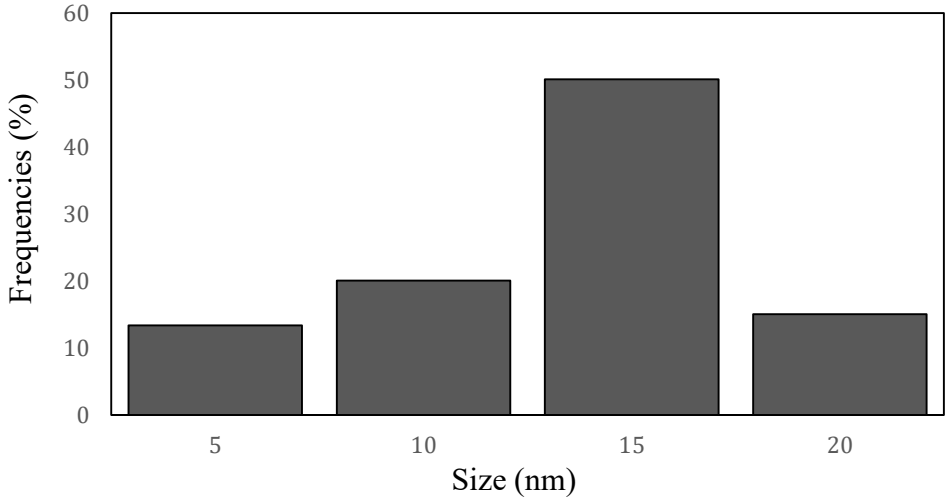

Figure 4-3: Particle size distribution of the synthesized nanoparticles (method 1)

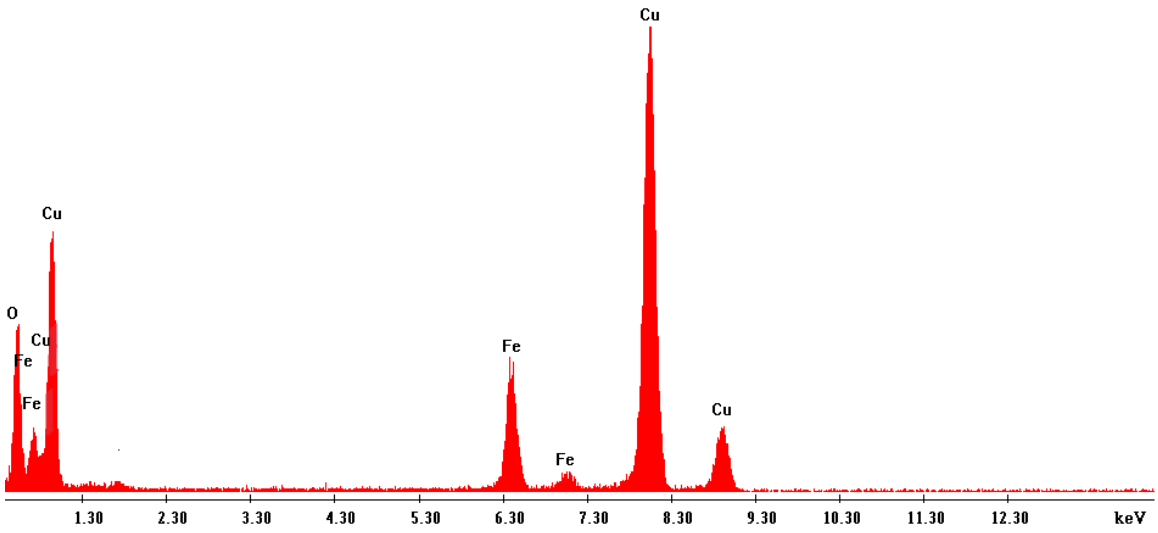

Figure 4-4: Elemental distribution for the sample of iron/copper nanoparticles (method 1).

4.1.3 Surface Areas (BET)

The BET surface area for the Fe/Cu nanoparticles was 79.5 m^2/g. This value is more than three times higher than that of Fe nanoparticles (25 m^2/g) (Yuvakkumar et al., 2011; Kanel et al., 2005). To put it into perspective, the BET surface area of the Fe/Cu NPs is more than 40 times higher than that of granular iron (less than 2 m^2/g) which is currently the most commonly used absorption medium in permeable reactive barriers (Su and Puls, 1999; Suk et al., 2009).

This increase in specific surface area means an increase in the total amount of surface iron. Since reactivity of NPs is directly correlated with the overall particle surface area, the rate of reaction will increase. Increasing the specific surface area also results in an increase in the fraction of iron atoms that are on the particle surface, which provides greater reductive capacity per gram of NPs. Overall, the higher specific surface area of Fe/Cu NPs will lead to using smaller amounts of iron to treat contaminated media.

4.2 Characterization of Fe/Cu nanoparticles by XRD, TEM and BET (method 2)

4.2.1 X-ray Diffraction

The XRD peaks of synthesized bimetallic Fe/Cu nanoparticles are shown in Figure 4-5. According to the XRD analyses of synthesized bimetallic nanoparticles, the peaks are composed of phases of ferric oxide (Fe_3O_4) and copper oxide (Cu_2O) with a higher percentage of copper oxide. Similar to the result of the first method, peaks at 30.2 [220], 35.6 [311], 43.3 [400], 57.3 [511], and 62.9 [440]º 2θ are associated with iron oxide (Fe_3O_4), which agree with that reported by Peng & Sun (2007). The peaks at 36.4 [111] and 42.3 [200]º 2θ correspond to copper oxide (Cu_2O); this is in agreement whit the work of Kuo et al. (2007).

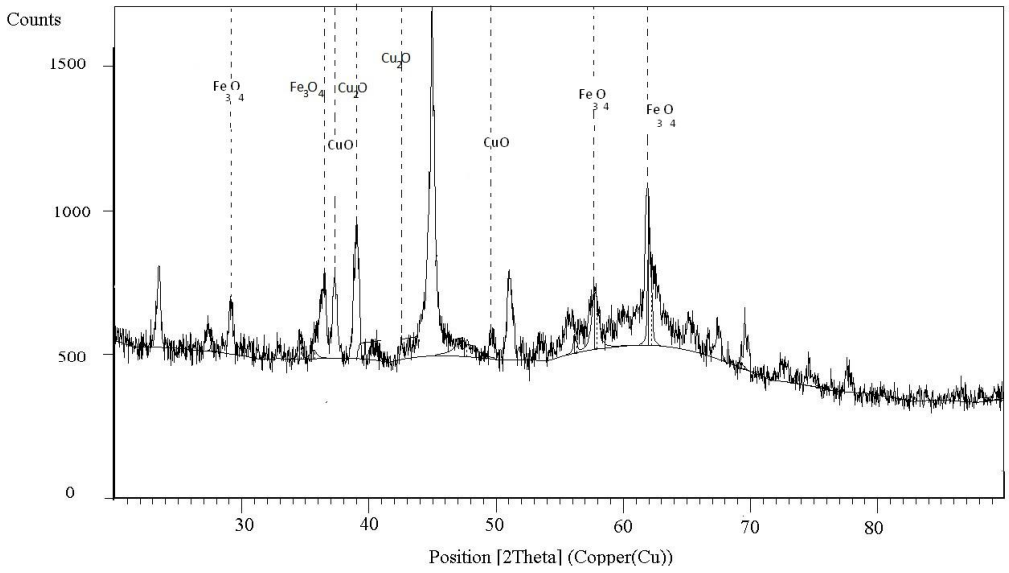

Figure 4-5: XRD pattern of Fe/Cu nanoparticles (method 2)

4.2.2 Transmission Electron Microscopy

Figure 4-6 shows the TEM images of the synthesized Fe/Cu nanoparticles. According to these images, nanoparticles (1 to 100 nm in size) were obtained. An overview image (Fig 4-6 (a)) at low magnification illustrates that the sample consists of nano-sized individual particles with a relatively wide size distribution which include smaller particles as well as larger particles. The particles are not uniform in size, but they are mostly spherical and uniform in shape. Typically, particle diameter ranges from 12 to 50 nm with an average of 27.15 nm although the mean diameter calculated based on Scherer's equation is 20.65. Similar to the result obtained from the characterization of first nanoparticle, the image of an isolated nanocrystal at higher magnification (Fig 4-6 (b)) shows a clear core–shell structure. Figure 4-7 shows statistical information about Fe–Cu nanoparticle size, which was obtained by measuring every nanoparticle on the same TEM photograph. It can be seen from Figure 4-7 that the 30 nm size is the largest group, 20 nm is the second largest, and 25nm is the third largest. The percentage of the nanoparticles with diameters of 30, 20, and 25 nm are 27.3%, 25.0% and 18.2%. This means that about 70.45% of the nanoparticles have a diameter between 17.5 and 32.5 nm. The elemental distribution for the sample of Fe/Cu nanoparticles is illustrated in Fig. 4-8.

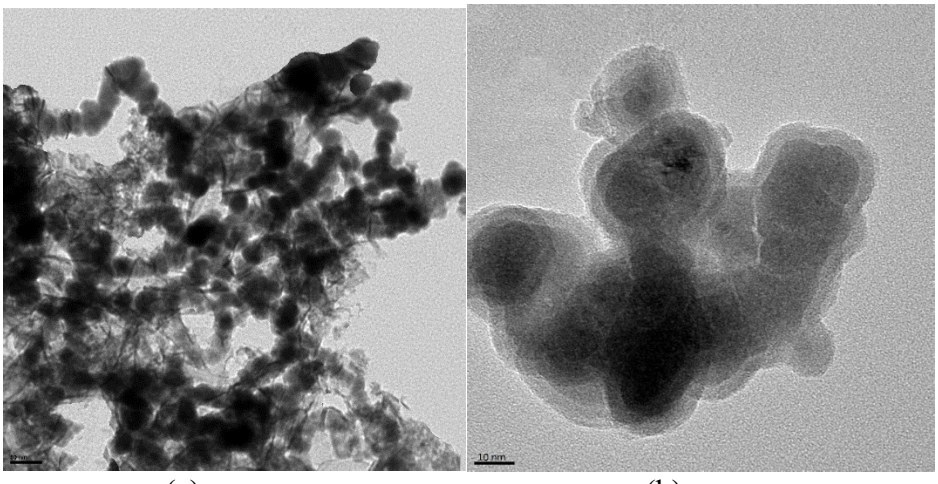

(a) (b)

Figure 4-6: TEM images of Fe/Cu nanoparticles (method 2)

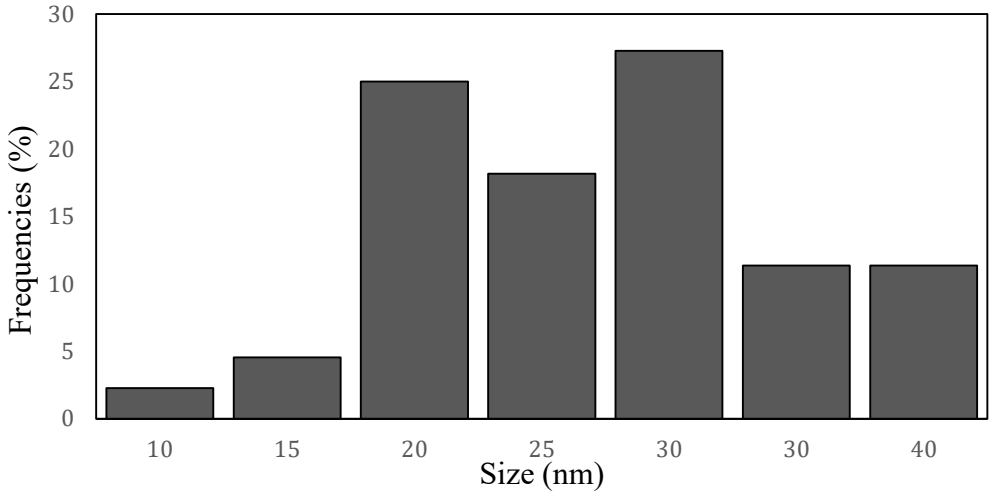

Figure 4-7: Particle size distribution of the synthesized nanoparticles (method 2)

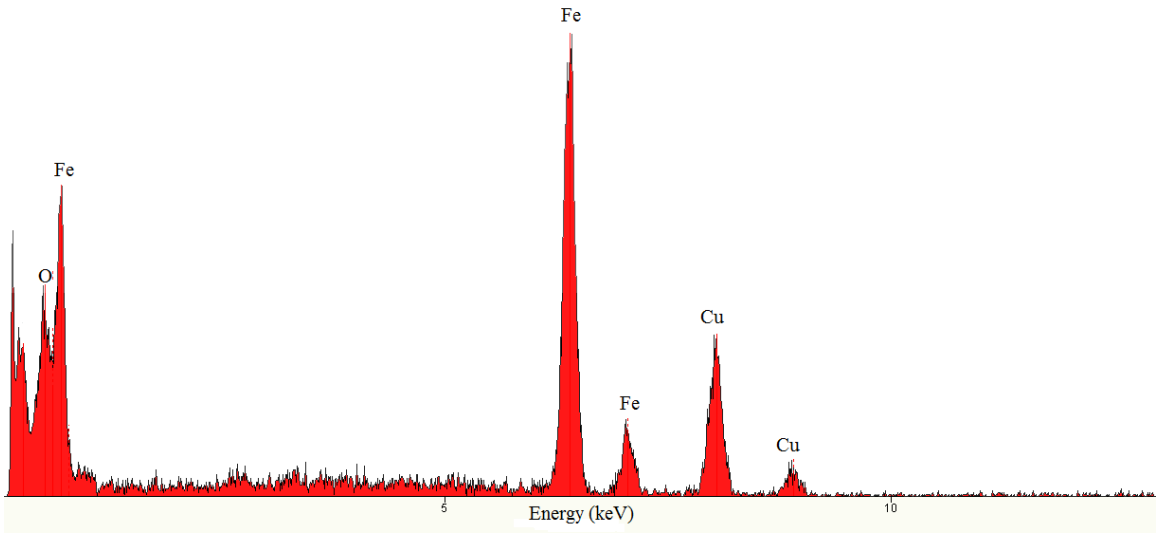

Figure 4-8: Elemental distribution for the sample of iron/copper nanoparticles (method 2).

4.2.3 Surface Areas (BET)

The BET surface area for the Fe/Cu nanoparticles from the second method was 40.4 m^2/g. Similar to the first nanoparticle, the BET surface area of this nanoparticle is greater than that of Fe nanoparticles and granular iron used in permeable reactive barriers (Yuvakkumar et al., 2011; Kanel et al., 2005; Su and Puls, 1999; Suk et al., 2009). As it was discussed earlier, this high surface area can attribute to a higher reaction rate for remediation of contaminants. However the BET surface area of the smaller nanoparticle is two times higher than that of the larger nanoparticle indicating that the smaller nanoparticle will be far more effective in a remediation process.

4.3 Effect of initial concentration and adsorbent dose

By using 100 mg/L of nanoparticles for the initial concentration of 1000 µg/L, 69% removal of As(III) was observed with the smaller size nanoparticles and 44% with the larger size nanoparticles. The percent removal was higher for As(V) (89% and 85% with the smaller and the larger particles, respectively). For the initial concentration of 500 µg/L, 78% removal of As(III) was observed with the smaller size nanoparticle and 46% with the larger size nanoparticle. For As(V) these percentages become 96% and 91%, respectively. 80% and 75% removal efficiency of As (III) were achieved using the smaller size nanoparticles and the larger size nanoparticle respectively at the initial concentration of 100µg/L. For As(V), these percentages become 97 and 94, respectively.

It is evident that the percent removal of arsenic decreases with an increase in the initial concentration of arsenic. With an increase in arsenic concentration, competition for the active adsorption sites increases and the adsorption percentage will decrease accordingly.

As can be seen, for all initial concentrations, the removal percentage is higher for smaller size nanoparticle. This is due to the higher ratio of surface to volume. As the nanoparticles

become smaller in size (diameter), the ratio of surface to volume goes up with the same mass, meaning more adsorption sites are available.

Adsorbent dose is an important parameter for arsenic removal by adsorption. The effect of nanoparticles dose (10 mg/L, 50 mg/L and 100 mg/L) on the percentage removal of As(III) & As(V) for both nanoparticles at three different initial concentrations 100, 500 and 1000 µg/L is shown in Figures 4-9 and 4-10. It was observed that arsenic removal increased with increased adsorbent dose up to 0.1 g/L. An increase in adsorption with the increase in adsorbent dose can be attributed to greater adsorbent surface area and availability of more adsorption sites. However, when the dose of nanoparticles is increased from 50 mg/L to 100 mg/L, the increase in the rate of arsenic removal is less than in comparison with the rate of removal when the dose of nanoparticles increased from 10 mg/L to 50 mg/L, indicating a saturation of adsorption sites. The saturation of the active sites may also be due to overlapping of active sites at higher dosages as well as the decrease in the effective surface area, resulting from the accumulation of particles.

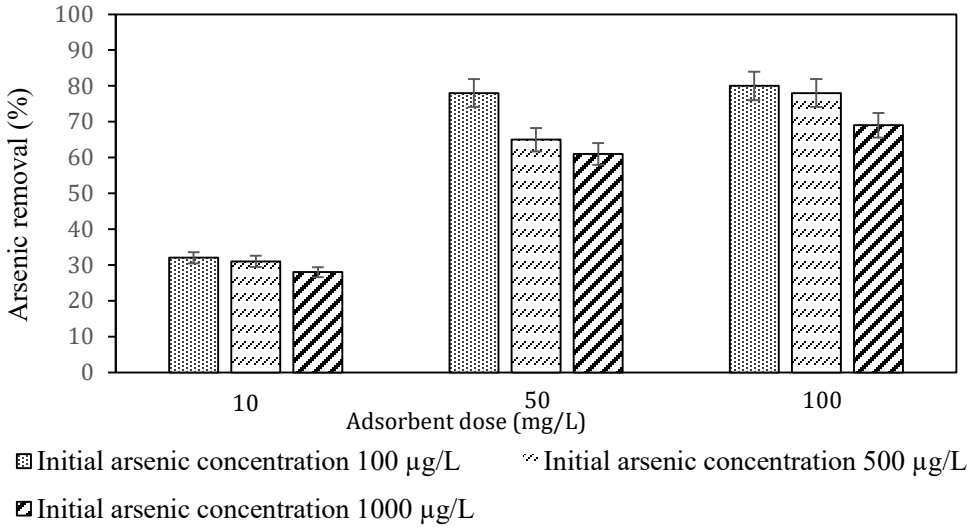

(a)

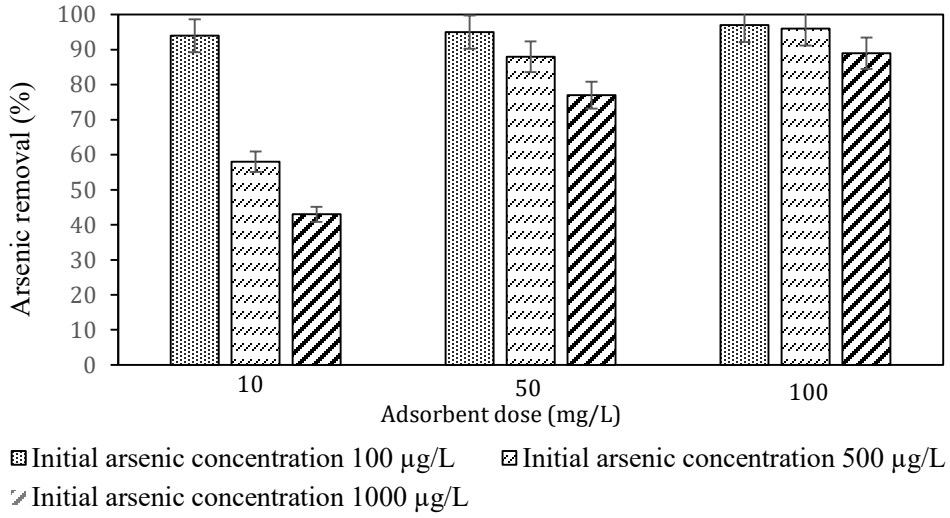

(b)

Figure 4-9: Effect of adsorbent dose on the removal of arsenic (method 1) (a) As(III), (b) As(V) (error bars indicate the standard deviation)

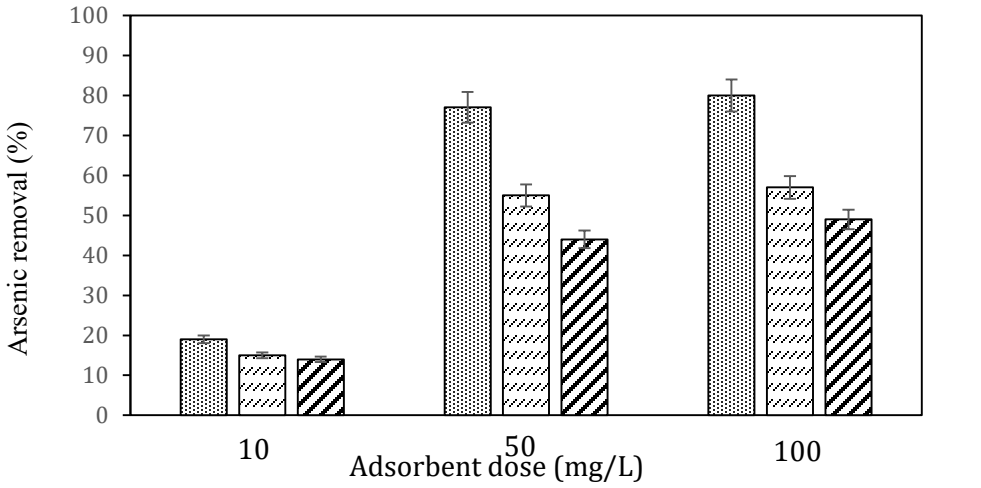

(a)

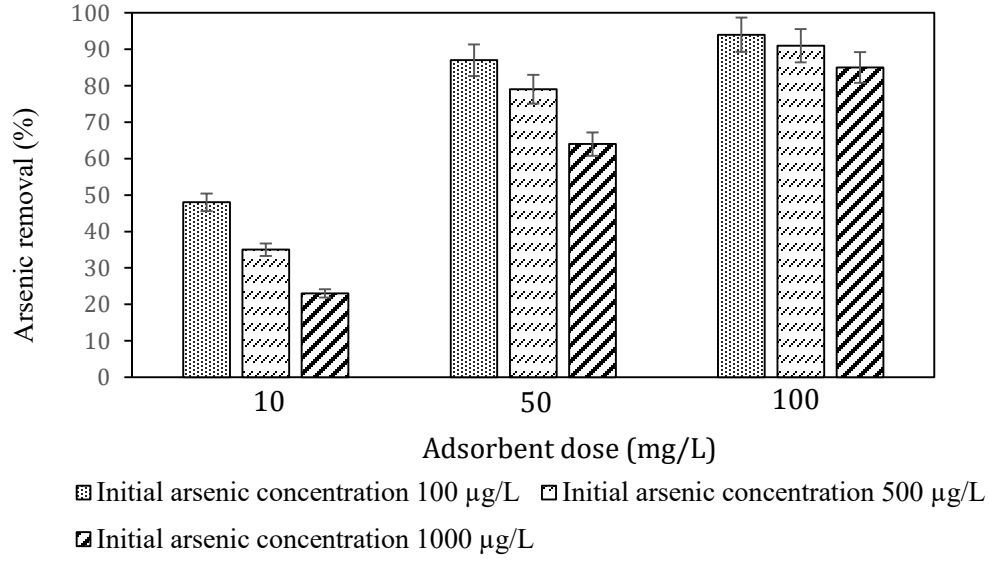

(b)

Figure 4-10: Effect of adsorbent dose on the removal of arsenic (method 2): (a) As(III), (b) As(V) (error bars indicate the standard deviation)

4.4 Sorption Isotherms

The adsorption capacity is defined by the adsorption isotherms. In general, an adsorption isotherm is a curve describing the phenomenon governing the retention (or release) or mobility of a substance from the aquatic environment to a solid-phase at a constant temperature and pH (Limousin et al., 2007; Allen et al., 2004). Adsorption equilibrium (the ratio between the adsorbed amount with the remaining in the solution) is established when an adsorbate containing phase has been contacted with the adsorbent for sufficient time, with its adsorbate concentration in the bulk solution is in a dynamic balance with the interface concentration (Foo & Hameed, 2010).

Over the years, in order to correlate the equilibrium adsorption data, various models like Langmuir and Freundlich have been developed. In this research in order to study the dominant adsorption mechanisms and to compute various adsorption parameters, these two models were evaluated. The Langmuir empirical model assumes monolayer adsorption (the adsorbed layer is one molecule in thickness), with adsorption can only occur at a finite number of definite localized sites that are equivalent (Vijayaraghavan et al., 2006). The Langmuir model assumes that the sorption energy of each molecule is the same. This isotherm has the following form:

$$q_e = \frac{q_0 b C_e}{1 + b C_e} \qquad (4-2)$$

which may be written in the linearized form as follows:

$$\frac{C_e}{q_e} = \frac{1}{q_0 b} + \frac{1}{q_0} C_e \qquad (4-3)$$

where q_0 is the maximum adsorption capacity of the adsorbent, *Ce* is the liquid phase equilibrium concentration of, q_e is the amount of arsenic adsorbed, and b is the constant related to the energy

or net enthalpy of adsorption. The essential characteristics of Langmuir isotherm can be explained in terms of a dimension-less separation factor, R_L which describes the type of isotherm, as defined by (Hall et al., 1966):

$$R_L = \frac{1}{1 + bC_0} \qquad (4-4)$$

where C_0 (μg/L) is the initial arsenic concentration. For favorable isotherms, the R_L value should lie between 0 and 1. In this system, R_L values for adsorption of As(III) and As(V) for both nanoparticles was found to be less than 1, suggested that the adsorption system strictly followed Langmuir isotherm. Figures 4-11 and 4-12 show the Langmuir isotherm plots of Fe/Cu nanoparticles and Tables 4-1 and 4-2 show the isotherm parameters.

The Freundlich isotherm (Freundlich, 1906) is the earliest known relationship describing the non-ideal and reversible adsorption, not restricted to the formation of monolayer. This empirical model can be applied to multilayer adsorption, with non-uniform distribution of adsorption affinities over the heterogeneous surface. The Freundlich equation has the following form:

$$q_e = K_F C_e^{\frac{1}{n}} \qquad (4-5)$$

which may be written in the linearized form as follows:

$$\log q_e = \log K_F + \frac{1}{n} \log C_e \qquad (4-6)$$

where q_e is the amount of arsenic adsorbed, C_e is the equilibrium concentration of arsenic in solution, K_F can be taken as a relative indicator of adsorption capacity, and *1/n* is indicative of

energy or intensity of the reaction ranges between 0 and 1. Adsorption becomes more heterogeneous as the amount of *1/n* value gets closer to zero, whereas, a value below unity implies a chemisorption process.

As the adsorption isotherms follow the Langmuir model, Freundlich isotherms were not been plotted, although the isotherm parameters have been presented in Tables 4.2 and 4.3. It is observed from Tables 4-1 and 4-2 that the maximum adsorption capacity of the smaller size Fe/Cu nanoparticle for As (III) is 19.68 mg/g and for As (V) is 21.32 mg/g. For the larger nanoparticles these amounts drop to 5.6 and 7.8 mg/g. It is clear that there is a large difference between the adsorption capacities of these two nanoparticles, although both adsorbents are almost same in composition. The adsorption capacity of an adsorbent mainly depends on the adsorbent surface area and the initial adsorbate concentration. The initial adsorbate concentration is the same in both cases. However the smaller nanoparticle has a larger surface area (79. 6 m^2/g) in comparison with the larger one (40.5 m^2/g) and the discrepancy in adsorption can be attributed to this.

Table 4-1: Langmuir and Freundlich isotherm constants for arsenic adsorption (method 1)

Form of As	Langmuir			Freundlich		
	q_0 (mg/g)	b(L/mg)	R^2	K_F((mg/g)/((mg/L)1/n))	n	R^2
As(III)	19.68	0.002	0.99	0.19	1.69	0.94
As(V)	21.32	0.016	0.99	1.003	2.31	0.91

Table 4-2: Langmuir and Freundlich isotherm constants for arsenic adsorption (method 2)

Form of As	Langmuir			Freundlich		
	q_0 (mg/g)	b(L/mg)	R^2	K_F((mg/g)/((mg/L)1/n))	n	R^2
As(III)	5.55	.006	.99	0.116	1.68	.99
As(V)	10.41	.046	.99	0.3	1.63	.98

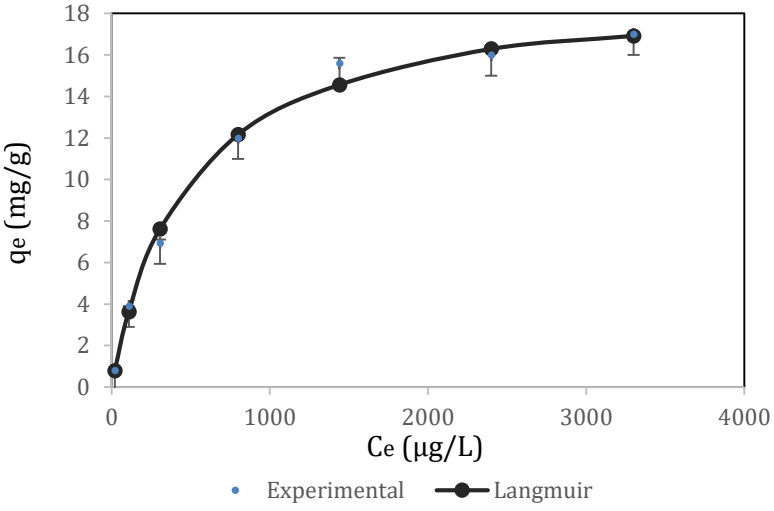

(a)

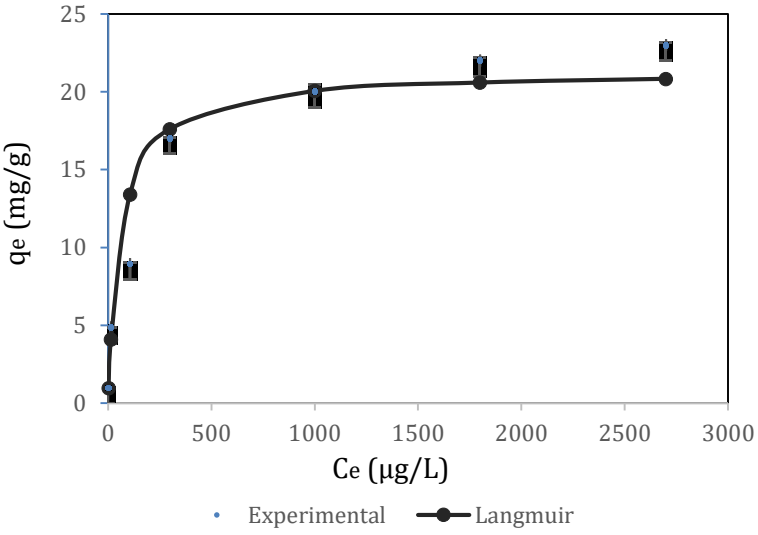

(b)

Figure 4-11: Equilibrium isotherm model for arsenic adsorption (method 1): (a) As(III), (b) As(V) (error bars indicate the standard deviation)

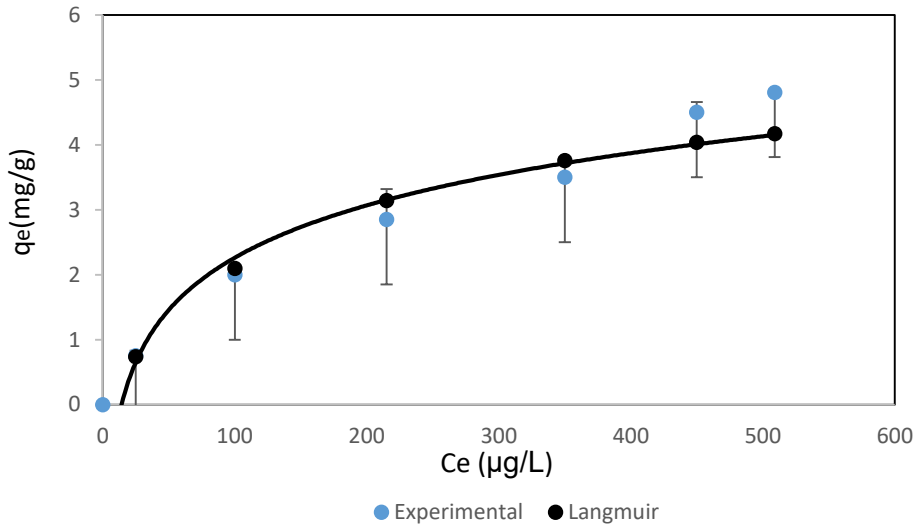

(a)

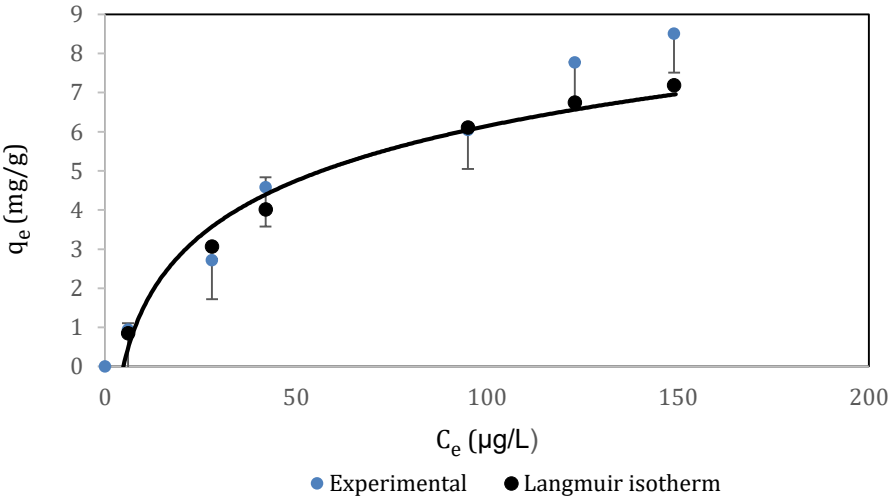

(b)

Figure 4-12: Equilibrium isotherm model for arsenic adsorption (method 2): (a) As(III), (b) As(V) (error bars indicate the standard deviation)

For comparison, arsenate and arsenite removal capacities of some of iron or copper based nanoparticles are listed in Table 4-3. As observed, Fe/Cu nanoparticles do not necessarily have the highest adsorption capacity. However, it should be noted that effective pollutant removal by adsorption is dependent on many factors, including kinetics of reaction, pH sensitivity of the process, possibility of secondary pollution, difficulties in separation from water solutions, and the presence of common competing anions. These factors can negatively affect and hinder the adsorption process (Martinson & Reddy, 2009). Moreover, in the case of nanoparticles, other factors, like the preparation method and particle resistance due to aging, are of high importance. In this study, Fe/Cu nanoparticles were prepared very quickly and easily, and it was demonstrated that it is possible to produce them in any environmental engineering lab, or in situ.

Table 4-3: Comparison of arsenic adsorption capacity of Fe/Cu nanoparticles with selected iron or copper based nanoparticles. (Langmuir model)

Adsorbent	Concentration range	qe (mg/g)	Arsenic species	pH	References
ɤ-Fe_2O_3	10 to 150 mg/L	59.25 (10ºC)	As(III)	6	Lin et al., 2012
	10 to 200 mg/L	88.44 (10ºC)	As(V)	3	
Fe-TNTs	1 to 50 mg/L	80.67	As(V)	2	Wang et al., 2015
Cupric oxide nanoparticles	0.1–100 mg/L	26.9	As(III)	8	Martinson and Reddy, 2009
		22.6	As(V)		
FeMag-250	1-70 mg/L	46.5	As(III)	7	Cheng et al., 2015
Fe-Cu	1-5 mg/L	19.68	As(III)	7	This study
		21.32	As(V)		
Maghemites (Mechanochemical)	1-11 mg/L	20.0	As(V)	7	Tuutijärvi et al., 2009
Fe_3O_4-RGO	3–7 mg/L	13.1	As(III)	7	Chandra et al., 2010
		5.83	As(V)		
nZVI	100-1000 mg/L	12.21 14	As(III) As(V)	7	Mosaferi et al., 2014
Copper (II) oxide	0.5–1.0 mg/L	1.0862	As(III)	7	Goswami et al., 2011

4.5 Kinetic models

The rate of arsenic uptake defined by the kinetic models is very important in designing a proper adsorption technique. Pseudo-first-order and pseudo second-order models were studied to investigate the reaction kinetics. The simple pseudo-first-order kinetic model also known as the Lagergren equation (Lagergren, 1898) is represented as:

$$d_q = k_a(q_e - q_t) \qquad (4-7)$$

where q_e and q_t are the amounts of arsenic adsorbed per unit weight (mg/g) of adsorbent at equilibrium and at any time (t), respectively, and k_a is the rate constant of pseudo-first order sorption. The linearized plots of log (q_e–q_t) versus t give the rate constants.

$$ln(q_e - q_t) = lnq_e - k_a d_t \qquad (4\text{-}8)$$

If the rate of adsorption is a second-order mechanism, the chemisorption kinetic rate equation is expressed as:

$$\frac{dq}{dt} = ka(qe - qt)^2 \qquad (4\text{-}9)$$

The linear equation (Lagergren, 1898) for which can be written as:

$$\frac{t}{qt} = \frac{1}{h} + \frac{t}{qe} \quad h = kq_e^2 \qquad (4\text{-}10)$$

where q_t is the amount of arsenic adsorbed at time t (mg/g), q_e is the amount of arsenic adsorbed at equilibrium (mg/g), and h is the initial sorption rate (mg/g min). The values of q_e (1/slope), k (slope ^{2}/intercept) and h (1/intercept) can be calculated from the plots of t/q_t versus t.

Adsorption kinetic results are presented in Figure 4-13. There was a rapid uptake of As(V) in the first 15 minutes, and then it quickly reached equilibrium. For As(III), all adsorption occurred in the first 30 minutes, after which time it reached equilibrium.

The experimental data was fitted to pseudo-first-order and pseudo-second-order equations. The kinetic model parameters are shown in Tables 4-4 and 4-5. The correlation coefficient (R^2) values represent that the pseudo-second-order model is more suitable than the pseudo-first-order model for arsenic adsorption on Fe/Cu nanoparticles.

In addition, the calculated q_e from the pseudo-second-order model is in good agreement with the experimental results. Moreover, the pseudo-second-order rate constant reflects the adsorption rate of adsorbate onto adsorbent. As it is implied in the table, the pseudo-second order rate constant decreased as the initial concentration of arsenic increased, this is because of abundant of arsenic ions competed for adsorption sites located on Fe/Cu nanoparticles at higher arsenic concentration and resulted in a low adsorption rate (Wang et al., 2015).

Table 4-4. Kinetic model parameters (As (III))

C_0 (mg/L)	Pseudo First			Pseudo Second		
	q_e (mg/g)	K (1/min)	R^2	q_e (mg/g)	K (g/mg min)	R^2
0.5	0.34	0.06	0.94	3.93	0.72	0.99
1	0.89	0.13	0.88	6.98	0.47	0.99
2	3.61	0.14	0.97	12.16	0.11	0.99
4	7.29	0.07	0.99	16.69	0.02	0.99

Table 4-5. Kinetic model parameters (As (V))

C_0 (mg/L)	Pseudo First			Pseudo	Second	
	q_e (mg/g)	K (1/min)	R^2	q_e (mg/g)	K (g/mg min)	R^2
0.5	0.12	0.23	1	4.85	14.15	1
1	0.42	0.17	0.97	8.94	1.43	1
2	0.91	0.18	0.98	17.03	0.76	1
4	2.12	0.11	0.95	22.12	0.17	1

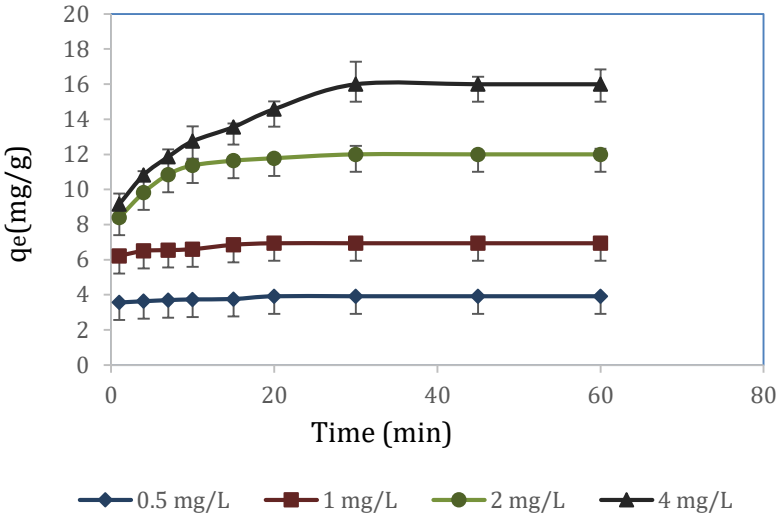

(a)

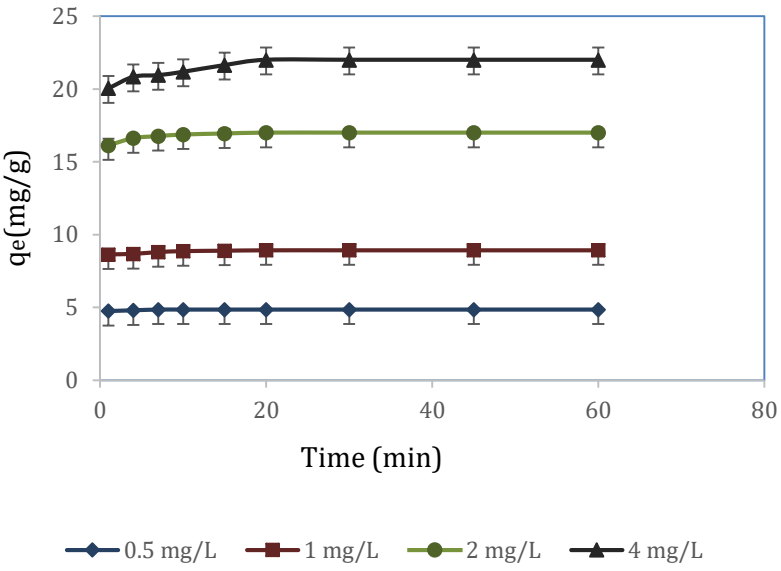

(b)

Figure 4-13**:** Adsorption kinetic data of arsenic at different initial concentrations: (a) As(III), (b) As(V) (error bars indicate the standard deviation)

4.6 pH effect

As(V) and As(III) removal percentage for Fe/Cu nanoparticles at pH 4-11 are presented in Figure 4-14. As clearly shown, pH has a significant effect on arsenic adsorption of nanoparticles. In fact, the surface charge of the adsorbent material and arsenic speciation in the aquatic solution can affect the adsorption capacity, which both are pH dependent factors (Cheng et al., 2015, Tuutijärvi et al., 2009).

Measurements of the zeta potentials at various pH levels in Figure 4-15 demonstrate that the point of zero charge (PZC) of Fe/Cu nanoparticles is between pH 8 and pH 9 as the positively charged nanoparticles at pH 8 or below become negatively charged at pH 9 or above. As(V) adsorption capacity decreased as the pH increased from 4 to11. The dominant As(V) species at pH 3 to 5 was $H_2AsO_4^-$ and from pH 5 to 11 it was $HAsO_4^{2-}$. The electrostatic interaction between As(V) anions and the positively charged surfaces of nanoparticles below the point of zero charge caused the arsenic species adsorbed to the nanoparticles, and by increasing the pH above the point of zero charge, a more and more negative surface charge occurs and the adsorption capacity decreases.

As it can be seen in Figure 2-2, below pH 9.2, As(III) mainly exists as neutral H_3AsO_3, while above pH 9.2, the ionic form of $H_2AsO_3^-$ dominates. The adsorption efficiency of As(III) below the point of zero charge is lower than As(V), but above the point of zero charge the stronger electrostatic repulsion between As(V) and nanoparticle lowers the efficiency of As(V) removal in comparison with As(III), as the particles become negatively charged and the concentration of negative charge is higher in As(V).

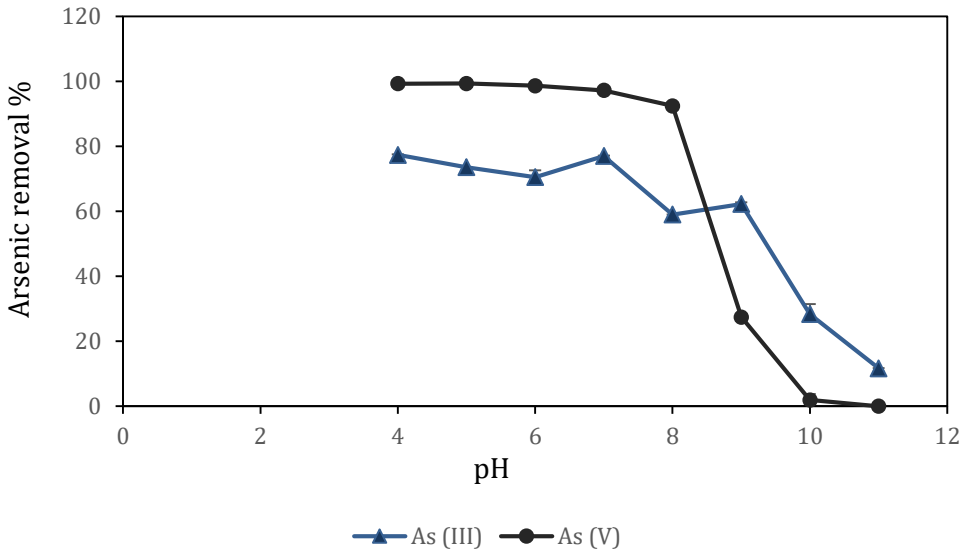

Figure 4-14: Effect of pH on adsorption of As(III) and As(V) onto Fe/Cu nanoparticles.

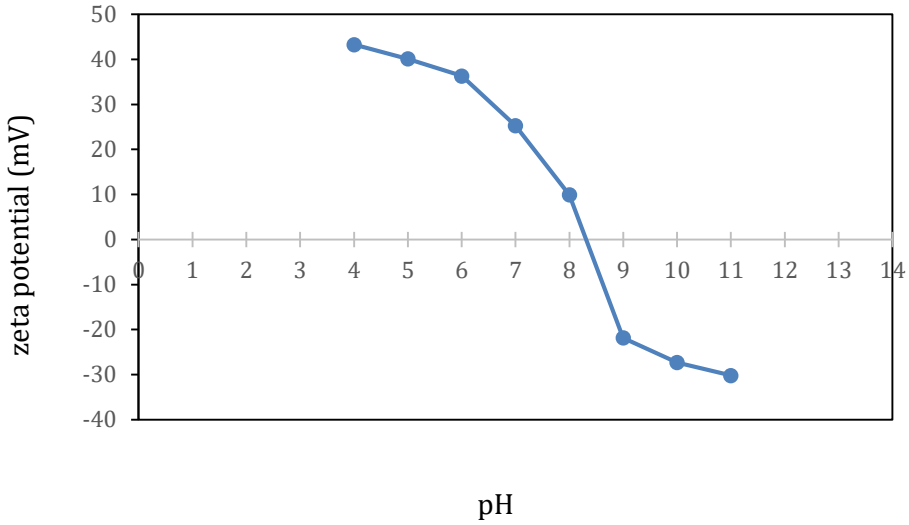

Figure 4-15: Zeta potential of Fe/Cu nanoparticle at various pH levels.

4.7 Effect of competing ions

The presence of bicarbonate, sulfate, and phosphate ions at the studied concentrations did not affect arsenate and arsenite adsorption on Fe/Cu nanoparticles as the amount of arsenic adsorbed on nanoparticles was the same in the presence of these ions. These results are in agreement with previous studies where HCO_3^- and SO_4^{2-} ions at concentrations up to 10 mM had no effect on As(III) (1 mg/L) uptake by zero valent iron nanoparticles (Kanel et al., 2005). As well, no sulfate inhibition was observed with maghemite nanoparticles with an initial concentrations of 0.5 mg/L of As(V) and 20 and 250 mg/L of sulfate (Tuutijärvi et al., 2012). Martinson and Reddy (2009) reported that the presence of sulfate, even at very high concentrations (5 mM), decreased the percentage of As(III) (0.9 mg/L) removal through CuO nanoparticles by less than 10% and had no effect on the adsorption of As(V) (0.9 mg/L).

Although the presence of phosphate ions in this study did not reduce the adsorption of arsenic, at higher concentrations, it may affect the amount of arsenic adsorption. In one study, the presence of 10 mM $H_2PO_4^{2-}$ reduced the uptake of As(III) from 99.9% to 66.3% on zero-valent iron nanoparticles (Kanel et al., 2005). In the case of CuO nanoparticles, removal of As(III) was decreased by more than 10% when phosphate concentrations was greater than 0.2 mM and removal of As(V) was slightly hindered by the presence of phosphate (0.2 mM).

The reason for competition between phosphate and arsenate is that they both have similar structures, chemical behaviors (O'Reilly et al., 2001), and both are adsorbed as an inner-sphere complex onto iron oxides (Arai and Sparks, 2001). Although phosphate is an analogue to arsenate, arsenate is more prominent than phosphate for adsorption on iron (hydr)oxides. The larger size arsenate ion makes it able to interact more strongly with some of the OH groups on the adsorbent surface (Tuutijärvi et al., 2012). These results are informative for in-situ remediation using iron-based nanoparticles due to regular coexistence of competing anions in natural groundwater.

4.8 Desorption studies

Considering the practical applicability of using these nanoparticles in the field, it is essential to examine the possibility of arsenic desorption from the nanoparticles. In previous studies, desorption of arsenic from metal nanoparticles was achieved by use of either alkali or strong acids (Reddy, 2007). As mentioned earlier in this study, a 0.1 or 0.01 M NaOH solution can be used for this purpose. The results of desorption of arsenic from Fe/Cu nanoparticles are presented in Figure 4-16.

As apparent from the results, the amount of As(III) and As(V) leached into the solution increases as NaOH concentration increases. 100% desorption of As(V) was achieved with a 0.1 M NaOH solution, while for As(III) there was 80.3% desorption using the same solution. With the 0.01 M NaOH solution, these amounts were 79.4% and 57.5% respectively for As(V) and As(III). In the natural pH of groundwater (6.5 to 8), there is less possibility of arsenic desorption from these nanoparticles as a very alkaline environment is needed for this purpose.

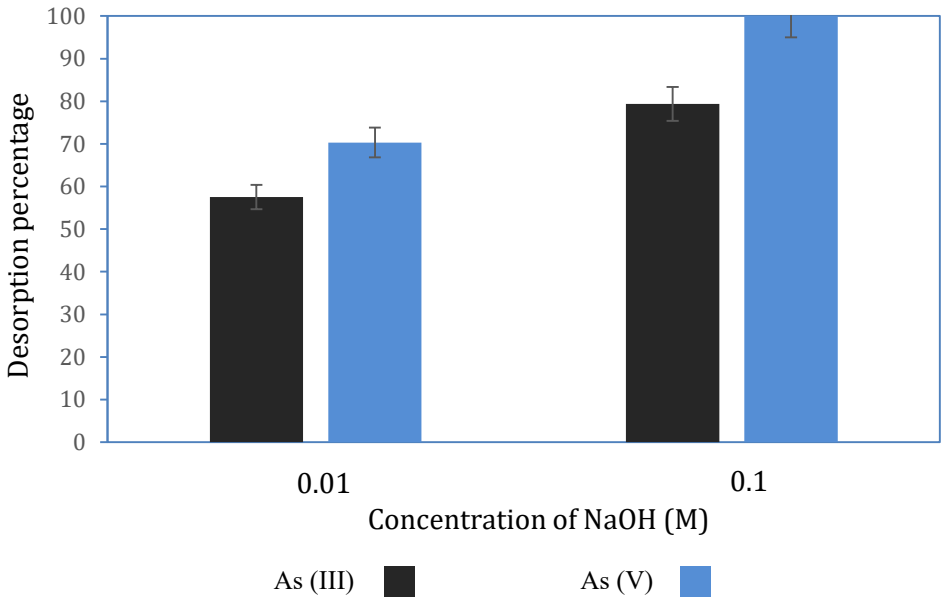

Figure 4-16: Desorption of arsenic from Fe/Cu nanoparticles with two different concentrations of sodium hydroxide. (error bars indicate the standard deviation)

4.9 Adsorption mechanism

To understand the arsenic adsorption mechanism by Fe/Cu nanoparticles, X-ray photoelectron spectroscopy was performed. Fig. 4-17 presents XPS wide scan spectra of Fe/Cu nanoparticles before and after As(III) & As(V) adsorption.

As shown in the survey spectra, three major peaks at binding energies of 530.03, 710.88, and 933.88 eV, designated for O1s, Fe2p and Cu2p respectively, were observed for the virgin sorbent. Changes were seen after As(III) & As(V) adsorption; in As(III) loaded material, two new peaks at binding energies of 1326.26 & 44.94 eV, corresponding to As2p3 & As3d3 appeared, while As(V) peaks at binding energies of 1326.88, and 45.32 eV correspond to As2p3 & As3d, indicating arsenic was adsorbed onto the material. In XPS data, adventitious elements (carbon and oxygen) spectra are very important as these elements can change the reactivity of surfaces even if the sample is prepared in vacuum (Chowdhury et al., 2011).

O1s narrow scans of the bimetal adsorbent before and after arsenic adsorption at pH 7 are illustrated in Fig. 4-18. Due to the chemical adsorption between the adsorbent and adsorbate the peak of the O1s spectra of the surface complexes has shifted to a lower negative binding energy after arsenic adsorption from 530.03 to 529.98 and 529.93 eV for As(III) & As(V) respectively (Peak binding energies extracted from excel files have been presented in appendix IV).

The O(1s) spectra of Fe/Cu nanoparticles (before and after adsorption) was composed of overlapped peaks of oxide oxygen (O^{2-}) and hydroxyl (OH^-). All spectra were analyzed using xpspeak41 software and satisfactory fitting results were obtained. As shown in Figure 4-19, O^{2-} was the most abundant (84.7%) followed by OH^- (15.3%) in the virgin material. After adsorption, changes in peak position and composition percent of O^{2-} and OH^- were observed due to the interaction between surface –OH and As. In As (III) loaded material the percentage of O^{2-} decreased to 79.7% while the percentage of OH^- increased to 20.3%. In As(V) loaded material, these percentages were 79.3% and 20.7% respectively.

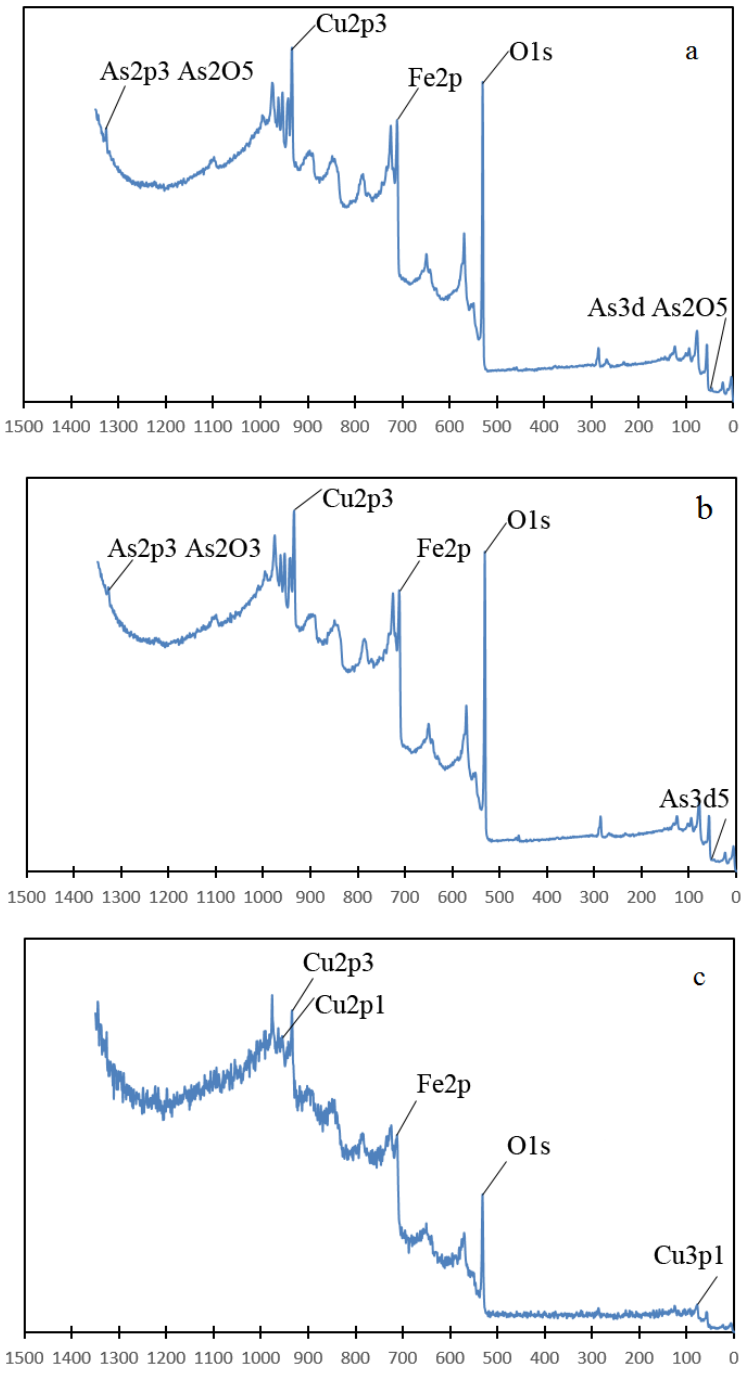

Figure 4-17: The XPS spectra of nanoparticles before and after arsenic adsorption. (a) after adsorption of As(V), (b) after adsorption of As(III), (c) before adsorption

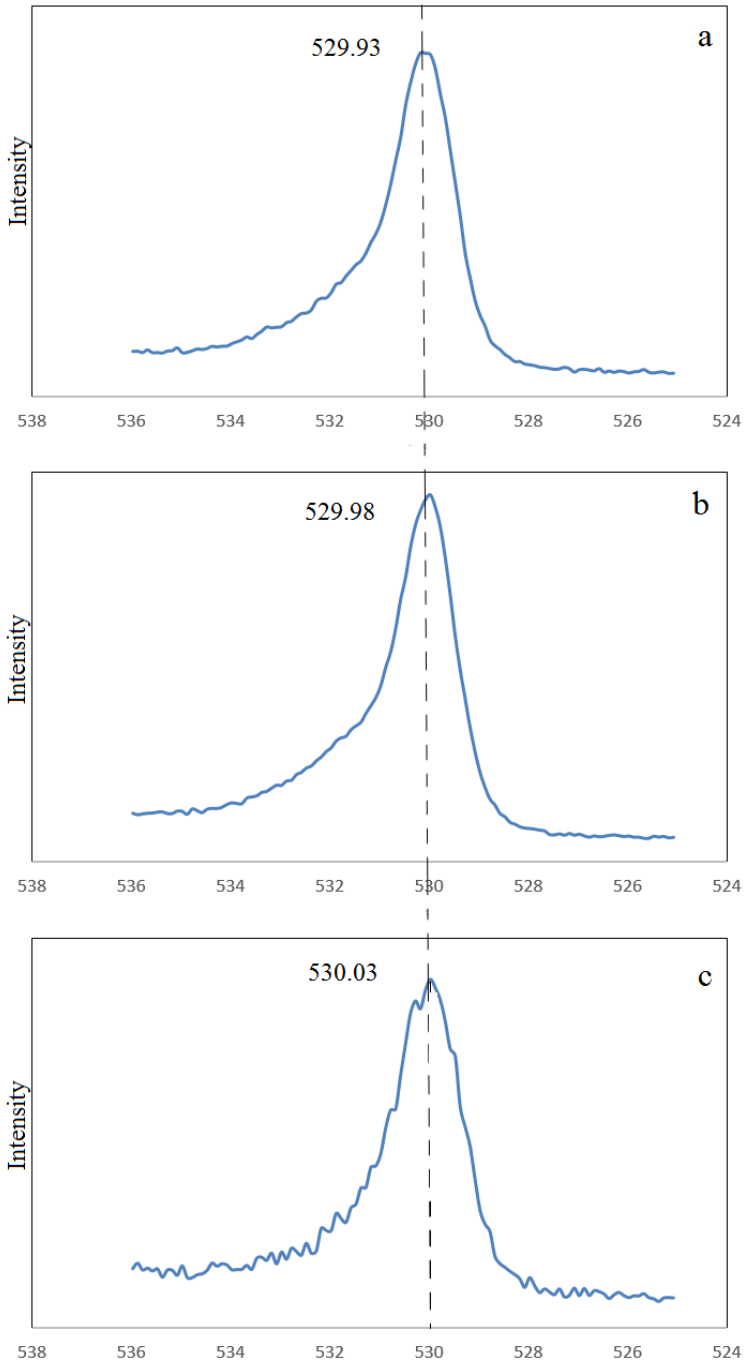

Figure 4-18: The O1s spectra of nanoparticles before and after arsenic adsorption. (a) after adsorption of As(V), (b) after adsorption of As(III), (c) before adsorption

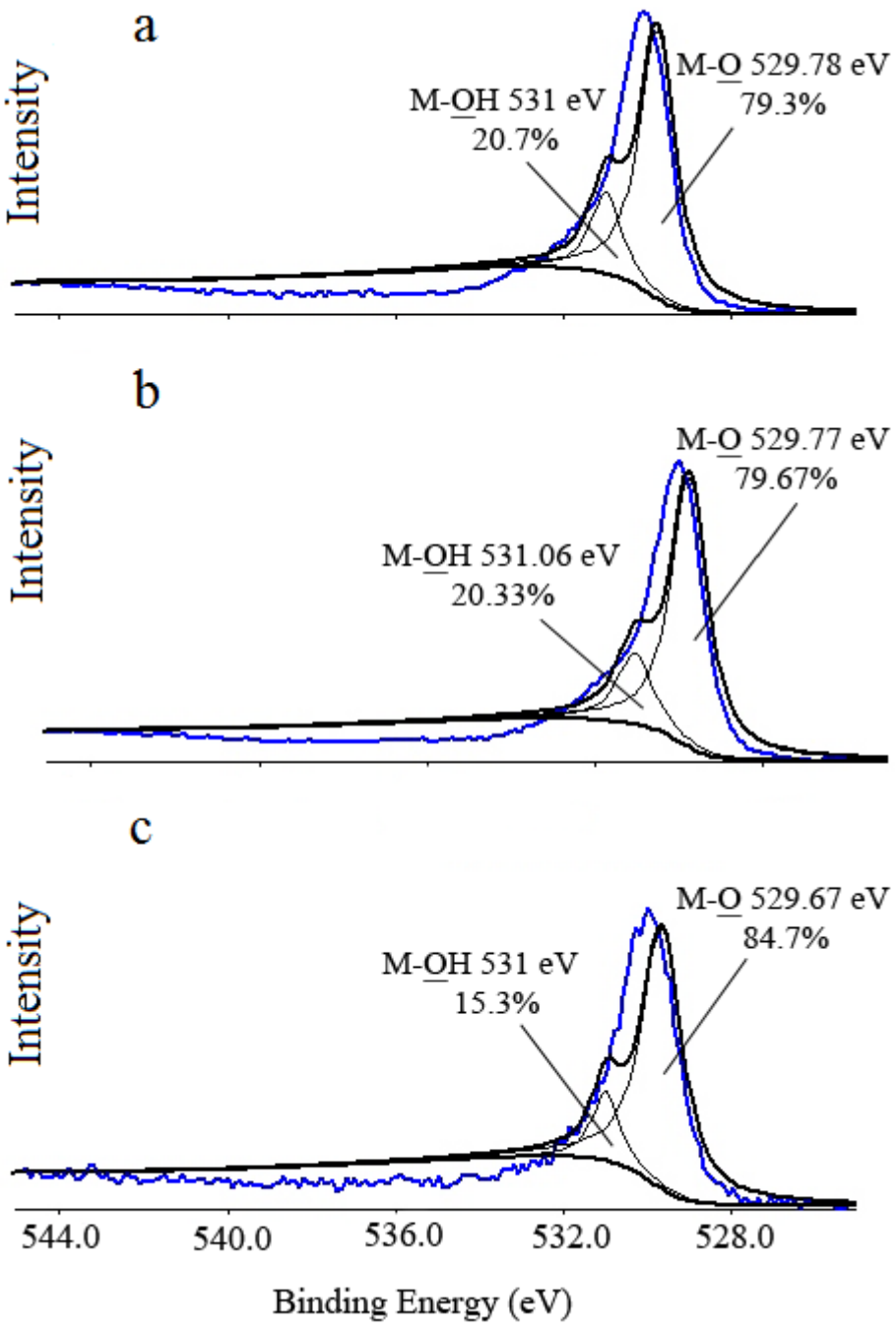

Figure 4-19: Deconvolution of O1s spectra of nanoparticles before and after arsenic adsorption.

(a) after adsorption of As(V) , (b) after adsorption of As(III), (c) before adsorption

In fact, surfaces of Fe/Cu nanoparticles became progressively more hydroxylated following arsenic adsorption perhaps because of the formation of highly hydroxylated arsenate surface complexes (Zhang et al., 2005). For the high resolution spectra of Fe2p, the peaks at 710.88 and 724.58 eV shifted to more negative binding energies after arsenic adsorption, indicating that the hydroxyl groups bonded to Fe may be involved in arsenic adsorption (Fig. 4-20). Photoelectron peaks at 933.88, 940.98, 953.78 and 961.78 eV in Fig. 4-21 corresponding to Cu2p have also shifted to more negative binding energies after arsenic adsorption showing the possible involvement of Cu bonded hydroxyl groups in arsenic adsorption. Therefore, both the hydroxyl groups bonded to Cu and Fe might be involved in arsenic adsorption, indicating these two types of adsorption sites are available at the surface of this nanoparticle. However, it should be noted that the main role of Cu is to modify the magnetite structure of the Fe(II)/Fe(III) system through oxidation of Fe^{2+} and to activate the Fe atoms to acquire more Fe-OH.

A significant amount of theoretical and experimental work on arsenic adsorption by iron oxides has been carried out, focusing mostly on elucidating reactions between adsorbents and arsenic (Zhang et al., 2010; Wang et al., 2015, Ding et al., 2000; Kubicki et al, 2007, Liu et al., 2015, Zhang et al., 2005). According to these studies, arsenic adsorption by Fe oxides is due to the formation of inner-sphere arsenic complexes on the particle surface, and the surface oxygen-containing functional groups involved in adsorption.

For As(V), there are three possible surface complexes resulting from the ligand exchange reaction: binuclear, bidentate, and monodentate complexes (Fig. 4-22) (Zhang et al., 2010). The monodentate and bidentate surface complexes have been used to explain the reaction step in anion adsorption by metal hydroxide on the basis of the quantitative relationship between hydroxyl ion release and As(V) adsorption (Zhang et al., 2005).

Although less studies have been performed for determination of As(III) complexes on the surface of metal oxides, some studies suggest formation of complexes similar to those seen with As(V) for As(III) as well (Dixit and Hering, 2003; Manning et al., 1998; Goffinet and Mason, 2012; Kubicki et al., 2007).

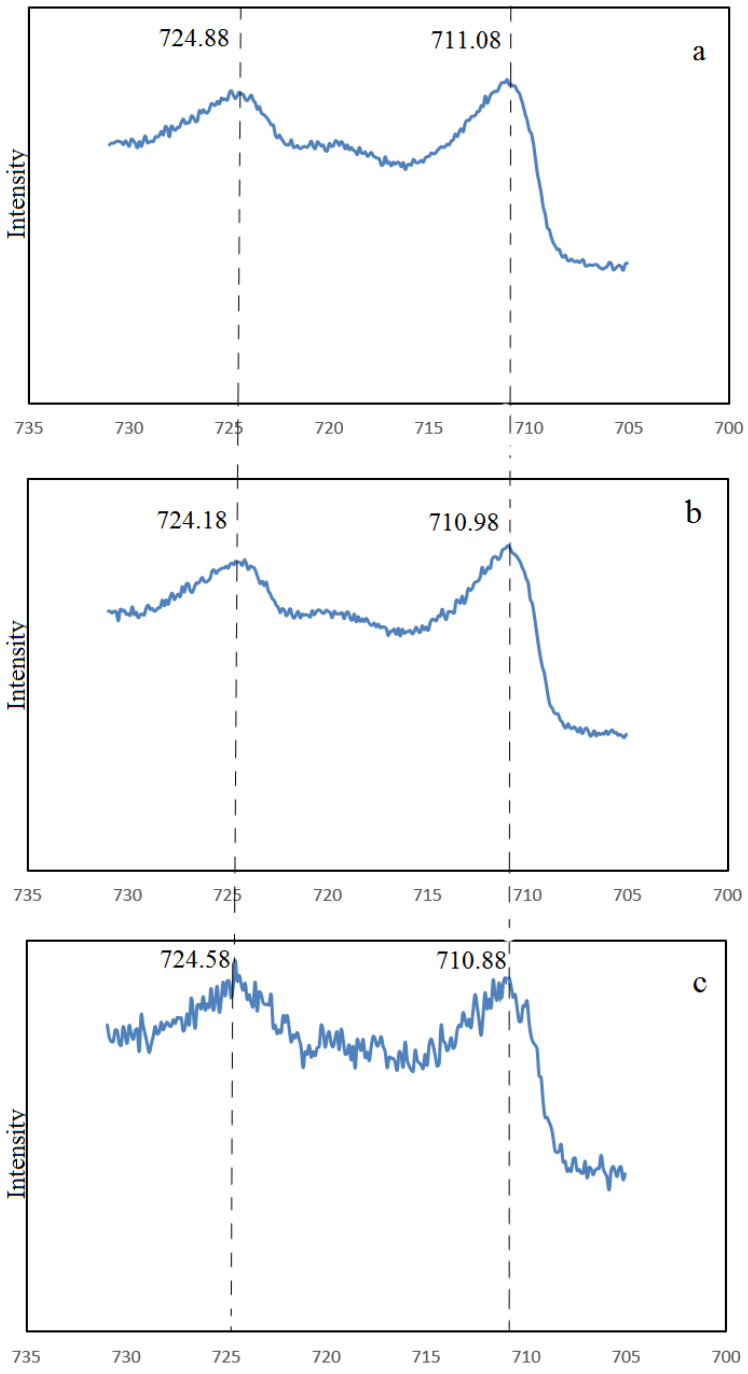

Figure 4-20: Fe2p spectra of nanoparticles before and after arsenic adsorption. (a) after adsorption of As(V), (b) after adsorption of As(III), (c) before adsorption

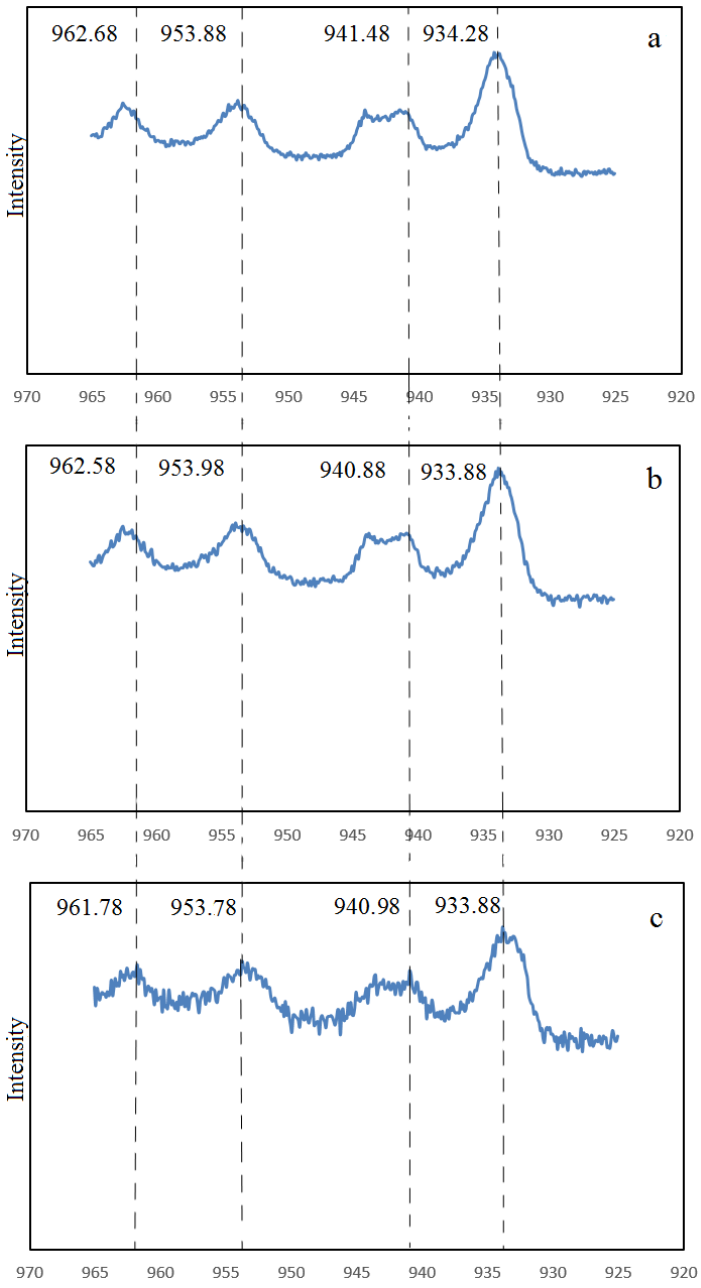

Figure 4-21: Cu2p spectra of nanoparticles before and after arsenic adsorption. (a) after adsorption of As(V) , (b) after adsorption of As(III), (c) before adsorption

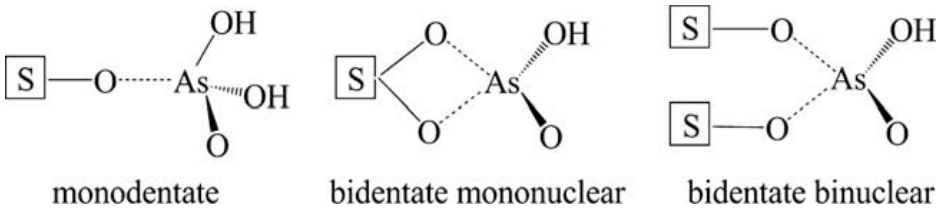

Figure 4-22: Possible configurations of the arsenate surface complexes (Zhang et al., 2010)

To elucidate the adsorption mechanism, FTIR spectra of the virgin Fe/Cu nanoparticles powder before adsorption and after arsenic adsorption on the surface of filter (the filter which was used to separate the nanoparticles from arsenic contaminated water) were also obtained. As it was not possible to remove the peaks related to filter after arsenic adsorption on the spectra, the FTIR spectra could not be used to draw any conclusion. However the spectra are presented in Appendix I.

Chapter 5

Experimental results of arsenic adsorption on starch stabilized Fe/Cu nanoparticles and immobilization in soil

5.1 Characterization of starch-stabilized Fe/Cu nanoparticles by XRD, TEM and BET

5.1.1 X-ray Diffraction

Figure 5-1 shows the XRD peaks of stabilized Fe/Cu nanoparticles (0.04 wt.% starch). According to XRD peak analyses of synthesized Fe/Cu nanoparticles, the peaks are mainly composed of phases of copper oxide (Cu_2O) with a small percentage of iron oxide (Fe_2O_3). The peaks at 36.4 [111], 42.3 [200], 61.4 [220], and 73.4[311]º 2θ correspond to copper oxide (Cu_2O) which is in agreement to the work of Kuo et al. (2007) and Qian et al. (2012). This result shows that iron has become encapsulated in a shell of copper oxide. Peaks other than the characteristic peaks of copper oxide hardly can be seen, indicating that there is little impurity.

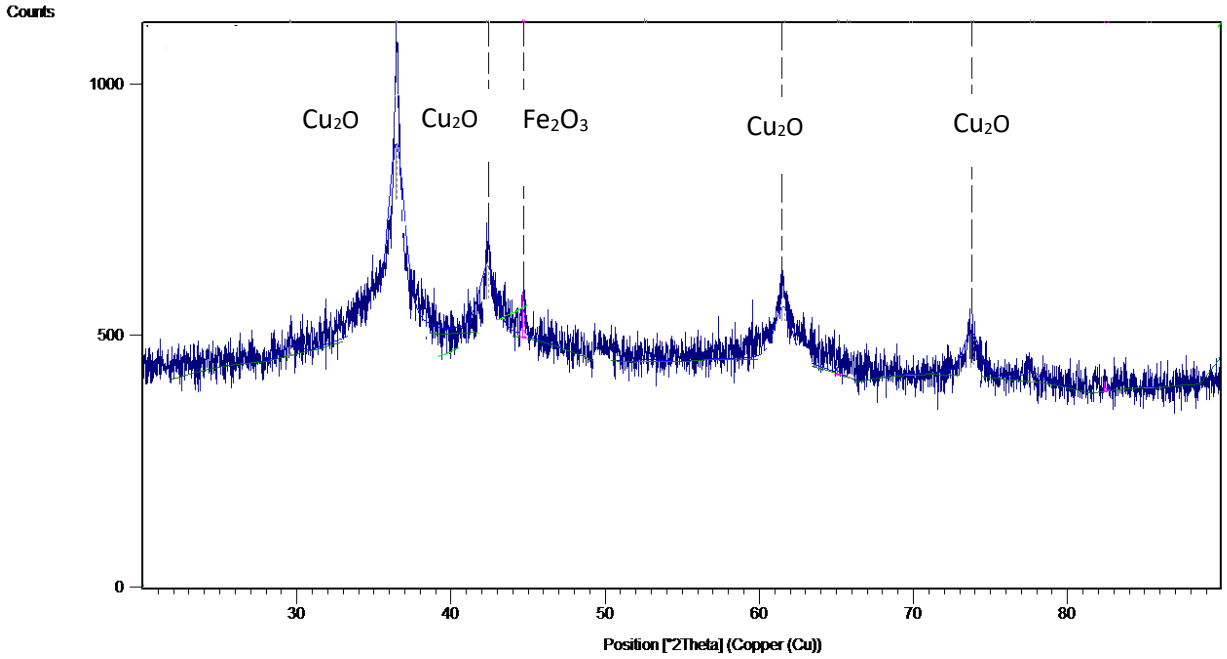

Figure 5-1: XRD pattern of starch stabilized Fe/Cu nanoparticles

5.1.2 Transmission Electron Microscopy

The representative TEM images of the synthesized nanoparticles shown in Figure 5-2 indicate that starch stabilized Fe/Cu nanoparticles were obtained. An overview image at low magnification, illustrates that 0.06 wt. % starch (Figure 5-2 (a)) resulted in completely dispersed and well defined Fe/Cu nanoparticles. The images also show that the sample consisted of nano-sized individual particles with a relatively narrow size distribution, without the presence of larger aggregates. The particles are mostly spherical and almost uniform in size and shape.

The nanoparticles prepared with 0.04 wt. % starch (Figure 5-2 (b)) were not completely dispersed and appeared as interbridged nanoparticles with a mean diameter of (calculated by Scherrer's equation) 8.75nm.

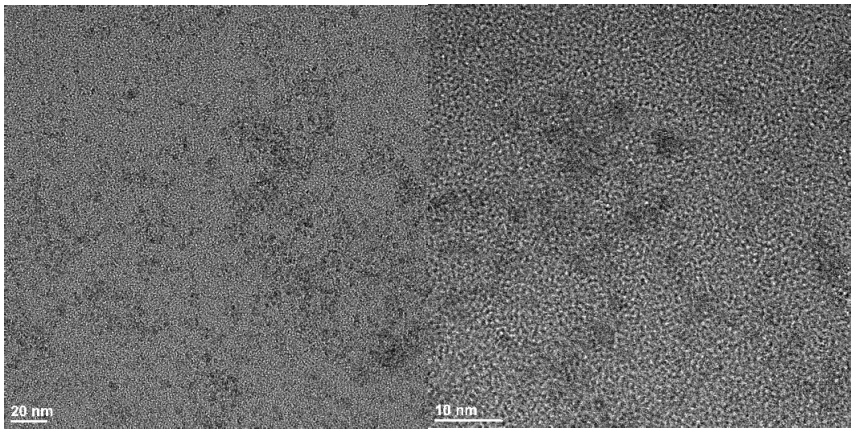

(a) Fe/Cu nanoparticles with 0.06 wt.% starch

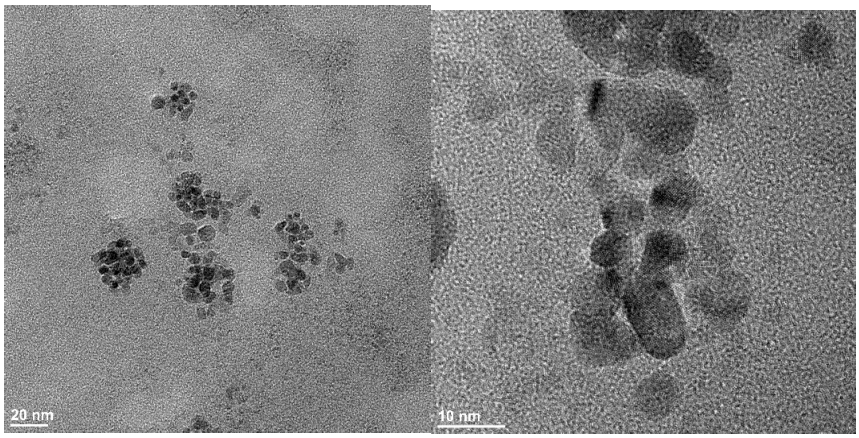

(b): Fe/Cu nanoparticles with 0.04 wt.% starch

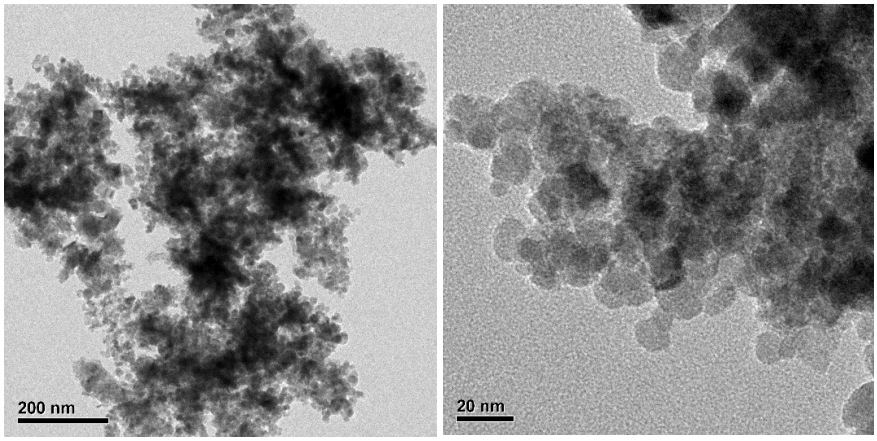

(c): Fe/Cu nanoparticles without starch

Figure 5-2: TEM images of starch stabilized Fe/Cu nanoparticles

However, as the concentration of Fe/Cu nanoparticles, as measured by atomic absorption, was 0.1 g/L at least 48 hours after synthesis, the suspension is still considered to be well stabilized. In comparison to these stabilized nanoparticles, Figure 5-2 (c) shows the tendency of bare Fe/Cu nanoparticles to aggregate, appearing like nanoclusters. It is obvious from the images that the higher starch concentration resulted in smaller nanoparticles (see effect of stabilizer for more details). The EDS spectrum of this nanoparticle is presented in Figure 5-3.

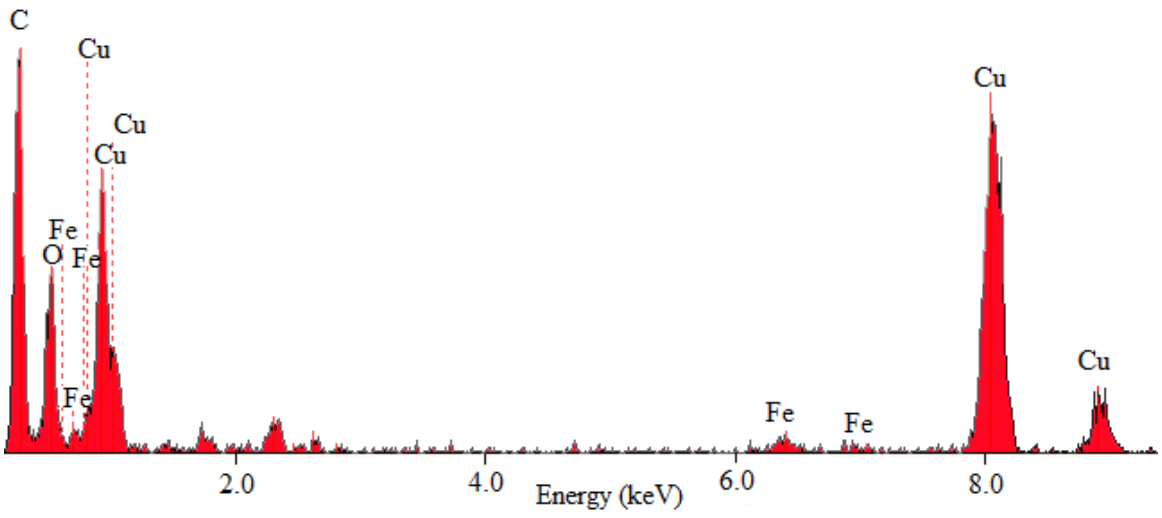

Figure 5-3: Elemental distribution for the sample of starch stabilized Fe/Cu nanoparticles.

5.1.3 XPS Analysis

Figure 5-4 shows the starch stabilized Fe/Cu spectrum. The Cu peak lies at 935.04eV and Fe the peak lies at 715.76 eV. As shown in Figure 5-3, the O peak lies at 532.39eV and for C the peak lies at 288.52 eV. Thus, the XPS results showed that the starch stabilized Fe/Cu has been formed and the sample is composed of iron, copper and carbon.

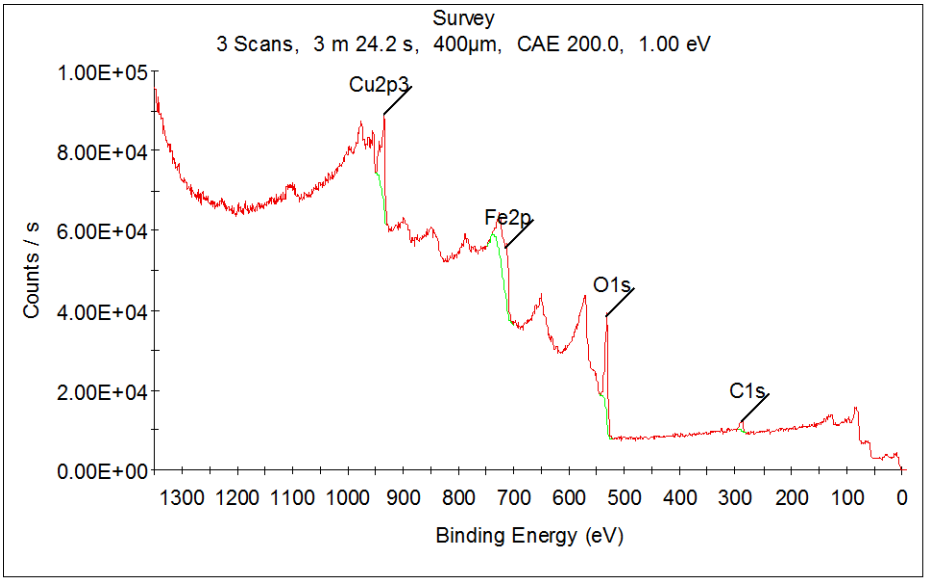

Figure 5-4. XPS spectrum of starch stabilized Fe/Cu nanoparticles.

5.2 Effects of Starch Concentration on Nanoparticle Stability

Figure 5-5 shows the physical stability of Fe/Cu nanoparticles suspensions which have been prepared with the same concentration (0.1 g/L) of nanoparticles, but with various concentrations of starch ranging from 0 to 0.06 wt %. As can be seen, complete particle stabilization occurred at a starch concentration of 0.04% and higher. Non-stabilized nanoparticles and nanoparticles synthesized with 0.02% wt/wt of starch agglomerated, settled within a few minutes after synthesis while completely stabilized Fe/Cu nanoparticles remained in suspension as the concentration of nanoparticles measured by atomic adsorption did not change. In one study by Liang et al. (2012), magnetite nanoparticles remained suspended in water for more than 12 months with ~60% settled based on Fe concentration in the supernatant.

Adsorption of starch macromolecules on the particle surface can significantly change the particle surface characteristics and interactions of the nanoparticles. Regarding the electrostatic interactions between the particles, the ζ potential is an important factor which governs the

stability of nanoparticles in a water environment. Figure 5-6 shows the ζ potential of 0.04 wt.% starch stabilized Fe/Cu nanoparticles as a function of pH.

Due to the starch stabilization, a slightly neutral surface can be observed at a pH range of 5−7. It becomes gradually more negative above pH 7, and reaches a ζ value of −7.7 mV at pH 9. Starch is a neutral polysaccharide and it provides nanoparticles with steric stabilization. In fact, overlapping of two interacting coated starch layers results in a greater repulsive osmotic force. The higher starch concentration translates to a greater osmotic force, and smaller and more stable nanoparticles will be formed as a result (Liang et al., 2012).

When nanoparticles are synthesized in a starch matrix, the hydroxyl groups of starch act as the passivating contacts and prevent the resultant nanoparticles from agglomeration as it can be noticed for the non-stabilized nanoparticles (Raveendran et al., 2003; He and Zhao, 2005).

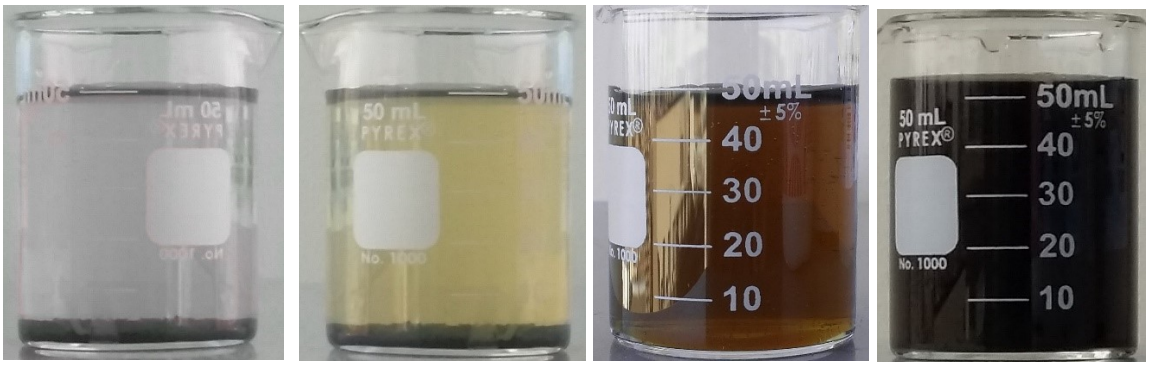

Figure 5-5: Fe/Cu (0.1 g/L) nanoparticles synthesized in the presence of (a) 0, 0.02, 0.04, and 0.06 wt % starch.

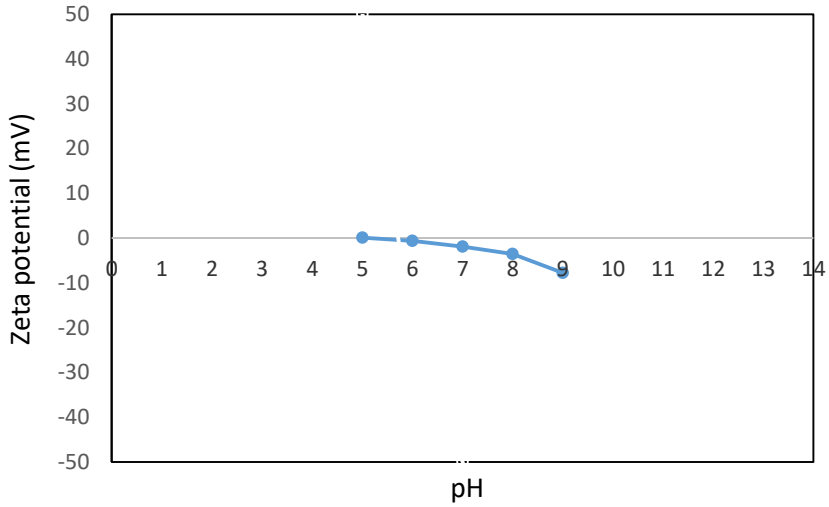

Figure 5-6: ζ potential of 0.04 wt.% starch stabilized Fe/Cu nanoparticles as a function of pH.

5.3 Efficiency of starch stabilized Fe/Cu nanoparticles for removal of arsenic from groundwater

Figure 5-7 shows arsenic sorption isotherms at a fixed pH 7 ± 0.1 for the nanoparticles stabilized with 0.04 wt. % starch. The Langmuir isotherm model was used to interpret the equilibrium data. Table 5-1 gives the best-fitted Langmuir parameters b and q. For this nanoparticle, a very favorable, almost rectangular isotherm was evident with a q value of 90.1 mg/g for As(III) and 126.58 mg/g for As(V). In comparison with the arsenic adsorption capacity of other nanoparticles which is presented in Table 4-3, this nanoparticle has the highest adsorption for arsenic.

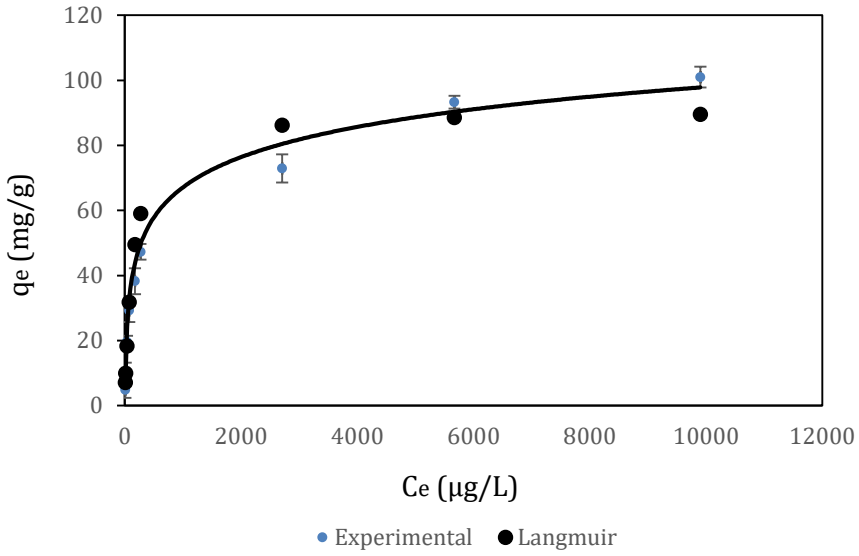

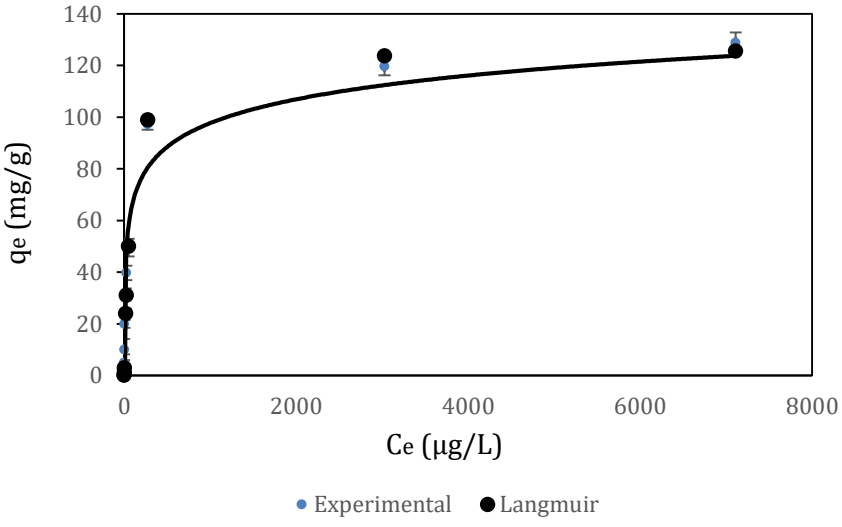

Figure 5-7: Arsenic sorption isotherm of starch stabilized nanoparticles: (a) As(III), (b) As(V) (error bars indicate the standard deviation)

Table 5-1: Langmuir sorption isotherm parameters for starch-stabilized Fe/Cu nanoparticles at pH 7 ± 0.1

Form of As	q_0 (mg/g)	b(L/mg)	R^2
As(III)	90.1	.007	.97
As(V)	126.58	.013	.99

Figure 5-8 shows the rate of arsenic adsorption by nanoparticles (0.04 wt. % starch) over the time. For the initial concentration of 4000 µg/L of As, most adsorption occurs within the first 4 hour as for both As(III) and As(V). Here, the concentration of arsenic falls to less than 30 µg/L. Since, in most cases, the concentration of arsenic in groundwater of contaminated areas has reported to be less than 4000 µg/L (Chakraborti et al., 2003; Ahamed et al., 2006), this nanoparticle can act to effectively remove arsenic from groundwater in a very short time. As the initial concentration of arsenic increases lower removal efficiencies over time can be expected (Figure 5-8 (b)). Although an initial concentration of 10000 µg/L of arsenic in water was tested, this concentration is not usually found naturally in the environment. This is an attempt to replicate the high concentration conditions seen with mine tailings. It should be noted that the control samples (the same solution without the nanoparticles) did not show any changes of arsenic concentration during the experiment.

Besides the high capacity of this nanoparticle to adsorb arsenic from water in a short period of time, previous experiments showed that non-stabilized Fe/Cu nanoparticles were effective in adsorbing arsenic, even 18 months after synthesis. There was no decrease in removal efficiency of arsenic from water after this period. As these nanoparticles were synthesized to remove arsenic from ground water by immobilizing it in the soil matrix, it is very significant that they can remain active for such a long period of time after the injection into the soil matrix.

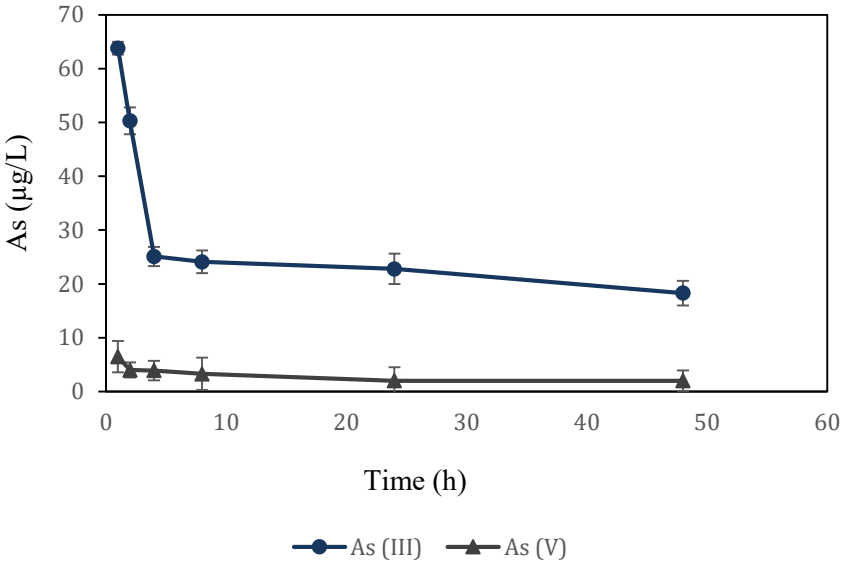

(a)

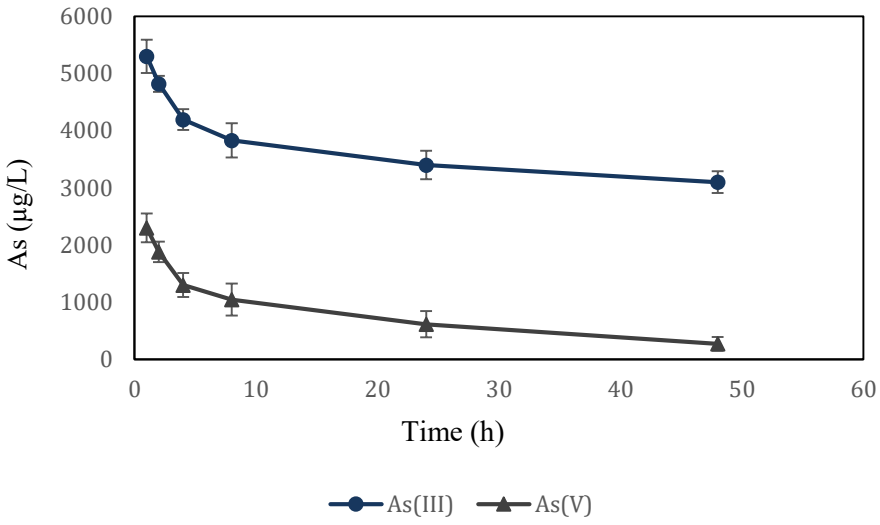

(b)

Figure 5-8: Concentration of arsenic in water after adsorption by starch-stabilized Fe/Cu nanoparticles according to the time: (a) initial concentration of 4 mg/L, (b) initial concentration of 10 mg/L.

It should be noted that stabilizing the nanoparticles results in higher removal efficiency as smaller nanoparticles will form and more adsorption sites will be available. It was observed that higher concentrations of starch result in smaller nanoparticles. However, at the same time, a higher concentration of starch translates to a higher viscosity of solution, which can hinder the movement of nanoparticles in subsurface environment (see column test for more details). Then although a higher concentration of starch will result in more contaminant removal, it may not be necessarily preferable for use in soil environments.

5.4 Soil Characterization

Physicochemical characteristics of the chromated copper arsenate (CCA) contaminated soil are presented in Table 5-2 (particle size distribution and the list of concentration of all elements in the soil are presented in appendices II & III). This soil is classified as a loamy soil and as it is shown in the Table 5-2, the concentration of arsenic in soil (120.6±14 mg/kg) is 10 times higher than the guideline value (12 mg/kg) (Environment Canada, 1996) for arsenic in soil. This high concentration of arsenic in soil requires further treatment as leaching to the groundwater may cause contamination of water resources nearby.

Table 5-2: Physicochemical characteristics of the soil.

Textural Class	Clay %	Silt %	Sand %	pH (DI water)	pH ($CaCl_2$ solution)	Organic content %	As (mg/kg)
Loam	8	45	47	7.7	7.6	4.5×10^{-3}	120.6± 14

Table 5-3: Particle size analysis result.

D_{10}	D_{30}	D_{50}	D_{60}	D_{90}	C_u	C_c
6	11	51	107	132	17.83	0.188

Table 5-3 presents the results of particle size analysis. The coefficients of uniformity (C_u) and curvature (C_c) were calculated by the following equations to have a better idea of the sample textures.

$Cu = D_{60}/D_{10}$

$Cc = (D_{30})^2/(D_{10} \times D_{60})$

Where, D10, D30 and D60 are the grain sizes at which 10, 30 and 60 percent of the soil are finer than, respectively.

5.5 Immobilization of arsenic: batch tests

The effectiveness of starch stabilized Fe/Cu nanoparticles for immobilization of arsenic in a chromated copper arsenate contaminated soil was investigated in batch tests at two different dosages of stabilized Fe/Cu nanoparticles (0.1 and 0.4 g/L) and two different soil to liquid ratios (SLR) of 0.1 and 0.4. Figure 5-9 (a) compares the concentrations of arsenic leached into the solution phase from the contaminated soil in the absence and the presence of different dosages of the nanoparticles at different soil to liquid ratios. In the absence of nanoparticles (i.e. when the contaminated soil was mixed with DI water and simulated ground water), the released arsenic concentration in the water phase was 55 µg/L and 59 µg/L for soil to liquid ratios of 0.1 and 0.4, respectively. In the presence of nanoparticles, the leachable concentration of arsenic from soil to the water was reduced to 4.23 µg/L by using 0.4 g/L of nanoparticles at a soil to liquid ratio of 0.1, which brings the concentration below the guideline value (10 µg/L) for arsenic contamination in water. As observed in Figure 5-9(a), when the dosage of nanoparticles

increases, higher removal efficiency was obtained. In contrast, when the ratio of soil to water increased, the removal efficiency reduced.

To investigate the leachability of arsenic remaining in the untreated or nanoparticle treated soil, TCLP leaching tests were performed on the soil samples following the batch treatments. Figure 5-9 (b) shows that the TCLP leachable arsenic concentration is between 60 to 80 µg/L for the soil sample before nanoparticle treatment. In all other samples, the concentration of arsenic is below the guideline level for arsenic in water except for the case when 0.1 g/L nanoparticles were used at a soil to liquid ratio of 0.4. By using 0.4 g/L nanoparticles at SLR of 0.1 the TCLP leachable arsenic was reduced by 98%. As mentioned previously, formation of inner sphere surface complexes between arsenic and Fe/Cu nanoparticles will cause arsenic to become stabilized at the surface of nanoparticles and as a result become sorbed in the soil matrix. These findings show that this nanoparticle has potential to immobilize arsenic in contaminated sites which have been polluted industrially. In all cases the amount of TCLP leachable arsenic is less than the TCLP regulatory level for arsenic which is 5 mg/L (EPA, 1994).

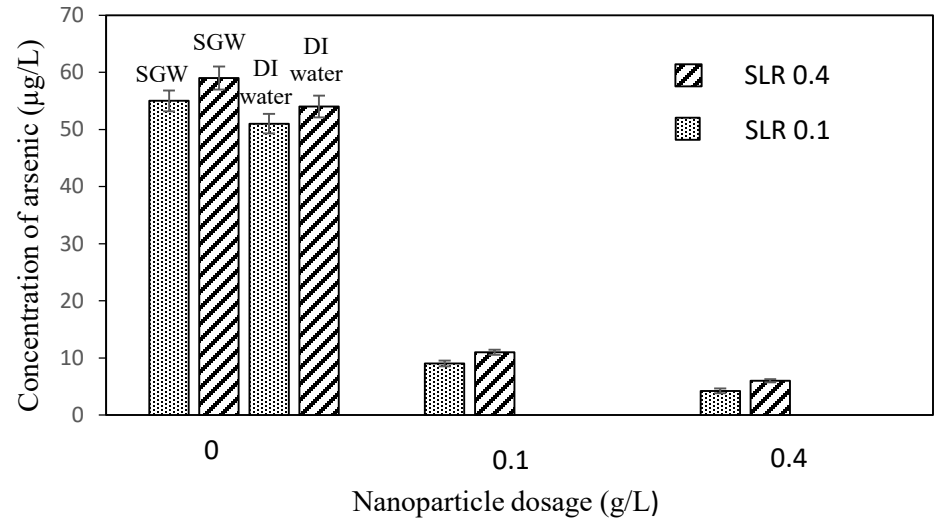

(a)

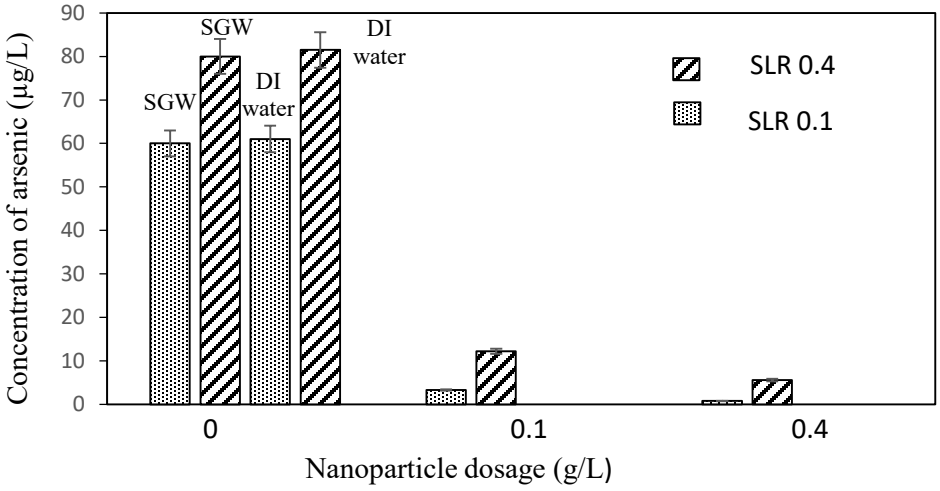

(b)

Fig 5-9:(a) Arsenic concentration in the aqueous phase of the CCA contaminated soil treated with DI water and simulated groundwater (as control solutions), and with different doses of stabilized Fe/Cu nanoparticles with various soil to liquid ratios; (b) Arsenic concentration in the TCLP fluid when the soil samples in (a) were subjected to TCLP tests.

5.6 Mobility of starch-stabilized Fe/Cu nanoparticles in soil

For effective in situ immobilization of contaminants in a soil environment by nanoparticles, they should be deliverable to the target zone of contamination. Also, when the external injection pressure is removed they should be able to act as an immobile sink for the removal of contaminants (Liang and Zhao, 2014; An and Zhao, 2012). Proper particle stabilization is a key factor for maintaining adequate delivery of nanoparticles in the subsurface environment. To examine the efficiency of starch-stabilized Fe/Cu nanoparticles for transport in the soil matrix, a soil column test was conducted with two concentrations of starch (0.04 and 0.06 wt/wt%) as stabilizers of nanoparticles and a tracer (bromide) for comparison. Fig. 5-10 shows breakthrough curves for the tracer and the starch-stabilized nanoparticles through the soil bed. For all experiments, the nanoparticles in the effluent reached a plateau after ~6 PVs (pore volumes) whereas for the tracer it happened after 4 pore volumes. It is assumed that the tracer is a nonreactive species and it does not sorb onto soil particles or column walls and does not suffer from any type of degradation or transformation, then the hydrodynamic properties of the soil column was confirmed with the tracer. Nanoparticles prepared with different concentrations of starch have different levels of breakthrough (C/C_0). As can be observed the nanoparticles stabilized with 0.04 wt.% of starch are more transportable ($C/C_0 = 0.85$) in comparison with the nanoparticles prepared with 0.06 wt.% ($C/C_0 = 0.82$). For 0.06 wt.% starch-stabilized nanoparticles after 10 PV, continuing the experiment was not possible as clogging of the pores happened. Similar results were observed by Liang & Zhao (2014) as the maximum transportability of magnetite nanoparticles occurred when they were stabilized with 0.04wt.% of starch. It should be noted in this study that higher concentrations of starch were not used because with 0.06 wt.%, of starch clogging occurred quickly and with a lower concentration of starch (0.02 wt.%), nanoparticles did not become stabilized.

Fifteen percent of the nanoparticles (0.04 wt.% starch) were removed which can be ascribed to the filtration effect. According to the classical filtration theory (Kretzschmar et al., 1999), filtration removal of fine particles in porous media includes mass transfer of particles to the matrix surfaces by Brownian diffusion, interception, and/or gravitational sedimentation

followed by deposition of particles to the matrix surface. Some factors including particle size, liquid viscosity, media pore size, and surface potential may affect mass transfer and particle-collector interactions (Liang & Zhao, 2014).

The contaminated soil used in this experiment was a loamy soil with 8 % clay and 45% silt, which translates to a high percentage of fine soil particles and extensive available surface area for deposition of Fe/Cu nanoparticles. Besides, due to the wide range of soil particle sizes, the pore size is small as finer particles will become entrapped between the larger particles. There is a higher chance of nanoparticle entrapment among soil particles.

As previously studied, a higher concentration of starch (0.06 wt.%) resulted in smaller nanoparticles, but less delivery in the soil column. It should be noted that a higher viscosity of suspension (because of the higher concentration of starch) may contribute to the slower mass transfer process and increased clogging of the soil pores. In addition, increased collisions between smaller particles and soil particle surfaces may cause more deposition of nanoparticles on collector surfaces (He et al., 2009).

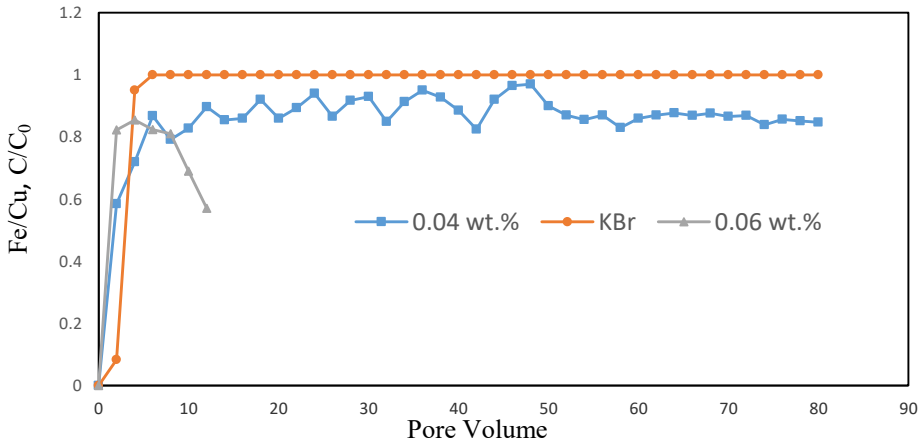

Figure 5-10: Breakthrough curves of the tracer (Br^-) and Fe/Cu nanoparticles prepared with different concentrations of starch through a CCA contaminated soil.

Overall, when nanoparticles are released into the subsurface environment, their behavior is dependent on the following factors: 1) particle-specific properties (e.g. size, shape, chemical composition, surface charge, and coating), 2) particle state (free or matrix incorporated), 3) the surrounding solution chemistry (e.g., pH, ionic strength, ionic composition, natural organic matter content), and 4) hydrodynamic conditions (Klaine et al., 2008 and Wiesner & Bottero, 2007). All these factors are important and affect particle aggregation with other particles or deposition onto various environmental surfaces (Petosa et al., 2010).

5-7 Immobilization of arsenic in soil: column tests

Starch-stabilized Fe/Cu nanoparticles were investigated for their potential ability to immobilize arsenic in a CCA contaminated soil through a fixed-bed column test. Arsenic elution during three column tests (with DI water, simulated groundwater and a starch stabilized Fe/Cu nanoparticle suspension) under identical conditions are presented in Figure 5-11 (a and b). In both cases, the elution curves displayed an immediate peak during the first 5 PVs for the nanoparticle amended soil column and 28 PVs for the soil column with SGW, after which both curves were followed by a gradual tailing. It can be observed that the nanoparticle amended soil eluted arsenic 4.76 times more than simulated groundwater and 5.45 times more than DI water. The reason to have more arsenic elution by SGW is that SGW contains 0.86 mM of $CaSO_4$ and that SO_4^{2-} offers greater affinity than non-specifically sorbed arsenic (An et al., 2005). Then the higher elution peak of As by SGW can be attributed to sulfate exchange for the loosely-bonded arsenic species.

When the effluent samples of the nanoparticle suspension were digested and analyzed for iron and arsenic, it was revealed that ~94% of the eluted arsenic by the stabilized Fe/Cu suspension was associated with the nanoparticles, while all arsenic eluted by DI water and SGW was soluble (as in DI water and SGW experiments nanoparticles had not been applied). In fact, nanoparticles adsorbed nearly all water soluble arsenic. Once the injection pressure is removed, nanoparticles moves for a while under natural groundwater conditions, but eventually they

deposit on the surface of the collector (soil grains) and will act as an immobilized bed to capture water leachable arsenic. It should be noted based on the mass balance in this experiment less than one percent (0.81%) of the total arsenic in soil matrix was eluted by nanoparticles (for more details see the sequential extraction results).

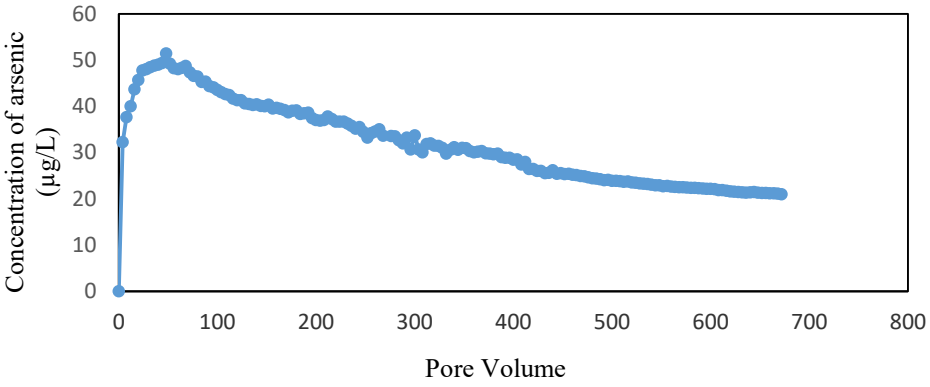

(a)

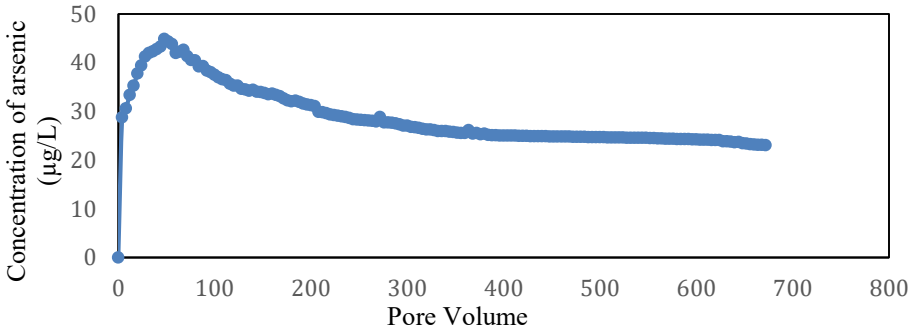

(b)

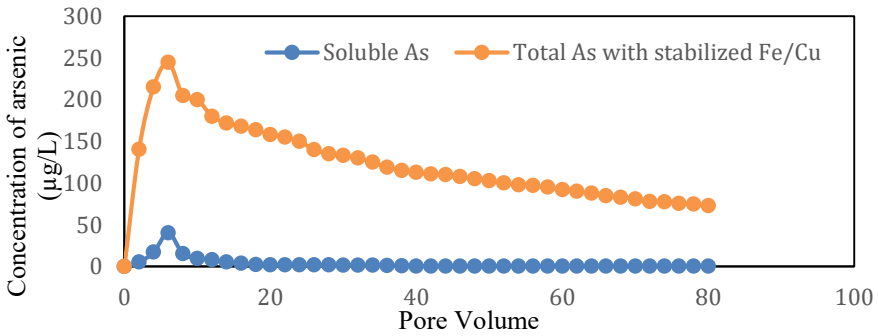

(c)

Figure 5-11: Arsenic elution profiles using (a) simulated groundwater, (b) DI water and (c) starch stabilized Fe/Cu nanoparticle suspensions (soluble As refers to As concentration after nanoparticles removed).

Following the elution trials, the TCLP tests were performed for the soil samples which were subjected to DI water, SGW or treated with nanoparticle suspension. Noting that just 15% of total mass of nanoparticles were entrapped in the soil column, Figure 5-12 shows that the nanoparticle amendment reduced the TCLP leachability by more than 70%, which can be associated with the elevated sorption capacity due to the Fe/Cu nanoparticles retained in the soil. In all cases the amount of TCLP leachable arsenic is less than the TCLP regulatory level for arsenic which is 5 mg/L (EPA, 1994). The presence of iron in the soil has been known to retain more arsenic in the soil phase (Hartley et al., 2004 & An and Zhao, 2012). The results from Figure 5-12 show that the starch stabilized Fe/Cu nanoparticle cannot only immobilize the groundwater soluble arsenic, but also can reduce the leachability of the remaining arsenic in the soil phase.

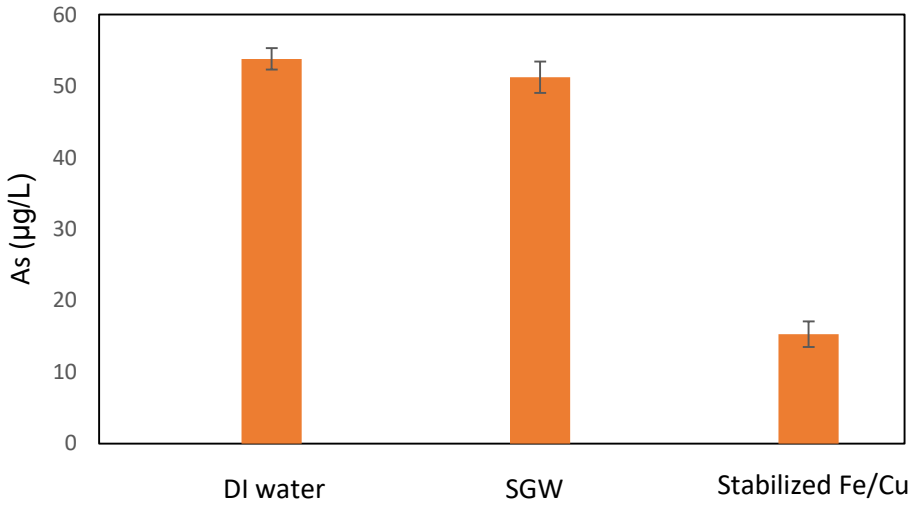

Figure 5-12: Arsenic concentration in the TCLP fluid when the soil samples from were subjected to TCLP tests.

5-8 Selective sequential extraction

A six step sequential extraction test was performed to evaluate the fractionation of As among the soil fractions and changes that occur after nanoparticle treatment. Each step targeted a specific solid phase associated with arsenic and could provide information on relative liability. The arsenic fractions determined in the chromated copper arsenate contaminated soil are presented in Figure 5-13.

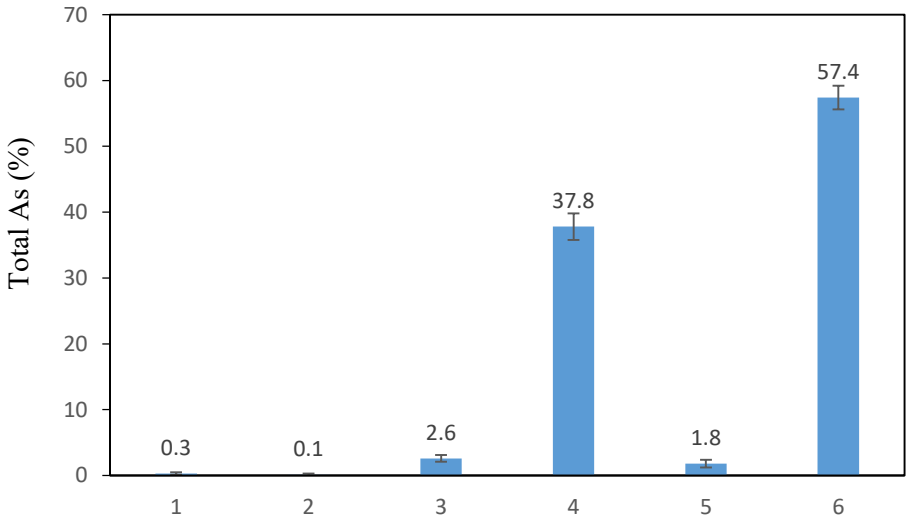

Figure 5-13: Arsenic percent in fractions of the CCA contaminated soil before nanoparticle treatment (fraction 1: water soluble, fraction 2: exchangeable, fraction 3: carbonate associated, fraction 4: oxide associated, fraction 5: organic matter associated, fraction 6: residual)

As is illustrated in Figure 5-13 arsenic mainly was associated in the oxide and residual fractions followed by the fractions associated with the carbonate and organic fractions. Water soluble and exchangeable levels are quite low, accounting only for 0.3% and 0.1% of the total arsenic. Exchangeable arsenic is usually sorbed by electrostatic attraction with the amphoteric surfaces of the amorphous compounds present, and also with broken clay edge surfaces (Yong et al., 1993). As shown in Figure 5-13, arsenic associated with carbonate accounted for 2.8% of the total arsenic while arsenic associated with oxides and hydroxides is quite high (37.8% of the

total). The oxide and hydroxide associated arsenic are related to the detrital metals. This is the result of ligand exchange of arsenic oxyanions on the mineral surfaces and diffusion of arsenic into the minerals (Yong et al., 1993). Arsenic in this fraction is less mobile and its release requires diffusion of arsenic out of the mineral structures and/ or dissolution of the minerals which may happen under some environmental conditions such as acidification or weathering. Arsenic in the oxidizeable fraction associated with organic matter and sulphide made up less than 2% of the total arsenic. This fraction is fairly stable and may be released when the organic matter is decomposed over time.

A significant portion of arsenic (57.5 % of total) was found in the residual fraction. This arsenic is hosted by silicate or sulfide minerals, and significant changes in subsurface chemistry over a long period of time would allow it to become mobile. Overall the SSE result shows that the arsenic in this CCA contaminated soil is potentially of relatively low mobility. The result indicated that the arsenic was concentrated in the last three fractions. The amount of arsenic extracted in the last three fractions was 97% of the total arsenic content in the sample.

Table 5-4 shows the change of arsenic percentage in soil fractions after nanoparticle amendment. After nanoparticle treatment, 0.81 % (less than 1%) of the total arsenic in the soil body was reduced. As it is observed from Table 5-4, starch stabilized nanoparticles removed all water soluble and exchangeable fractions as well as 0.47% of the carbonate fraction.

As the soil was treated with the nanoparticle suspension which was prepared in a water environment, extraction of all water soluble arsenic is expected. Exchangeable arsenic, as previously mentioned is usually sorbed by electrostatic attraction and can become mobile where electrostatic forces of the system are altered or when anion exchange reactions occur. As the nanoparticle suspension was prepared using aqueous solutions of $FeSO_4.7H_2O$ and $CuSO_4.5H_2O$ salts, the suspension contains a considerable amount of SO_4^- ions (Fe and Cu form the nanoparticle and SO_4^- remains in the solution), then the balance of electrostatic forces in soil changes and exchangeable arsenic becomes mobile. Moreover, the presence of SO_4^- in the nanoparticle suspension may have attributed to reducing the carbonate associated arsenic fraction since sulfate exchanges for the loosely-bonded arsenic species (An et al., 2005). Then starch stabilized Fe/Cu nanoparticles remove these fractions of arsenic which were released to the suspension.

Table 5-4: Percentage of arsenic in different soil fractions before and after treatment with starch stabilized Fe/Cu nanoparticles

	F1	F2	F3	F4	F5	F6
Before treatment	0.3± 0.2	0.1± 0.2	2.6± 0.4	37.8± 2	1.8± 0.6	57.4±1.8
After treatment	0	0	2.1± 0.4	37.8± 2	1.8± 0.6	57.4±1.8

Although the main concern of this project was removal of arsenic and tracking its changes in different soil fractions, the concentration of chromium as a potential contaminant in different fractions of soil were examined as well. The chromium fractions percentage determined in the chromated copper arsenate contaminated soil are presented in Figure 5-14. As is illustrated in Figure 5-14 arsenic mainly was associated in the oxide and residual fractions followed with the fractions associated with the organic and carbonate fractions. Water soluble fraction level is quite low, accounting only for 0.1% of the total chromium and no chromium was found in exchangeable fraction.

The total concentration of chromium in this soil calculated as 225.45 ± 0.4 mg/kg which is above the Canadian Soil Quality Guidelines (1999) (64 mg/kg) for residential areas, although the water soluble part accounts just for 0.1% of the total chromium in soil and can leach to the water up to a maximum concentration of 40±0.3 µg/L, which is below the Guidelines for Canadian Drinking Water Quality (50 µg/L) (Health Canada, 2014). During sequential extraction procedure, it's revealed that all water soluble part of chromium was removed by Fe/Cu nanoparticles, but there was not any change in concentration of chromium associated with other fractions of soil.

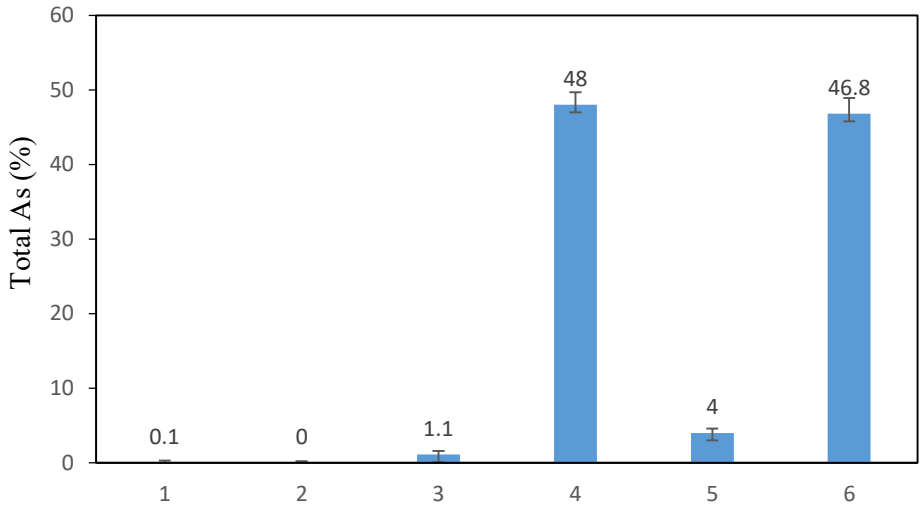

Figure 5-14: Chromium percent in fractions of the CCA contaminated soil before nanoparticle treatment (fraction 1: water soluble, fraction 2: exchangeable, fraction 3: carbonate associated, fraction 4: oxide associated, fraction 5: organic matter associated, fraction 6: residual)

5.9 Arsenic speciation

The result of arsenic species analysis performed by liquid chromatography (LC) showed that 97.5 % of arsenic leaching from the soil is As(V) and 2.5% is As (III) without the presence of methylated forms of arsenic. In this experiment, soil was contaminated initially with pentavalent arsenic (As_2O_5) in the wood preservative, but certain conditions were favorable and allowed its reduction to trivalent arsenic. It is generally recognized that arsenate is the major species present in oxidized acidic environment, while in reducing and alkaline conditions, arsenite becomes significant (Sadiq et al., 1983; Peters et al., 1996). In this study because of the soil alkaline environment (pH 7.6) conditions which are favorable for reduction of arsenate to arsenite, a small percentage (2.5%) of arsenate was reduced to arsenite. In the case of field soils, some authors found As(III) in large proportions even in conditions theoretically favorable to the presence of As(V) (Balasoiu et al., 2001). For example, in acidic soils (average pH of 5.3)

contaminated by mine tailings, Bowell et al. (1994) found that arsenite was present in a large proportion in aerobic soils (up to 45% of total arsenic) and it was the major species in anaerobic soils (79% of total arsenic).

Generally, the precise mechanisms controlling the reduction in soils are poorly understood. According to Bowell et al. (1994), the reduction of As(V) to As(III) is predominantly chemically controlled in both aerobic and anaerobic soils, although Pongratz (1998) and McGeehan and Naylor (1994) reported that this reduction can occur as a result of biotic processes. In this study, the soil alkaline environment and biota activities may have attributed to reduction of this small percentage of arsenate to arsenite.

5.10 Comparison of the results of this study with similar work

Applying nanoparticles is one of the newest and innovative treatment approaches that recently has been tried in many contaminated sites across the word especially in North America. Research is being performed to introduce new nanoparticles for this purpose or to optimize the conditions leading to a better performance. In this research starch stabilized Fe/Cu nanoparticles were synthesized and used to immobilize arsenic in a chromated copper arsenate (CCA) contaminated soil which was from a contaminated site in Quebec. In Table 5-5 the result of this experiment has been compared with two similar studies (due to limited number of research in this context, just these two studies with all required information were found). It should be noticed that some factors like the soil condition and elemental composition, source of contamination or presence of other contaminants make this comparison difficult. Although for all these three nanoparticles, the conditions of experiments are different, they all show a good arsenic removal efficiency from the water leaching from the soil matrix, proving the possibility of arsenic immobilization in soil matrix. The soil used for the present study is the most contaminated in comparison with other studies. However as the soil is actually contaminated and due to formation of strong bonds with arsenic and soil components, the water leachable part is considerably lower.

Table 5-5: Comparison of the result of this study with similar work

Nanoparticle	Langmuir adsorption capacity (mg/g)	pH	Type of soil	Source of contamination	Soil As concentration (mg/kg)	Form of As in soil	Water leaching As concentration (µg/L)	Removal percentage
CMC stabilized Fe-Mn (An and Zhao, 2012)	272 (As V)/338 (As III)	5.5	Sand	Spiking in lab	103.5	As(III)	3800	91
Starch stabilized magnetite (Liang and Zhao, 2014)	62.1 (As V)	6.8	Sand	Spiking in lab	31.45	As (V)	2200	98
This study	126.6 (As V)/90.1 (As III)	7	Loam	CCA (from a contaminated site)	120.6	As (V)	59	90

It should be noted many of the remediation projects using nanoparticles are just beginning or ongoing and as a result cost and performance data are limited. However, using nanoparticles for environmental decontamination in comparison to other methods of site remediation has such advantages like extending the range of treatable contaminants, improving the extent and speed of contaminant destruction and compatibility with other treatments methods. In addition there will not be any production of waste, energy requirements, undesirable byproducts or long term monitoring requirements. The main concern is the possibility of contaminants migration along with nanoparticles to other parts of the area. However as the particles eventually will adsorb in the subsurface environment and the contaminants already have been removed from the liquid phase, there would not be also a problem in this context.

Chapter 6

Conclusions, contributions to knowledge and suggestions for further research

6.1 Summary and conclusions

In this PhD thesis, simple chemical reduction methods were used to produce iron/copper nanoparticles for the removal of As(III) and As(V) from water, as well as to immobilize arsenic in the soil matrix. In order to investigate the nanoparticle size effects for water experiments iron/copper nanoparticles were synthesized using two different protocols, resulting in two different sizes of particles. To use the nanoparticles in a soil environment, nanoparticles were stabilized with a water soluble starch. A comprehensive physicochemical characterization of the nanoparticles was performed using XRD, TEM, BET and XPS techniques. To examine the adsorption capacity and kinetics, and the effect of different parameters (dose of nanoparticles and initial concentration of arsenic on adsorption, pH, competing ions, desorption possibility and etc.) for aqueous solutions batch experiments were performed.

To gauge the ability of starch-stabilized nanoparticles in immobilizing arsenic in the soil environment, nanoparticles were synthesized with various concentrations of starch and their physiochemical characteristics were examined. The physical and chemical properties of the contaminated soil were determined to create a soil profile. In order to elucidate the

transportability and effect of starch stabilized Fe/Cu nanoparticles on adsorption and immobilization of arsenic in the chromated copper arsenate contaminated soil, batch and column tests were performed as well as toxicity characteristic leaching procedure (TCLP) test to see the possibility of leaching in landfill conditions. Finally, a selective sequential extraction procedure was conducted to elucidate the partitioning of arsenic in different fractions of soil and the effect of nanoparticle treatment on it.

Characterization of nanoparticles resulting from the first method of synthesis indicated that all nanoparticles had a crystalline phase with a core-shell structure. The mean diameter of nanoparticles was 13.17 nm and they were uniform in size and shape. The mean diameter of nanoparticles resulting from the second method was calculated as 27.15 nm. Results demonstrated that arsenic can be removed by adsorption on Fe/Cu nanoparticles of both methods at concentrations typical of contaminated ground waters, and with an increase in the dose of nanoparticles, the removal efficiency would be enhanced.

Adsorption isotherms fit well into the Langmuir equation and the maximum sorption capacity for As(III) and As(V) were 19.68 mg/g and 21.32 mg/g, respectively, at pH 7.0 for the first nanoparticle, and 5.55 mg/g and 10.41 mg/g for As(III) and As(V), respectively, for the second nanoparticle. As the nanoparticles resulting from the first method showed higher adsorption capacity, for following experiments only this nanoparticle was used.

For this nanoparticle, sorption follows pseudo-second-order kinetics with adsorption occurring in the first 15 for As(V) and the first 30 minutes for As(III). The result of competing ions experiments showed that coexisting HCO_3^- , SO_4^{2-}, and PO_4^{3-} had little influence on arsenic adsorption at initial concentrations equal to As concentration. The pH effect experiments revealed that acidic conditions were favored for arsenic adsorption and desorption of arsenic from this nanoparticle would occur in alkaline environments. To elucidate the adsorption mechanism, XPS spectra before and after arsenic adsorption were examined and this revealed that arsenic was adsorbed on the surface of Fe/Cu nanoparticles by incorporating into the inner sphere surface complexes.

Based on transport studies, for the immobilization of arsenic in chromated copper arsenate contaminated soil, 0.04 wt.% starch stabilized Fe/Cu nanoparticles were used. The

Langmuir adsorption isotherm was fitted and showed a maximum sorption capacity of 90.1 mg/g for As(III) and 126.58 mg/g for As(V) at pH 7.0 from arsenic aqueous solutions.

The physiochemical characterization of the contaminated soil showed that the soil has a loamy texture with 120.4 mg/kg contamination of arsenic. Column breakthrough tests and elution profiles demonstrated the mobility of the starch stabilized nanoparticles (0.04 wt.%) with 15% of the nanoparticles were retained in the soil bed.

Starch-stabilized Fe/Cu nanoparticles were highly effective for immobilization of arsenic in the CCA contaminated loamy soil. When the soil was treated in batch experiments with nanoparticles (0.4 g/L) at a soil to liquid ratio of 0.1, the water leachable arsenic was reduced from 50 µg/L to 4.23 µg/L and the TCLP leachability of arsenic was reduced by 98%. Column elution tests indicated that application of starch stabilized Fe/Cu suspension transferred nearly all water-soluble arsenic to the nanoparticle phase. As a result, arsenic can become immobilized in the soil bed as the nanoparticles are immobilized in the soil matrix. The TCLP leachability of arsenic remaining in the soil was reduced by 70%. The result of selective sequential extraction revealed that nanoparticles are able to remove all arsenic presented in water soluble and leachable fractions as well as 47 % of the arsenic associated with carbonate fraction.

Overall, the Fe/Cu nanoparticles have potential for ex-situ as well as in-situ remediation of arsenic, already present in soil or groundwater.

6.2 Contribution to Knowledge

In general, the findings of this research study will be important in improving and developing the use of nanoparticles as a new class of adsorbents for removal of arsenic from contaminated waters or immobilization of arsenic in contaminated soils. Use of nanoparticles for arsenic remediation can be applied as an environmentally friendly remedial option to reduce arsenic concentration in aquatic environments and avoid further contamination of groundwater by immobilizing the compound in contaminated soils.

Specifically this research contributes to scientific knowledge in the following aspects:

- Demonstrates the feasibility of using Fe/Cu nanoparticles for the removal of arsenic from aqueous solutions for the first time.
- Demonstrates the effect and importance of nanoparticle size and specific surface area on adsorption.
- Elucidates the effect of nanoparticle dose and initial arsenic concentration on the adsorption process.
- Identifies the role of coexisting ions in aqueous solutions on arsenic adsorption by Fe/Cu nanoparticles.
- Determines the effect of pH on arsenic adsorption by this nanoparticle and the conditions that could lead to desorption of adsorbed arsenic.
- Demonstrates the mechanism of arsenic adsorption by Fe/Cu nanoparticles
- Investigates the possibility of arsenic immobilization in a chromated copper arsenate contaminated soil. As a result, prevention of leaching to groundwater by starch stabilized Fe/Cu nanoparticles for the first time.
- Examines the effect of starch concentration on nanoparticle size, stability, and transportability in soil environment.
- Determines the percentage of arsenic in different fractions of contaminated soil by performing selective sequential extraction procedure and elucidating the effect of nanoparticles on change of arsenic concentration in different fractions for the first time.

6.3 Future research

Based on the experiments performed for this research work and results obtained, the following research directions and experiments are recommended:

- After arsenic adsorption by nanoparticles, arsenic speciation should be performed on the solid phase to examine the redox reactions. This speciation can help to have a better understanding of the adsorption mechanism.
- The possibility of reuse of nanoparticles under real situations should be examined and pilot studies should be performed.
- The effect of different parameters such as nanoparticle concentration and injection velocity should be examined on nanoparticle transportability and effectiveness of arsenic removal in the subsurface environment.
- The environmental fate and impact of starch stabilized Fe/Cu nanoparticles on arsenic contaminated soil should be determined by examining some factors such as pH, ORP, DO and microbial community in soil over a period of time.
- The changes in adsorption capacity of nanoparticles in subsurface environment due to aging should be examined over a long period of time.
- A cost analysis needs to be performed in order to justify the economic feasibility of nanoparticles for adsorption process.

References

Adeniji, A. 2004. Bioremediation of Arsenic, Chromium, Lead, and Mercury. USEPA. Office of Solid Waste and Emergency Response Technology Innovation Office, Washington, DC, www.clu-in.org

Ahamed, S., Sengupta, M. K., Mukherjee, A., Amir Hossain, M., Das , B., Nayak, B., Pal, A., Mukherjee, S. C., Pati, S., Dutta, R. N., Chatterjee, G., Mukherjee, A., Srivastava, R., Chakraborti, D. 2006. Arsenic groundwater contamination and its health effects in the state of Uttar Pradesh (UP) in upper and middle Ganga plain, India: A severe danger. *Science of the Total Environment*, 370, 310–322.

Allen, S.J., Mckay, G., Porter J.F. 2004. Adsorption Isotherm Models for Basic Dye Adsorption by Peat in Single and Binary Component Systems. *Journal of Colloid Interface Science*. 280, 322–333.

Altavilla, C.& Ciliberto, E. 2011. Inorganic Nanoparticles. Boca Raton, Florida: CRC Press.

Arai, Y., Sparks, D.L. 2001. ATR-FTIR spectroscopic investigation on phosphate adsorption mechanisms at the ferrihydrite-water interface, *Journal of Colloid and Interface Science*, 241, 317-326.

An, B., Steinwinder, T.R., Zhao, D.Y. 2005. Selective removal of arsenate from drinking water using a polymeric ligand exchanger. *Water Research*. 39, 4993–5004.

An, B., Zhao, D. 2012. Immobilization of As(III) in Soil and Groundwater Using a New Class of Polysaccharide Stabilized Fe–Mn Oxide Nanoparticles. *Journal of Hazardous Materials,* 212, 332– 341.

Aschengrau, A., Zierler, S., Cohen, A. 1989. Quality of Community Drinking Water and the Occurrence of Spontaneous Abortion. *Archives of Environmental Health*, 44,283 -290.

Azcue, J.M. and Nriagu, J.O. 1994. Arsenic: Historical Perspectives. In: Arsenic in the Environment, Part I: Cycling and Characterization, Edited by J.O. Nriagu. John Wiley and Sons, Inc. New York, NY. 1-16.

Balasoiu, C. F., Zagury, G. J., Deschenes, L. 2001. Partitioning and Speciation of Chromium, Copper, and Arsenic in CCA-contaminated Soils: influence of soil composition. *The Science of the Total Environment*, 280, 239-255.

BCMWLAP (Ministry of Water, Land, and Air Protection, Province of British Columbia). 2002. Arsenic in Groundwater Well stewardship information series, BC.

Blowes, D.W.,Ptacek, C. J.,Benner, S. G., McRae, C. W.T., Bennett, T. A.,Puls, R. W. 2000.Treatment of Inorganic Contaminants Using Permeable Reactive Barrier. *Journal of Contaminant Hydrology*, 45, 123–137.

Boparai , H. K.,Joseph, M.,O'Carroll D. M. 2011.Kinetics and Thermodynamics of Cadmium Ion Removal by Adsorption onto NanoZerovalent Iron Particles. *Journal of Hazardous Materials*, 186, 458–465.

Bowell, R.J., Morley, N.H., Din, V.K. 1994. Arsenic Speciation in Soil pore Waters from Ashanti mine, Ghana, *Applied Geochemistry*, 9, 15-22.

Cao, J.,Xu , R., Tang , H., Tang , S., Cao , M. 2011. Synthesis of Monodispersed CMC-stabilized Fe–Cu Bimetal Nanoparticles for in Situ Reductive Dechlorination of 1, 2, 4-trichlorobenzene. *Science of the Total Environment*, 409, 2336–2341.

Canadian Council of Ministers of the Environment. 1999. Canadian soil quality guidelines for the protection of environmental and human health: Chromium (total 1997) (VI 1999). In: Canadian environmental quality guidelines, 1999, Canadian Council of Ministers of the Environment, Winnipeg.

CED (Environmental Defence Canada). 2003. Arsenic Lurks in Canadian Playgrounds: Is Your Child Safe? Toronto, ON, Canada: Environmental Defence Canada.

Chakraborti, D., Mukherjee, S. C., Pati, S., Sengupta, M. K. Rahman Uttam M. M., Chowdhury, K., Lodh, D., Chanda, C. R., Chakraborti, A.K. and Basu, G. K. 2003. Arsenic

Groundwater Contamination in Middle Ganga Plain, Bihar, India: A Future Danger?. *Environmental Health Perspectives*, 111 (9) 1194-1201.

Chandra, V., Park, J., Chun, Y., Woo Lee, J., Hwang, I.C., Kim, K.S. 2010. Water-Dispersible Magnetite-Reduced Graphene Oxide Composites for Arsenic Removal. *ACS Nano.* 4 (7), 3979–3986.

Chen, H.W., Frey, M.M., Clifford, D., McNeil, L.S., Edwards, M. 1999. Arsenic treatment considerations, *American Water Works Association*, 91: 74–85

Cheng, R., Wang , J-l., Zhang,W-X. 2007. Comparison of reductive dechlorination of p-chlorophenol using Fe0 and nanosized Fe0. *Journal of Hazardous Materials,* 144, 334–339.

Cheng, W., Xu, J., Wang, Y., Wu, F., Xu, X., Li. J.2015. Dispersion–precipitation synthesis of nanosized magnetic iron oxide for efficient removal of arsenite in water. *Journal of Colloid and Interface Science*, 445, 93–101.

Choe, S., Lee, S.H., Chang, Y.Y., Hwang, K.Y., Khim, J. 2001 Rapid Reductive Destruction of Hazardous Organic Compounds by Nanoscale Fe^0, *Chemosphere*, 42: 367–372.

Choi, W.H., Lee, S. R., Park, J. Y. 2009. Cement Based Solidification/Stabilization of Arsenic Contaminated Mine Tailings. *Waste Management*, 29, 1766–1771.

Choong,T., Chuah, T.G., Robiah, Y., Gregory Koay, F.L., Azni, I. 2007. Arsenic Toxicity, Health Hazards and Removal Techniques from Water: an Overview. *Desalination*, 217, 139–166.

Chowdhury, S. R., Yanful, E. K., Pratt, A. R. 2011. Arsenic removal from aqueous solutions by mixed magnetite–maghemite nanoparticles. *Environmental Earth Sciences.* 64 (2): 411-423.

Cullen, W.R., Reimer, K.J. 1989. Arsenic speciation in the environment. *Chemical Reviews,* 89, 713– 64.

Ding, M., Jong, B.H.W.S., Roosendaal, S.J., Vredenberg, A. 2000. XPS studies on the electronic structure of bonding between solid and solutes: Adsorption of arsenate, chromate,

phosphate, Pb21, and Zn21 ions on amorphous black ferric oxyhydroxide. *Geochimica et Cosmochimica Acta*, Vol. 64, No. 7, pp. 1209–1219.

Dixit, S., Hering, J.G. 2003. Comparison of arsenic(V) and arsenic(III) sorption onto iron oxide minerals: implications for arsenic mobility. *Environmental Science & Technolgy*, 37, 4182–4189.

Elliott, D.W., & Zhang, W. 2001. Field Assessment of Nanoscale Bimetallic Particles for Groundwater Treatment. *Environmental Science & Technology,* 35, 4922-4926.

Elliott, D.W., Lien, H-L., Zhang, W-X. 2009. Degradation of lindane by zero-valent iron nanoparticles, *Journal of Environmental Engineering*, 135, 317–324.

Environment Canada. 1990. Results from Inhalable Particulate Matter (PM10) Sampling Network (1984–1987) PMD-90-3 Ottawa, Canada.

Environment Canada. 1996. Canadian Soil Quality Guidelines for Arsenic: Environmental and Human Health Supporting document, Final draft Ottawa, Canada.

EPA-902-B-94-001. 1994. Technical Assistance Document for Complying with the TC rule and Implementing the Toxicity Characteristic Leaching Procedure (TCLP). United States Environmental Protection Agency, Region 2, RCRA Outreach Program, http://nepis.epa.gov/Exe/ZyPDF.cgi/P1007NTD.PDF?Dockey=P1007NTD.PDF

EPA-815-D00-001. 2000. Arsenic Occurrence in Public Drinking water Supplies, *Office of water (4607), Washington*, D.C. 20460.

EPA-542-R-02-004. 2002. Arsenic Treatment Technologies for Soil, Waste, and Water, Solid Waste and Emergency Response, (5102G) www.epa.gov/tioclu-in.org/arsenic.

EPA/600/R-09/148. 2009. Technology Performance Review: Selecting and Using Solidification/Stabilization Treatment for Site Remediation, National Risk Management Research Laboratory, Office of Research and Development, U.S. Environmental Protection Agency, Cincinnati, OH 45268, http://www.epa.gov/nrmrl.

Evanko, C. R., Dzombak, D. A. 1997. Remediation of Metals-Contaminated Soils and

Groundwater" Technology Evaluation Report, TE-97-01, Available at: Homepage: http://www.gwrtac.org.

Ferguson, J.E., Gavis, J. 1972. A Review of the Arsenic Cycle in Natural Waters. *Water Research*, 6, 1259-1274.

Freundlich, H.M.F. 1906. Over the Adsorption in Solution, *Journal of Physical Chemistry*, 57, 385–471.

Foo, K.Y., Hameed, B.H. 2010. Insights into the Modeling of Adsorption Isotherm Systems. *Chemical Engineering Journal*, 156, 2–10.

Gavaskar, A. R., Gupta, N., Sass, N. M., Janoy, R. J., O'Sullivan, D. 1998. Permeable Barriers for Goundwater Remediation—Design, Construction, and Monitoring, Battelle Memorial Institute, Columbus, OH.

Ghimirea, K.N., Inouea, K., Yamaguchia, H., Makinob, K., Miyajimaa, T. 2003. Adsorptive Separation of Arsenate and Arsenite Anions from Aqueous Medium by using Orange Waste. *Water Research*, 37, 4945–4953.

Goffinet, C.J., Mason, S.E. 2012. Comparative DFT study of inner-sphere As(III) complexes on hydrated a-Fe2O3(0001) surface models. *Journal of Environmental Monitoring*, 14, 1860-71.

Goswami, A., Raul, P.K., Purkait, M.K. 2012. Arsenic adsorption using copper (II) oxide nanoparticles. *Chemical Engineering Research and Design,* 90(9), 1387-1396.

Gu, B., Phelps, T. J., Liang, L., Dickey, M. J., Roh, Y., Kinsall, B. L., Palumbo, A. V., Jacobs, G. K. 1999. Biogeochemical Dynamics in Zero-Valent Iron Columns: Implications for Permeable Reactive Barriers. *Environmental Science & Technology*, 33, 2170–2177.

Hall, K.R., Eagleton, L.C., Acrivos, A., Vermeulen, T., 1966. Pore-and Solid-diffusion Kinetics in Fixed-bed Adsorption under Constant-pattern Conditions. *Industrial & Engineering Chemistry Fundamentals* , 5, 212–223.

Hartley, W., Edwards, R., Lepp, N.W. 2004. Arsenic and heavy metal mobility in iron oxide-amended contaminated soils as evaluated by short- and long-term leaching test. *Environmental. Pollution*, 131,495–504.

Health Canada (2014). Guidelines for Canadian Drinking Water Quality—Summary Table. Water and Air Quality Bureau, Healthy Environments and Consumer Safety Branch, Health Canada, Ottawa, Ontario

Health Canada (2014). Guidelines for Canadian Drinking Water Quality—Summary Table. Water and Air Quality Bureau, Healthy Environments and Consumer Safety Branch, Health Canada, Ottawa, Ontario.

Health Canada .2012.Guidelines for Canadian Drinking Water Quality—Summary Table. Water, Air and Climate Change Bureau, Healthy Environments and Consumer Safety Branch, Health Canada, Ottawa, Ontario.

He, F., and Zhao, D. 2005. Preparation and Characterization of a New Class of Starch-Stabilized Bimetallic Nanoparticles for Degradation of Chlorinated Hydrocarbons in Water. *Environmental Science & Technology*., 39, 3314-3320.

He, F., Zhang, M., Qian, T.W., Zhao, D.Y. 2009. Transport of carboxymethyl cellulose stabilized iron nanoparticles in porous media: column experiments and modeling. *J. Colloid Interf. Sci*, 334, 96–102.

Hoch, L. B., Mack, E. J., Hydutsky, B. W., Hershman, J. M., Skluzacek, I. M., Mallouk, T. E. 2008. Carbothermal synthesis of carbon-supported nanoscale zero-valent iron particles for the remediation of hexavalent chromium. *Environmental Science and Technology*, 42, 2600–2605.

Hopenhayn-Rich, C., Browning, S.R., Hertz-Picciotto, I., Ferreccio, C., Peralta, C., and

Gibb, H. 2000. Chronic Arsenic Exposure and Risk of Infant Mortality in Two Areas of Chile .*Environmental Health Perspectives*, 108, 667-673.

Hosseini, M. S., Ataie-Ashtiani,B., Kholghi, M. 2011. Nitrate Reduction by Nano-Fe/Cu Particles in Packed Column. *Desalination*, 276, 214–221.

IPCS .2001. Arsenic and arsenic compounds, 2nd ed. Geneva, World Health Organization, International Program on Chemical Safety (Environmental Health Criteria 224; http://whqlibdoc.who.int/ehc/WHO_EHC_224.pdf.

Ignatow, A., McCutcheon, W., Hoskin, W., Fong, D., Koren, E. 1991. Specialty Metals: Arsenic. In: Canadian minerals yearbook 1990: Review and outlook. Mineral Report 39. Energy, Mines and Resources Canada, Ottawa.

Jadia, C.D., Fulekar, M.H. 2009. Phytoremediation of Heavy Metals: Recent Techniques. *African Journal of Biotechnology*, 8(6), 921-928.

Jang, M., Hwang, J.S., Choi, S. I., Park, J. K. 2005. Remediation of Arsenic-Contaminated Soils and Washing Effluents. *Chemosphere*, 60, 344–354.

Kanel, R.S., Manning, B., Charlet, L., Choi,H. 2005. Removal of Arsenic (III) from Groundwater by NanoscaleZero-Valent Iron. *Environmental Science Technology*, 39, 1291-1298.

Karn, B., Kuiken, T., Otto, M. 2009. Nanotechnology and in Situ Remediation: A Review of the Benefits and Potential Risks, *Environmental Health Perspectives*, 117(12): 1823-1831.

Keil, P., Lützenkirchen-Hecht, D., Frahm, R.2006. Investigation of Room Temperature Oxidation of Cu in Air by Yoneda-XAFS. *AIP Conference*, 9-14 July 2006, Stanford, California (USA).

Khin, M.M., Sreekumaran Nair, A., JagadeeshBabu,V., Murugan, R., Ramakrishna, S. 2012. A Review on Nanomaterials for Environmental Remediation. *Energy & Environmental Science*, 5, 8075–8109.

Kim, H.J., Phenrat T., Tilton, R. D., Lowry, G. V. 2012. Effect of Kaolinite, Silica Fines and pH on Transport of Polymer-modified Zero Valent Iron Nano-particles in Heterogeneous Porous Media. *Journal of Colloid and Interface Science,* 370, 1–10.

Klaine, S. J., Alvarez, P. J. J., Batley, G. E., Fernandes, T. F., Handy, R. D., Lyon, D. Y., Mahendra, S., McLaughlin, M. J., Lead, J. R. 2008. Nanomaterials in the environment:

Behavior, fate, bioavailability, and effects, *Environmental Toxicology and Chemistry*, 27(9), 1825–1851.

Klimkova, S., Cernik, M., Lacinova, L., Filip, J., Jancik, D. 2011. Zero-valent Iron Nanoparticles in Treatment of Acid mine Water from In situ Uranium Leaching, *Chemosphere*, 82, 1178–1184.

Kretzschmar, R., Borkovec, M., Grolimund, D., Elimelech, M. 1999. Mobile subsurface colloids and their role in contaminant transport. *Advances in Agronomy*, 66, 121–193.

Kubicki, J.D., Kwonk, D., Paul,W., Sparks, D.L. 2007. Surface complex structures modelled with quantum chemical calculations: carbonate, phosphate, sulphate, arsenate and arsenite European Journal of Soil Science. *European Journal of Soil Science*, 58, 932−944.

Kuo, C.H., Chen, C.H., Huang, M.H. 2007. Seed-Mediated Synthesis of Monodispersed Cu_2O Nanocubes with Five Different Size Ranges from 40 to 420 nm, *Advanced Functional Materials,* 17, 3773–3780.

Lagergren, S. 1898. Zur theorie der sogenannten adsorption geloster stoffe, Kungliga Svenska Vetenskapsakademiens. *Handlingar,* 24 (4): 1−39.

Li, X., Elliott, D. W., Zhang, W. 2006. Zero-Valent Iron Nanoparticles for Abatement of Environmental Pollutants: Materials and Engineering Aspects. *Critical Reviews in Solid State and Materials Sciences,* 31:4, 111-122.

Li, X-Q., Zhang,W-X. 2007. Sequestration of Metal Cations with Zerovalent Iron Nanoparticles - A Study with High. Resolution X-ray Photoelectron Spectroscopy (HR-XPS). *Journal of PhysicalChemistry*, C 111, 6939-6946.

Liang, Q.Q., Zhao, D.Y., Qian, T.W., Freeland, K., Feng, Y.C. 2012. Effects of stabilizers and water chemistry on arsenate sorption by polysaccharide-stabilized magnetite nanoparticles, *Industrial and Engineering Chemistry Research*, 51, 2407–2418.

Liang, W., Dai, C., Zhou, X., Zhang, Y. 2014. Application of Zero-Valent Iron Nanoparticles for the Removal of Aqueous Zinc Ions under Various Experimental Conditions. PLoS ONE 9(1): e85686. doi:10.1371/journal.pone.0085686.

Liang, Q., and Zhao, D., 2014. Immobilization of arsenate in a sandy loam soil using starch-stabilized magnetite nanoparticles. *Journal of Hazardous Materials*. 271, 16–23.

Lien, H-L., Wilkin, R.T. 2005. High-level Arsenite Removal from Groundwater by Zerovalent Iron. *Chemosphere*, 59, 377–386.

Limousin, G., Gaudet, J.P., Charlet, L., Szenknect, S., Barthes, V., Krimissa, M. 2007. Sorption Isotherms: A Review on Physical Bases, Modeling and Measurement. *Applied Geochemistry*. 22, 249–275.

Lin, S., Lu, D., Liu. Z. 2012. Removal of arsenic contaminants with magnetic ɤ-Fe2O3 nanoparticles. *Chemical Engineering Journal,* 211–212, 46–52.

Liou, Y.H., Lo, S.L., Lin, Ch. J., Kuan, W.H., Weng, Sh.Ch. 2005. Chemical reduction of an unbuffered nitrate solution using catalyzed and uncatalyzed nanoscale iron particles. *Journal of Hazardous Material*. 127, 102–110.

Liu, C.H., Chuang, Y.H., Chen, T.Y., Tian, Y., Li, H., Wang, M.K., Zhang, W. 2015 .Mechanism of Arsenic Adsorption on Magnetite Nanoparticles from Water: Thermodynamic and Spectroscopic Studies. *Environmental Science and Technology*, 49 (13), 7726–7734.

López-Téllez, G., Barrera-Díaz, C. E., Balderas-Hernández, P., Roa-Morales, G., Bilyeub,B. 2011. Removal of Hexavalent Chromium in Aquatic solutions by Iron Nanoparticles Embedded in Orange peel pith. *Chemical Engineering Journal*, 173, 480–485.

Mance, G., Musselwhite, C., Brown, V. M. 1984. Proposed Environmental Quality Standards for List II substances in water: Arsenic. TR 212. Prepared for the Department of the Environment (DoE). Medmenham, Buckinghamshire: WRc.

Maharjan, M., Watanabe, C., Aktar Ahmad, S.K., Ohtsuka, R., 2005. Short Report: Arsenic Contamination in Drinking Water and Skin Manifestations in Lowland Nepal: the First

Community-Based Survey. *American Journal of Tropical Medicine and Hygiene*, 73(2), 477-479.

Manning, B.A., Fendorf, S.E., Goldberg, S. 1998. Surface Structures and Stability of Arsenic(III) on Goethite: Spectroscopic Evidence for Inner-Sphere Complexes. *Environmental Science and Technology,* 32, 2383-2388.

Martinson, C. A., Reddy, K.J. 2009. Adsorption of Arsenic (III) and Arsenic (V) by Cupric oxide Nanoparticles. *Journal of Colloid and Interface Science*, 336, 406–411.

Matschullat, J. 2000. Arsenic in the Geosphere - A Review. *The Science of the Total Environment*, 249, 297-312.

McGeehan, S.L., Naylor, D.V. 1994. Sorption and Redox Transformation of Arsenite and Arsenate in Two Flooded Soils. *Soil Science Society of America Journal,* 58, 337-342.

Mohana, D., Charles, U., Pittman, J.R. 2007. Arsenic Removal from Water/Wastewater using Adsorbents— A Critical Review. *Journal of Hazardous Materials*, 142, 1–53.

Mondal , K.,Jegadeesan , G., Lalvani, S. B.2004. Removal of Selenate by Fe and NiFeNanosized Particles. *Industrial & Engineering Chemistry Research*, 43, 4922–4934.

Morales-Luckie, R. A., Sanchez-Mendieta, V., Arenas-Alatorre, J. A., López-Castañares, R., Perez-Mazariego, J.L., Marquina-Fabrega, V., Wayne Gómez, R. 2008. One-step aqueous synthesis of stoichiometric Fe–Cu nanoalloy. *Materials Letters*, 62, 4195–4197.

Mosaferi, M., Nemati, S., Khataee, A., Nasseri, S., Asl Hashemi, A. 2014. Removal of Arsenic (III, V) from aqueous solution by nanoscale zero-valent iron stabilized with starch and carboxymethyl cellulose. *Journal of Environmental Health Science & Engineering,* 12:74.

Mulligan, C.N., Yong, R.N., Gibbs, B.F., 2001. Remediation Technologies for Metal Contaminated Soils and Groundwater: an Evaluation. *Engineering Geology*, 60, 193-207.

National Research Council (NRC). 1999. Arsenic in Drinking Water. National Academy Press. Washington, D.C. pp. 310

Nimic, D.A., Moore, J.N., Dalby, C.E., and Savaka, M.M. 1998. The Fate of Geothermal Arsenic in the Madison and Missouri Rivers, Montana and Wyoming. *Water Research*, 34(11), 3051-3067.

O'Carroll, D., Sleep, B., Krol, M., Boparai, H., Kocur, C. 2013. Nanoscale zero valent iron and bimetallic particles for contaminated site remediation. *Advances in Water Resources.* 51, 104–122.

O'Neill, P. 1990. Arsenic. In "Heavy Metals in Soils" (B. J. Alloway, ed.), pp. 83-99.Blackie. London.

O ′ Reilly, S.E., Strawn, D.G., Sparks, D.L.2001. Residence time effects on arsenate adsorption/desorption mechanisms on goethite, *Soil Science Society of America Journal,* 65, 67-77.

Ollson, C.C. 1999. Arsenic Contamination of the Terrestrial and Freshwater Environment Impacted by Gold Mining Operations Yellowknife, NWT. MEng. Thesis, Royal Military College of Canada, Kingston, Canada.

Peng, S., and Sun, S. 2007. Synthesis and Characterization of Monodisperse Hollow Fe3O4 Nanoparticles. *Angwandte chemie*, 119, 4233 –4236.

Peters, G.R., McCurdy, R.F., Thomas, J., Hindmarch, J.T. 1996. Environmental Aspects of Arsenic Toxicity. *Critical Reviews in Clinical Laboratory Sciences*, 33,457-493.

Petosa, A.R., Jaisi, D.P., Quevedo, I.R., Elimelech.M., Tufenkji. N., 2010. Aggregation and Deposition of Engineered Nanomaterials in Aquatic Environments: Role of Physicochemical Interactions. *Environmental Science and Technology*, 44, 6532–6549.

Phenrat, T., Saleh, N., Sirk, K., Kim, H. J., Tilton, R. D., Lowry, G. V. 2008. Stabilization of aqueous nanoscale zerovalent iron dispersions by anionic polyelectrolytes: adsorbed anionic polyelectrolyte layer properties and their effect on aggregation and sedimentation. *Journal of Nanoparticle Research*, 10 (5), 795–814.

Pillewan, P., Mukherjee, S., Roychowdhury, T., Das, S., Bansiwal, A., Rayalu, S. 2011. Removal of As(III) and As(V) from water by copper oxide incorporated mesoporous alumina. *Journal of Hazardous Materials*, 186, 367–375.

Pongratz, R. 1998. Arsenic Speciation in Environmental Samples of Contaminated Soil. *Science of the Total Environment*, 224,133-141.

Qian, Y., Ye, F., Xu, J., Le, Z.G. 2012. Synthesis of Cuprous Oxide (Cu_2O) Nanoparticles/Graphene Composite with an Excellent Electrocatalytic Activity Towards Glucose. *International Journal of Electrochemical Science*, 7, 10063 – 10073.

Raj Kanel, S., Manning, B., Charlet, L., Choi,H. 2005. Removal of Arsenic (III) fromGroundwater by NanoscaleZero-Valent Iron. *Environmental Science Technology*, 39, 1291-1298.

Ravenscroft, P., Brammer, H., Richards, K. 2009. Arsenic Pollution. Wiley-Blackwell, A John Wiley & Sons, Ltd, Publication.

Raveendran, P., Fu, J., Wallen, S. L. 2003. Complete "Green" Synthesis and Stabilization of Metal Nanoparticles. *J. Am. Chem. Soc.,* 125, 13940-13941.

Reddy, K.J., McDonald, K.J., King, H. 2013. A Novel Arsenic Removal Process for Water Using Cupric oxide Nanoparticles. *Journal of Colloid and Interface Science*, 397, 96–102.

Reddy, K.J. 2007. Method for removing arsenic from water, U.S. Patent 7,235,179.

Reese, R.G. 1998. Arsenic In: United States Geological Survey Minerals Yearbook, Fairfax, VA.

Reese, R.G. 1999. Arsenic In: United States Geological Survey Minerals Commodities Summeries, Fairfax, VA.

Rhine, E.D., Phelps, C.D., Young, L.Y. 2006. Anaerobic Arsenite Oxidation by Novel Denitrifying Isolates. *Environmental Microbiology*, 8,899–908.

Sadiq, M., Zaidi, T.H., Mian, A.A. 1983. Environmental Behavior of Arsenic in Soils: Theoretical. *Water Air Soil Pollution*, 20, 369-377.

Saleh, N., Sirk, K., Liu, Y. et al. 2007. Surface modifications enhance nano iron transport and NAPL targeting in saturated porous media. *Environmental Engineering Science*. 24(1): 45-57.

Satterfield, C. N. 1991. Heterogeneous Catalysis in Industrial Practice, second ed. McGraw-Hill, Inc., New York, NY.

Scherer, M.M., Richter, S., Valentine, R.L., Alvarez, P.J. 2000. Chemistry and Microbiology of Permeable Reactive Barriers for In Situ Groundwater Clean up. *Critical Reviews in Microbiology*, 26(4), 221-64.

Schrick B., Hydutsky B.W., Blough, JL., 2004. Delivery vehicles for zerovalent metal nanoparticles in soil and groundwater. *Chemistry of Materials*. 16(11):2187-2193.

Shah, K., Nongkynrih, J.M. 2007. Metal Hyperaccumulation and Bioremediation. *BiologiaPlantarum*, 51 (4), 618-634.

Shih, M.C. 2005. An Overview of Arsenic Removal by Pressure Driven Membrane Processes. *Desalination*, 172, 85-97.

Silver. S., Phung, L.T. 2005. Genes and Enzymes Involved in Bacterial Oxidation and Reduction of Inorganic Arsenic. *Applied and Environmental Microbiology*, 71: 599-608.

Sirk, K.M., Saleh, NB., Phenart T et al. 2009. Effect of adsorbed polyelectrolytes on nanoscale zerovalent iron particle attachment to soil surface models. *Environmental Science Technology*, 43:3803-3808.

Singh, N., Kumar, D., Sahu, A.P. 2007. Arsenic in the Environment: Effects on Human Health and Possible Prevention. *Journal of Environmental Biology*, 28(2), 359-365.

Smedley, P.L., Kinniburgh, D.G. 2002.A Review of the Source, Behaviour and Distribution of Arsenic in Natural Waters. *Applied Geochemistry,* 17 (5), 517-568.

Smith, E., Naidu, R., Alston, A. M. 1998. Arsenic in the Soil Environment: A Review. *Advances in Agronomy*, Volume 64. Academic Press, New York, NY, pp.149-195.

Suk, J.O., Jeen, S.W., Gillham, R.W., Gui., L. 2009. Effects of Initial Iron Corrosion Rate on Long Term Performance of Iron Permeable Reactive Barriers: Column Experiments and Numerical Simulation. *Journal of Contaminant Hydrology*, 103, 145-156.

Su, C., Puls., R.W. 1999. Kinetics of Trichloroethene Reduction by Zerovalent Iron and Tin: Pretreatment Effect, Apparent Activation Energy, and Intermediate Products. *Environmental Science and Technology*, 33, 163-168.

Tamaki, s., Frankenberger, J.R. 1992. Environmental Biochemistry of Arsenic. *Reviews of Environmental Contamination and Toxicology,* 124, 79-110.

Tuutijärvi, T., Lu, J., Sillanpää, M., Chen, G. 2009. As(V) adsorption on maghemite nanoparticles. *Journal of Hazardous Materials*, 166, 1415–1420.

Tuutijärvi, T., Repo, E., Vahala, R., Sillanpää, M., Chen, G. 2012. Effect of Competing Anions on Arsenate Adsorption onto Maghemite Nanoparticles. *Chinese Journal of Chemical Engineering,* 20(3) 505-514.

United States Environmental Protection Agency, 1998b. Locating and Estimating Air Emissions from Sources of Arsenic and Arsenic Compounds. USEPA Office of Air Quality Planning and Standards, Research Triangle Park, NC. Document No. EPA- 454- R-98-013. June 1998.

United States Environmental Protection Agency, 1999b. US EPA List of Pesticides Banned and Severely Restricted in the United States, Original U.S. Nominations to the U.N. PIC Procedure. USEPA Office of Prevention, Pesticides, and Toxic Substances. Washington, D.C. At http://www.epa.gov/oppfead1/international/piclist.htm February 1999.

U.S. EPA. 2000. Technologies and Costs for Removal of Arsenic from Drinking Water. EPA-R-00-028. Office of Water. December. http://www.epa.gov/safewater/ars/ treatments_and_costs.pdf

Üzüm, Ç., Shahwan, T., Eroğlu, A.E.,Lieberwirth, I., Scott, T.B.,. Hallam, K.R2008. Application of zero-valent iron nanoparticles for the removal of aqueous Co^{2+} ions under various experimental conditions. *Chemical Engineering Journal*, 144, 213–220.

Üzüm, Ç., Shahwan, T., Eroğlu, A.E., Hallam, K.R., Scott, T.B., Lieberwirth, I. 2009. Synthesis and Characterization of Kaolinite-supported Zero-valent Iron Nanoparticles and their Application for the Removal of Aqueous Cu^{2+} and Co^{2+} Ions. *Applied Clay Science*, 43, 172–181.

Vaclavikova, M., Gallios, G. P., Hredzak, S., Jakabsky, S., 2008. Removal of Arsenic from Water Streams: an Overview of Available. *Clean Technologies and Environmental Policy*, 10, 89–95.

Vijayaraghavan, K., Padmesh, T.V.N., Palanivelu, K., Velan, M. 2006. Biosorption of Nickel(II) Ions onto Sargassum wightii: Application of Two parameter and Three parameter Isotherm Models. *Journal of Hazardous Materials*. B133, 304–308.

Wang, S., Mulligan, C.N. 2006. Occurrence of Arsenic Contamination in Canada: Sources, Behaviour and Distribution. *Science of the Total Environment*, 366 (2-3), 701-721.

Wang, S., Mulligan, C.N. 2009. Effect of natural organic matter on arsenic mobilization from mine tailings. *Journal of Hazardous Material,* 168, 721–726.

Wang, S., Zhao, X. 2009. On the Potential of Biological Treatment for Arsenic Contaminated Soils and Groundwater. *Environmental Management,* 90, 2367–2376.

Wang, Y., Liu, W., Wanga, T., Ni, J. 2015. Arsenate adsorption onto Fe-TNTs prepared by a novel water–ethanol hydrothermal method: Mechanism and synergistic effect. *Journal of Colloid and Interface Science,* 440: 253–262.

Welch, A.H., Lico, M.S., Hughes, J. L. 1988. Arsenic in Ground Water of the Western United States. *Groundwater*, 26 (3), 333–347.

Wiesner, M. R., Bottero, J.-Y.2007. Environmental Nanotechnology; The McGraw-Hill Companies: New York, p 540.

Wu, T.H., 1976. Soil Mechanics. Allyn and Bacon, Boston.

Xu, J. F., Ji, W., Shen, Z. X., Tang, S. H. Ye, X. R., Jia, D. Z., Xin X. Q. 1999. Preparation and Characterization of CuO Nanocrystals, *Journal of Solid State Chemistry,* 147, 516-519.

Yan, W., Herzing, A.A., Kiely, C. J., Zhang, W.2010. Nanoscale zero-valent iron (nZVI): Aspects of the core-shell structure and reactions with inorganic species in water. *Journal of Contaminant Hydrology,* 118, 96–104.

Yong, R.N., Galvez-Cloutier, R., Phadungchewit, Y., 1993. Selective sequential extraction analysis of heavy-metal retention in soil. *Canadian Geotechnical Journal*, 30(5): 834-847.

Yuvakkumar, R., Elango, V., Rajendran,V., Kannan, N. 2011. Preparation and Characterization of Zero Valent Iron Nanoparticles. *Digest Journal of Nanomaterials and Biostructures,* 6, 1771-1776.

Zhan, J., Zheng, T., Piringer, G., Day, C., McPherson, G. L., Lu, Y., Papadopoulos, K., John, V. T. 2008. Transport Characteristics of Nanoscale Functional Zerovalent Iron/Silica Composites for in Situ Remediation of Trichloroethylene. *Environmental Science and Technology*, 42 (23), 8871–8876.

Zhang, W., 2003. Nanoscale Iron Particles for Environmental Remediation: An Overview. *Journal of Nanoparticle Research*, 5, 323–332.

Zhang, Y., Yang, M., Dou, X-M., He, H., Wang, D-S. 2005. Arsenate Adsorption on an Fe-Ce Bimetal Oxide Adsorbent: Role of Surface Properties. *Environmental Science & Technology*, 39, 7246–7253.

Zhang, S., Li, X., Chen, J. P. 2010. An XPS study for mechanisms of arsenate adsorption onto a magnetite-doped activated carbon fiber. *Journal of Colloid and Interface Science,* 343: 232–238.

Zhu, J., Bi, H., Wang, Y., Wang X., Yang, X., Lu. 2007. Synthesis of Flower-like CuO Nanostructures via a Simple Hydrolysis Route, *Materials Letters,* 61, 5236–5238.

Zin, M. T., Borja, J., Hinode, H., Kurniawan, W. 2013. Synthesis of Bimetallic Fe/Cu Nanoparticles with Different Copper Loading Ratios, *International Journal of Chemical, Materials Science and Engineering*, 7 (12), 662-666.

Zouboulis, A.I., Katsoyiannis, I.A. 2005. Recent Advances in the Bioremediation of Arsenic-Contaminated Ground Waters. *Environment International,* 31, 213– 219

Appendix I: FTIR spectra

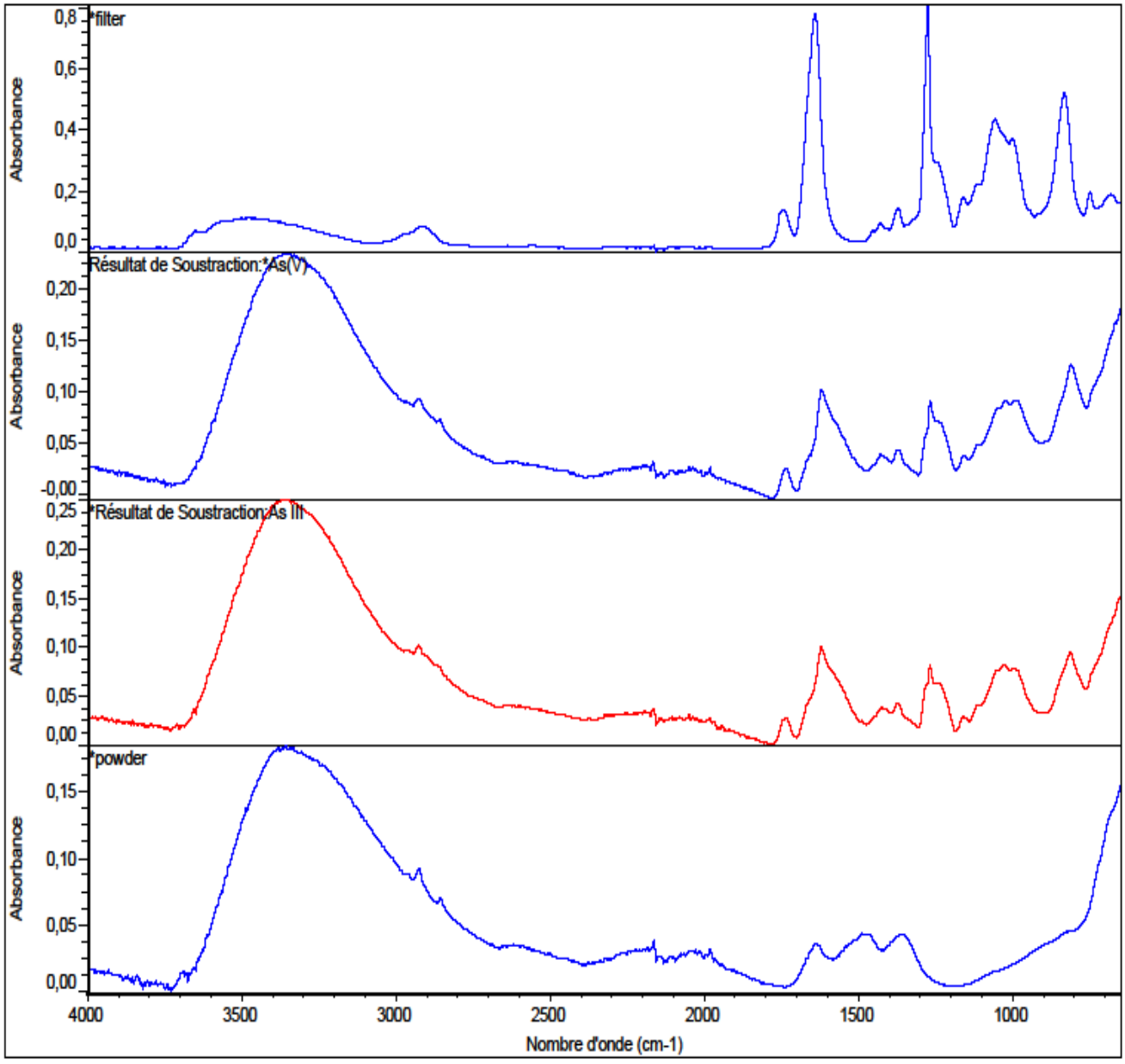

Appendix II: Soil particle size distribution

2015.07.02 11:09:15

HORIBA Laser Scattering Particle Size Distribution Analyzer LA-950

Sample Name	: CCA SOIL	Median Size	: 48.04263(μm)
ID#	: 2015070211072B7	Mean Size	: 149.18108(μm)
Data Name	: 2015070211072B7	Variance	: 27421(μm²)
Transmittance(R)	: 95.8(%)	Std.Dev.	: 165.5938(μm)
Transmittance(B)	: 94.3(%)	Mode Size	: 418.4389(μm)
Circulation Speed	: 5	Span	: OFF
Agitation Speed	: 3	Geo.Mean Size	: 42.6944(μm)
Ultra Sonic	: OFF	Geo.Variance	: 6.2871(μm²)
Form of Distribution	: Manual	Skewness	: 0.7602
Distribution Base	: Volume	Kurtosis	: 1.9941
Material	: SOIL	Diameter on Cumulative %	: (2)10.00 (%)- 5.8269(μm)
Source	: CONTAMINATED SITE		: (9)90.00 (%)- 422.4924(μm)
Lot Number	:		
Test or Assay. Number	: Test 1		
Refractive Index (R)	: CCA[Quartz(1.450 - 0.000i),Water(1.333)]		
Refractive Index (B)	: CCA[Quartz(1.450 - 0.000i),Water(1.333)]		

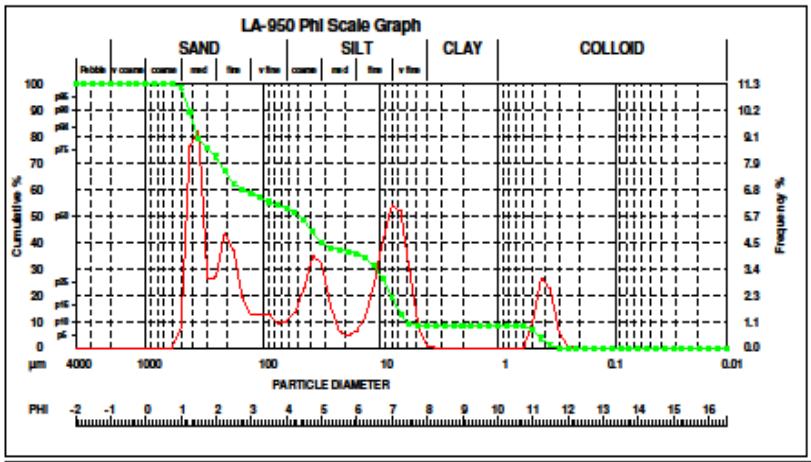

	Diameter	Phi	MILS	Microns	Frequency	Diameter Frequency	CUMULATIVE
F PEBBLE	5	-2.00	157.48	4000.00	0.00	0.00	100.00
	6	-1.75	132.43	3363.59	0.00		100.00
	7	-1.50	111.26	2828.43	0.00		100.00
	8	-1.25	93.64	2378.41	0.00		100.00
FINE PEBBLE	10	-1.00	78.74	2000.00	0.00	0.00	100.00
	12	-0.75	66.21	1681.79	0.00		100.00
	14	-0.50	55.68	1414.21	0.00		100.00
	16	-0.25	46.82	1189.21	0.00		100.00
V CRS SAND	18	0.00	39.37	1000.00	0.00	0.00	100.00
	20	0.25	33.11	840.90	0.00		100.00
	25	0.50	27.84	707.11	0.00		100.00
	30	0.75	23.41	594.60	0.00		100.00
CRS SAND	35	1.00	19.69	500.00	0.92	0.92	99.08
	40	1.25	16.55	420.45	9.54		89.54
	45	1.50	13.92	353.55	10.32		79.22
	50	1.75	11.70	297.30	3.25		75.97
MED SAND	60	2.00	9.84	250.00	3.35	26.45	72.62
	70	2.25	8.28	210.32	5.46		67.17
	80	2.50	6.96	176.78	4.62		62.54
	100	2.75	5.85	148.65	2.46		60.14
FINE SAND	120	3.00	4.92	125.00	1.55	14.03	58.59
	140	3.25	4.14	105.11	1.58		57.01
	170	3.50	3.48	88.39	1.60		55.41
	200	3.75	2.93	74.33	1.18		54.23
V FINE SAND	230	4.00	2.46	62.50	1.23	5.58	53.01
	270	4.25	2.07	52.56	1.68		51.33
	325	4.50	1.74	44.19	2.81		48.52
	400	4.75	1.46	37.16	4.38		44.15
CRS SILT	450	5.00	1.23	31.25	4.05	12.91	40.10
	500	5.25	1.03	26.30	2.05		38.05
	625	5.50	0.87	22.10	0.79		37.25
		5.75	0.73	18.58	0.58		36.67
MED SILT		6.00	0.62	15.63	0.76	4.21	35.89
		6.25	0.52	13.14	1.45		34.44
		6.50	0.43	11.05	3.06		31.39
		6.75	0.37	9.29	5.10		26.27
FINE SILT		7.00	0.31	7.81	6.75	16.36	19.52
		7.25	0.26	6.57	6.58		13.05
		7.50	0.22	5.52	3.61		9.42
		7.75	0.18	4.65	1.07		8.34

	Diameter	Phi	MILS	Microns	Frequency	Diameter Frequency	CUMULATIVE
V FINE SILT	8.00		0.15	3.91	0.10	11.28	8.25
	8.25		0.13	3.26	0.00		8.25
	8.50		0.11	2.76	0.00		8.25
	8.75		0.09	2.32	0.00		8.25
	9.00		0.08	1.95	0.00		8.25
	9.25		0.06	1.64	0.00		8.25
	9.50		0.05	1.38	0.00		8.25
	9.75		0.05	1.16	0.00		8.25
CLAY	10.00		0.04	0.98	0.00	0.00	8.25
	10.25		0.03	0.82	0.00		8.25
	10.50		0.03	0.69	0.00		8.25
	10.75		0.02	0.58	0.02		8.23
	11.00		0.02	0.49	1.19		7.03
	11.25		0.02	0.41	3.31		3.72
	11.50		0.01	0.35	2.94		0.88
	11.75		0.01	0.29	0.77		0.12
	12.00		0.01	0.24	0.12		0.00
	12.25		0.01	0.21	0.00		0.00
	12.50		0.01	0.17	0.00		0.00
	12.75		0.01	0.15	0.00		0.00
	13.00		0.00	0.12	0.00		0.00
	13.25		0.00	0.10	0.00		0.00
	13.50		0.00	0.09	0.00		0.00
	13.75		0.00	0.07	0.00		0.00
	14.00		0.00	0.06	0.00		0.00
	14.25		0.00	0.05	0.00		0.00
	14.50		0.00	0.04	0.00		0.00
	14.75		0.00	0.04	0.00		0.00
	15.00		0.00	0.03	0.00		0.00
	15.25		0.00	0.03	0.00		0.00
	15.50		0.00	0.02	0.00		0.00
	15.75		0.00	0.02	0.00		0.00
	16.00		0.00	0.02	0.00		0.00
	16.25		0.00	0.01	0.00		0.00
COLLOID	16.50		0.00	0.01	0.00	8.25	0.00

1 / 1

Appendix III: Soil elements

Concentration of different elements in soil (mg/kg)

Ca	Mg	Al	Mn	Fe	Co	Ni	Cu	Zn	Se	Mo	Pb
18497.2	163177.3	8561.9	836.6	18166.3	12.2	37.5	304	76.4	0.7	0.2	5.6

Appendix IV: Binding energy of elements in XPS spectra

Peak binding energies (extracted from excel files)

Name	*Peak BE (before adsorption)*	*Peak BE (after adsorption As(III))*	*Peak BE (after adsorption As(V))*
O1s	530.03	529.98	529.93
Cu2p	933.88	933.88	934.28
	940.98	940.88	941.48
	953.78	953.98	953.88
	961.78	962.58	962.68
Fe2p	710.88	710.98	711.08
	724.58	724.18	724.88